

**University of
Reading**

A Bioactive Hyperbranched Polymer Disclosure System for Bacteria

PhD Chemistry

Department of Chemistry

A thesis submitted in part fulfilment of the degree of
Doctor of Philosophy

Oliver Balmford

Supervised by
Professor Wayne Hayes and Dr Simon Clarke

September 2018

Declaration

I confirm the research described in this thesis is my own work and that the use of all materials from other sources has been properly and fully acknowledged.

Oliver Balmford

Acknowledgements

Firstly, I would like to thank Professor Wayne Hayes and Dr Simon Clarke for their guidance and support throughout my PhD. I would also like to thank Dr Alistair Bishop, Dr Camilla Robinson and Dr Mark Sambrook at DSTL for providing Chemical and Microbiological insight and for funding this work.

I am grateful for the expertise and knowledge passed on to me by the Post-Doctoral researchers I have had the pleasure to work with: Dr Lewis Hart, Dr Kate Lim, Dr Antonio Feula, Dr Daniel Smith, Dr Kelly Melia, Dr Flavien Leroux and Dr Ashfaq Afsar. I would also like to thank my fellow labmates for the years of fun and friendship: Dr Tahkur Babra, Jessi Godleman, Dr Priya Sonkar, Dr Ben Baker, Dr Clare Gosling, Dr Michael Budd, Sam Burholt, Dr Hannah Bowden, Dr Charlotte Marriot, Iain Hopkins, Markus Knappert, Sara Salimi, Alex Gavriel, Adam O'Donnell, Jasraj Babra and Zoe Selfe.

A special mention to Jessi Godleman for many essential coffee breaks and sharing in the highs and lows that come with a Chemistry PhD.

Dr Radoslaw Kowalczyk for his insight into NMR spectroscopy, Nicholas Michael for his invaluable assistance with ESI Mass Spectrometry and MALDI-TOF Mass Spectrometry and Amjed Mohsen for his advice with the routine microbiological procedures.

Dr Tahkur Babra, having started with you back in 2014 following our masters together it has been a pleasure to work alongside you since. Your insight and advice as well as your friendship has made my time here even more enjoyable.

I would like to thank my family for all their support throughout my PhD and for helping me reach my childhood goal of becoming a scientist.

I could not have completed this PhD without the unconditional support of my wife Laura Kane. You have helped me through the lowest points and celebrated with me through the highest and I am forever grateful.

Finally, I thank the reader, for if you have made it this far, you have read at least one page of my thesis.

Abbreviations

δ	Chemical shift
η_{inh}	Inherent viscosity
η_{rel}	Relative viscosity
AChE	Acetylcholinesterase
AIBN	Azobisisobutyronitrile
ATP	Adenosine Triphosphate
<i>B.</i>	Bacillus
BoNT	Botulinum Neurotoxin
Bp	Boiling Point
BWA	Biological Warfare Agent
BWC	UN Biological Weapons Convention
^{13}C NMR	Carbon 13 Nuclear Magnetic Resonance Spectroscopy
CaDPA	Calcium Dipicolinate
CBRN	Chemical, Biological, Radiological or Nuclear Weapons
COSY	Correlation Spectroscopy
CWA	Chemical Warfare Agent
d	Doublet
dd	Double Doublet
EF	Edema Factor
DLS	Dynamic Light Scattering / Quasi-elastic Light Scattering
DMSO	Dimethylsulfoxide
DPA	Dipicolinate Anion
DSC	Differential Scanning Calorimetry

ESI	Electrospray Ionization
FRET	Förster resonance energy transfer
FT-IR	Fourier-Transform Infra-Red Spectroscopy
GPC	Gel Permeation Chromatography
GQDs	Graphene Quantum Dots
HCl	Hydrochloric Acid
HMBC	Heteronuclear Multiple Bond Correlation Spectroscopy
HSQC	Heteronuclear Single Quantum Coherence Spectroscopy
^1H NMR	Proton Nuclear Magnetic Resonance Spectroscopy
IG	Inverse-Gated Proton Decoupling
LCMS	Liquid Chromatography tandem Mass Spectrometry
LF	Lethal Factor
LMWG	Low Molecular Weight Gelators
Mp	Melting Point
MALDI-TOF MS	Matrix Assisted Laser Desorption/Ionization Time of Flight Mass Spectrometry
MS	Mass Spectrometry
NMR	Nuclear Magnetic Resonance Spectroscopy
NSET	Nanosurface Energy Transfer
OD	Optical Density
OPH	Organophosphorus Hydrolase
PA	Protective Antigen
PCR	Polymerase Chain Reaction
RPA	Recombinase Polymerase Amplification
SMA	Slow Monomer Addition

t	Triplet
TGA	Thermogravimetric analysis
T_g	Glass Transition Temperature
UV	Ultra-Violet
WHO	World Health Organization
WMD	Weapon of Mass Destruction

Synopsis

The disclosure of Biological Warfare Agents (BWAs) poses a considerable scientific and practical challenge as a result of the inherent lower reactivity afforded by natural products, viral and bacterial pathogens. In the 20th century throughout both the first and second world wars *Bacillus anthracis*, the causative agent of Anthrax, was studied for its potential use in biological warfare. *B. anthracis* is one of a limited number of bacteria capable of forming endospores. The endospore is a dormant and stable form of the organism in which all water is removed and cell metabolism ceases. Bacteria that can form these structures are capable of surviving thousands of years. Hence, land contaminated with pathogenic endospores can be rendered uninhabitable and, in some cases, impassable for decades. However, if the *B. anthracis* cell is in its vegetative state, the process of decontamination is made substantially easier by the increased susceptibility of the cells. It is, therefore, favourable to induce germination in spores before attempting decontamination.

This thesis is a multidisciplinary approach to develop a formulation capable of inducing germination of *B. anthracis* endospores and disclosing their presence to an end-user such that appropriate action can be taken to decontaminate the surface.

In this thesis Chapter 1 provides an overview to the obstacles that have so far restricted development of the desired formulation. It also encompasses the historical background, posed risks and detailed aims of this project.

Chapter 2 reports the synthesis and optimisation of processes towards materials that can provide favourable environments to promote endospore germination in a controlled fashion. Investigations focussed on the promising characteristics of a class of low molecular weight gelators (LMWGs) known as supergelators because of their exceptionally ability to form rigid structures at concentrations as low as 0.9 mM as well as hydrophilic branched polymers based upon the monomer glycerol. Investigations into hydrophilic materials capable of providing sufficient humectant properties to sustain germination suggested the hyperbranched polyether polyglycerol could fulfil many of the desired requirements of a formulation suitable for storage and spray dispersal. The polymers were further optimised by introduction of orthogonal reactive groups of furfuryl

alcohol capable of reacting via the facile thermoreversible Diels-Alder process to enable future bioactive sensors or dyes. The benefit of this method is that these reactions are typically conducted in very mild conditions and at low temperatures which allows for sensitive or less stable functional compounds to be attached to the polymer backbone without fear of degradation or damage to these materials. These materials were noted to possess LCST properties which were further investigated by means of DLS.

Chapter 3 focussed on the development of a suitable disclosure agent for the *B. anthracis* biomarker calcium dipicolinate (CaDPA). Based upon the fluorescent carbazole moiety, a sensor originally developed by Curiel *et al.* was resynthesized using optimised procedures to evaluate its suitability for use in an aqueous formulation. Following this, steps were taken to attempt to increase the effectiveness of the sensor by altering its colourimetric response through extension of the π -system of the carbazole fluorescent backbone. Further optimisations to increase its water solubility were explored via introduction of charged imidazolium species.

Chapter 4 details the steps taken to assess the suitability of the polyglycerol formulations prepared in Chapter 2 to assist in the germination of *B. thuringiensis*. *B. thuringiensis* endospores are used as a simulant for the more dangerous *B. anthracis* and were cultivated and purified before use. The degree of germination of the endospores was assessed through a plate counting method and compared to a rate of germination assessment carried out via optical density measurements.

The studies described herein provide a strong foundation for further development of a novel formulation capable of rapidly disclosing the presence of *B. anthracis* contamination.

Contents

Chapter 1 - Introduction.....	1
1.1. Biological Warfare	1
1.2. BWA Disclosure	2
1.2.1. Traditional Identification Methods	2
1.2.2. Rapid Identification Methods	5
1.3. <i>B. anthracis</i>	9
1.3.1. History	9
1.3.2. Method of Action	10
1.3.3. Endospores and Germination	12
1.4. <i>B. anthracis</i> Disclosure Agents	14
1.4.1. Lanthanide DPA Sensors.....	14
1.4.2. Organic DPA Sensors.....	15
1.5. Project Aims and Objectives	16
1.6. References	18
Chapter 2 – Gels and Polyols for <i>Bacillus anthracis</i> endospore germination.....	24
2.1. Introduction	24
2.1.1. Hydrogelators.....	24
2.1.2. Polyols	26
2.2. Results	29
2.2.1. Hydrogelators.....	29
2.2.2. Hyperbranched Polyglycerol	32
2.2.3. Glycidyl FGE copolymer.....	49
2.3. Conclusion and Future Work	59
2.4. Experimental.....	61

2.4.1.	General Experimental	61
2.4.2.	General procedure for initiator preparation	61
2.4.3.	General procedure for SMA polymer synthesis (2.19_{SMA})	61
2.4.4.	General procedure for Bulk polymer synthesis (2.19_{BULK})	62
2.4.5.	5-(3-(4-nitrophenyl)ureido)isophthalic acid (2.15).....	63
2.4.6.	Furfuryl Glycidyl Ether	63
2.5.	References	64
Chapter 3 – Organic based Bacillus anthracis disclosure agent.....		68
3.1	Introduction	68
3.1.1	Calcium dipicolinate-based sensors	68
3.2	Results and Discussion	71
3.2.1	Synthesis of the DPA sensor 3.1	71
3.2.2	Carbazole Modification	80
3.2.3	Binding site modification	87
3.3	Conclusion.....	96
3.4	Experimental.....	97
3.4.1	Materials	97
3.4.2	General Experimental	98
3.4.3	Synthesis of dimethyl 2-nitro-[1,1'-biphenyl]-4,4'-dicarboxylate (3.8).	98
3.4.4	Synthesis of dimethyl 9 <i>H</i> -carbazole-2,7-dicarboxylate (3.10).....	98
3.4.5	Synthesis of 9 <i>H</i> -carbazole-2,7-dicarboxylic acid (3.11).....	99
3.4.6	Synthesis of <i>N</i> ² , <i>N</i> ⁷ -bis((1 <i>H</i> -pyrrol-2-yl)-methyl)-9 <i>H</i> -carbazole-2,7-dicarboxamide (3.1).....	99
3.4.7	Synthesis of dimethyl 2-amino-[1,1'-biphenyl]-4,4'-dicarboxylate (3.25) ...	100
3.4.8	Synthesis of 1 <i>H</i> -pyrrole-2-carbaldehyde (3.15).	101
3.4.9	Synthesis of 1 <i>H</i> -pyrrole-2-carbaldehyde oxime (3.17).	101

3.4.10	Synthesis of <i>N</i> -Boc-ethanolamine (3.29)	102
3.4.11	Synthesis of 2-((Boc)-amino)-ethyl 4-methylbenzenesulfonate (3.30)	102
3.4.12	Synthesis of <i>Tert</i> -butyl (2-(1H-imidazol-1-yl)-ethyl)-carbamate (3.32)	103
3.4.13	Synthesis of 2-(2-(1H-imidazol-1-yl)-ethyl)-isoindoline-1,3-dione. (3.34)	103
3.4.14	Synthesis of 1-(2-(1,3-dioxoisindolin-2-yl)-ethyl)-3-methyl-1-imidazolium iodide. (3.35)	104
3.4.15	Synthesis of 1-(2-(1,3-dioxoisindolin-2-yl)-ethyl)-3-methyl-1-imidazolium hexafluorophosphate. (3.38)	104
3.5	References	105
Chapter 4 – In Vitro studies of bacterial germination and disclosure.....		107
4.1.	Introduction	107
4.2.	Results and Discussion	110
4.2.1.	Plate Counting.....	115
4.2.2.	Alternative Methods for measuring Germination.....	118
4.3.	Conclusion.....	122
4.4.	Methods	123
4.5.	References	123
Chapter 5 – Conclusions and Future Perspectives		126
5.1.	Materials for BWA Disclosure - Gels and Polyols.....	125
5.2.	Disclosure Agent.....	129
5.3.	Microbiological Studies.....	131
5.4.	References	133

Chapter 1

Introduction

1.1. Biological Warfare

Biological warfare agents (BWAs) are, in some cases, more challenging to define than their Chemical, Radiological and Nuclear counterparts. Using the definition from the World Health Organization (WHO) BWAs are those that depend on multiplication inside the host for their method of action such as viruses and bacteria.¹ However, the UN Biological weapons convention (BWC) bans the developing, producing, stockpiling or otherwise acquiring or retention of biological agents and toxins.² Since the treaty includes biological toxins certain agents that are derived from natural sources such as ricin fall are both a discrete chemical and also a biological agent. For the avoidance of doubt, BWAs discussed here will be categorized in accordance with the BWC definition.

The first recorded use of biological warfare dates back over 3000 years to the Hittite plague where an epidemic of tularaemia, caused by *Francisella tularensis*, was instigated by forcing infected individuals to travel to the enemy state.³ Although there is wide spread support for this hypothesis there remain some individuals who are sceptical because it does not align with main sources of infection which are rodents and lagomorphs such as rabbits.⁴ *Yersinia pestis*, the causative agent of bubonic plague has been suggested as one of the earliest BWA's used, with its use at the siege of Caffa (now Feodosia in Crimea) in 1346 a potential origin of the 14th century plague pandemic.⁵⁻⁷

Clostridium botulinum is the bacterium responsible for causing botulism in humans.⁸ Similarly to ricin this species is known mostly for the toxin it produces, botulinum neurotoxin (BoNT). BoNT is the most toxic substance known to humans requiring an intravenous dose of only 1.3-2.1 ng kg⁻¹ to be lethal.⁹⁻¹¹ The method of action of BoNT is counter to that of nerve agents such as VX which result in hyper-activation of the neuromuscular junction, BoNT prevents the release of the neurotransmitter acetylcholine thus paralysing muscle activation.⁹ Despite its exceedingly high toxicity this neurotoxin is

routinely used in the cosmetic industry to reduce the appearance of skin wrinkles by preventing facial muscle activation.

When compared to chemical warfare agents (CWAs), biological warfare agents are significantly slower in their action. Symptom timescales for CWA exposure range from minutes in the case of fast acting nerve and blood agents up to 24 hours in the case of certain blister agents and phosgene.¹² In contrast, biological warfare agents typically have incubation periods measured in days before symptoms arise.¹³ This slower mode of action allows for medical intervention and treatment but in the case of contagious species it also allows for further distribution.

1.2. BWA Disclosure

The disclosure of BWAs poses considerably more scientific and practical challenges than that of chemical warfare agents (CWAs) which is primarily as a result of the reactive nature of the agents involved. CWAs need to be inherently reactive such that upon contact they can quickly perform their designed function. Their functionality is usually very specific, and their molecular weight is typically less than 500 g mol^{-1} to permit efficient uptake by the human body. In contrast, BWAs are substantially less reactive as expected from natural products, viral and bacterial pathogens. There has been significant work in the area of BWA disclosure by commercial entities yet many of these options lack either rapid identification and/or large area disclosure.

1.2.1. Traditional Identification Methods

Traditional methods used to disclose the presence and identify typically involves the sampling of a surface using a moistened cotton wool tip. This method typically has a variety of problems associated with it, primarily the very poor recovery rate *ca.* 10%.¹⁴ The major limitation of this method is its restriction of the sample area since the degree and severity of the contamination can only be determined for the surface that passed directly under the swab.

It is unlikely that a contamination on a surface would be uniformly distributed, therefore inaccurate sampling could result in false negative results. Once acquired the sample still requires culturing through incubation on nutrient agar plates. These techniques require

extensive amounts of labour and expertise with technical microbiological techniques. Further potential methods for BWA detection and disclosure are discussed in sections 1.2.1.1 to 1.2.2.5.

1.2.1.1. pH Indication

The metabolic activity of bacteria on carbohydrates is known to produce acids which can be detected using simple pH colour change within the nutrient media on which the sample is cultivated. Cystine Lactose Electrolyte Deficient (CLED) agar is an example of such media where the fermentation process of lactose results in acid production which can be identified by the bromothymol blue indicator. Species such as *Escherichia coli* and *Staphylococcus aureus* can metabolize the lactose and as such produce identifiable yellow colonies as shown in Figure 1.1.

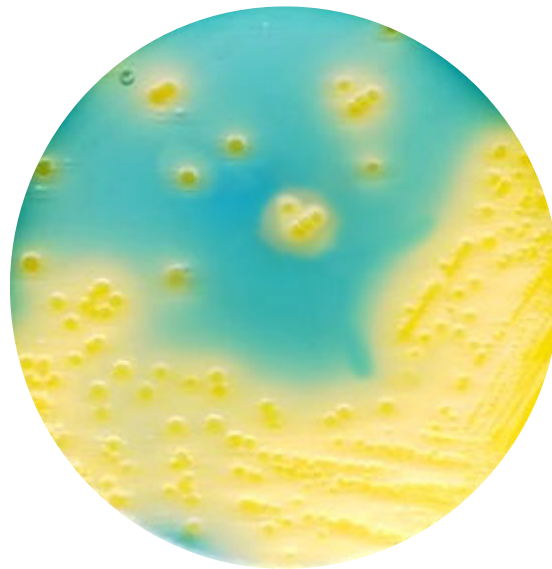


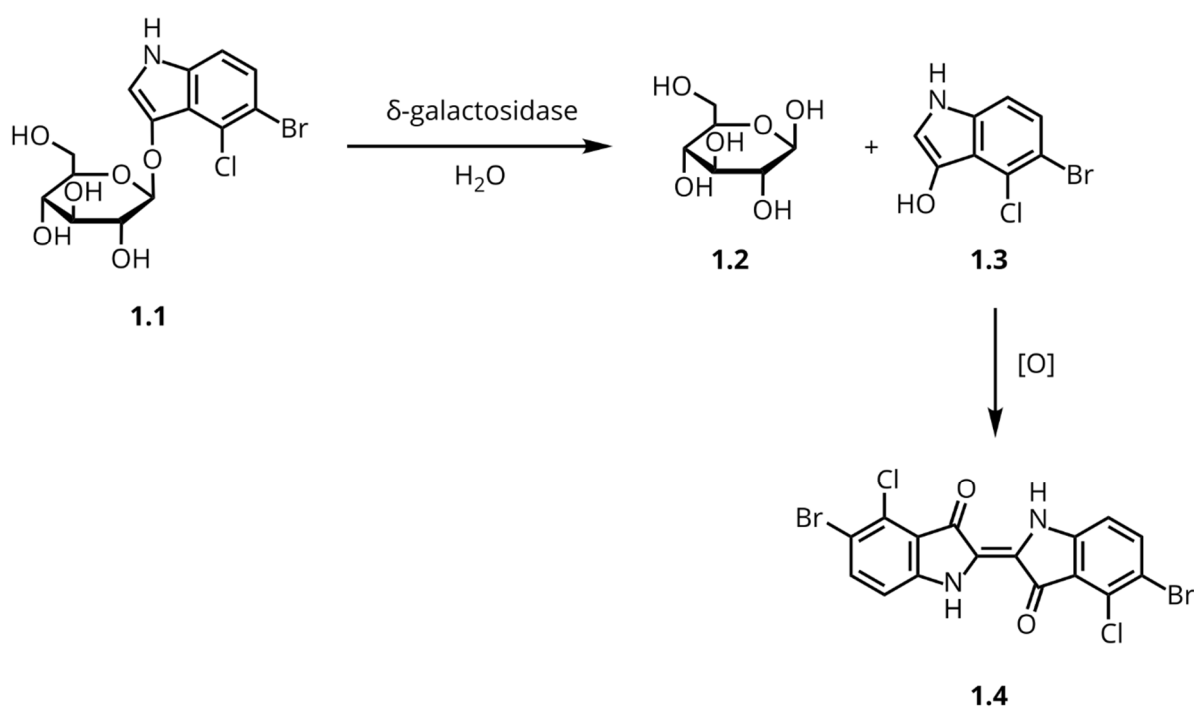
Figure 1.1: Cystine lactose electrolyte deficient (CLED) agar, a chromogenic agar impregnated with bromothymol blue.¹⁵

Bacteria can metabolize carbohydrates either via oxidation or fermentation, with the latter producing more acid compounds than the former. This varies the response based on the species, combined with this certain species of *Bacillus* can produce ammonia which neutralises the response of bromothymol blue.

1.2.1.2. Enzyme Assays

Enzyme assays are capable of utilising the specific enzymatic activity within viable cells to convert synthetic targets from an inactive state to a induce a colourimetric or fluorometric response or *vice versa*.

An example of this is the Brilliance™ chromogenic media developed by Oxoid Ltd. one type of which is the Bacillus cereus agar which is capable of identifying *Bacillus cereus* bacteria and its closely related genetic neighbours. In this case the synthetic chromogenic substrate 5-bromo-4-chloro-3-indolyl- β -glucopyranoside (**1.1**) provides an indication for the presence of active β -galactosidase enzyme. This enzyme cleaves the glycosidic bond and releases the 5-Bromo-4-chloro-3-hydroxyindole (**1.3**) which is then oxidised to form an analogue of the blue indigo dye (**1.4**).¹⁶



Scheme 1.1: Enzymatic cleavage of 5-bromo-4-chloro-3-indolyl- β -glucopyranoside leading to the production of the analogue of indigo dye.

The effects of this can be seen in the sample of Brilliance™ Bacillus cereus Agar inoculated with *B. thuringiensis* shown in Figure 1.2. This agar also contains two antibiotics Polymixin B and Trimethoprim to inhibit the growth of other species allowing for the analysis of impure samples. The development of the blue colonies is an indication of β -galactosidase enzyme within the species.

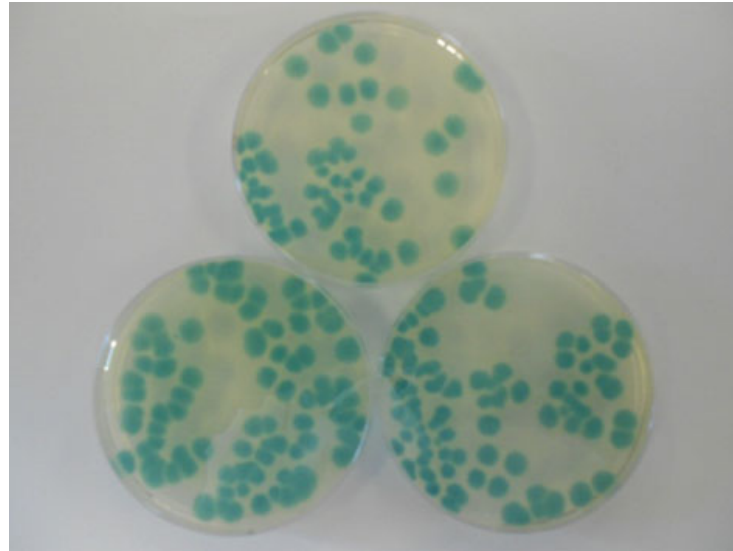


Figure 1.2: *Bacillus thuringiensis* growing on Brilliance™ *Bacillus cereus* Agar.^{17†}

While this method has been shown to be effective, the majority of enzyme assays are conducted on lysed cells. This is usually done to ensure the maximum contact between enzyme and chromogenic substrate as well as ensuring optimal conditions for the chromophore/fluorophore response. For example, *p*-nitrophenol requires basic conditions to exhibit a strong yellow colour as does the fluorophore 4-methylumbelliferone.

1.2.2. Rapid Identification Methods

It has been argued that rapid detection is not as necessary for BWAs as it is for CWAs.¹⁸ However, In the case of bioterrorism incidents or exposure to unknown BWAs within a military combat zone potential large area contamination necessitates fast identification of the location and class of hazard to enable area avoidance in the case of area denial and effective decontamination of surfaces and materials.¹⁹⁻²¹ For bacteria and viruses the option of using chemically reactive disclosure agents is unavailable. However, in place of this there are many methods that focus on these specific unreactive agents to effectively and rapidly identify imposing threats.

[†] Reproduced from Ref. ¹⁷ with permission from the Journal of Applied Microbiology.

1.2.2.1. Nucleic Acid Detection

Nucleic acid based detection has been widely investigated as a method to detect and identify potential BWA threats. These methods utilise procedures called Real-time Polymerase Chain Reaction (PCR) or Recombinase Polymerase Amplification (RPA) to amplify the quantity of a specific deoxyribonucleic acid (DNA) sample to enhance its sensitivity.²² Bell *et al.* took advantage of a modified version of this procedure to detect *B. anthracis* plasmids (i.e. short circular strings of DNA that are not part of the chromosomal DNA). One benefit of this method is its exceptionally high sensitivity. They report detection levels as low as one copy of DNA per microlitre. While culture methods usually take between 24 and 48 hours to yield a result, the approach of Cockerhill III *et al.* produced accurate results in under 1 hour using a Roche LightCycler[®].²³ While this method does offer excellent selectivity and sensitivity and has been shown to be effective in environmental samples, it is only capable of determining whether a sample contains *B. anthracis*. Therefore, full disclosure of a contaminated area can only be realised by extensive sampling. The one hour measurement time makes this method a viable candidate for identification of a specific biothreat.

1.2.2.2. SPR Biosensors

Biosensors, which convert biological responses into electrical signals to be measured by a device, were originally adapted to investigate immunoassays in 1983 by Liedberg *et al.*²⁴ A Surface Plasmon Resonance (SPR) sensor chip is made by attaching antibodies or antigens to the surface of a thin metal film (*ca.* 60 nm thickness) coated with a matrix such as dextran. An incident light beam through a prism creates surface plasmons on the opposing side of the metal layer. The plasmons are very sensitive to changes of the surface of the metal, therefore, upon binding of an analyte the light reflected from the metal surface undergoes a measurable change (see Figure 1.3). This approach has been successfully applied to detection of *B. anthracis*, however, the limit of detection (LOD) is much higher than other methods at between 10^7 and 10^5 endospores per mL of solution.²⁵⁻²⁸

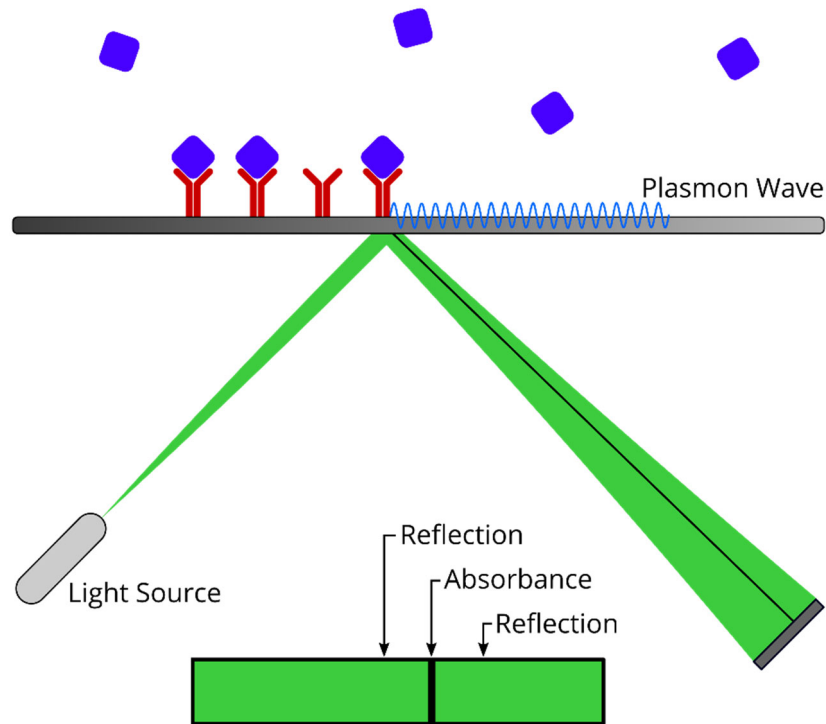


Figure 1.3: Schematic of a surface plasmon resonance detector with antibody receptors.

1.2.2.3. Antigen and Antibody Detection

Chanteau *et al.* in 2003 developed an antigen based rapid diagnostic test for *Y. pestis* designed to quickly identify infected patients.²⁹ Using sample strips infused with the monoclonal antibody anti-F1 Mab G6-18, tests were conducted on a variety of microbial samples showing its specificity and high concordance with an F1 immunoassay. This method of detection is effective but only help identify infected patients rather than the bacteria itself as the specific antigen is only produced at 37°C.³⁰

As previously mentioned there has been significant work in this area by commercial entities. BBI Detection produce the IMASS™ device³¹ (see Figure 1.4), originally developed by Dstl, capable of detecting and identifying 8 different BWAs including Ricin toxin, Botulinum Toxin A/B and *B. anthracis*. These devices offer rapid detection of these agents in 15 minutes. These antigen detection strips are contained in a plastic applicator to enable easy use by personnel in the field with little training.



Figure 1.4: IMASS™ device produced by BBI Detection.³¹

While these devices are ideal for first responders to the scene of a BWA contaminated zone their limited sampling area and single use nature mean that they are not suitable for identifying areas that require decontamination.

1.2.2.4. Bioluminescence / ATP Detection

Seto *et al.* reported the effectiveness of identifying the presence of adenosine triphosphate (ATP), a cellular energy source in bacteria and animals, by the bioluminescence of Luciferin-Luciferase solution part of the CheckLite™ 250 Plus kit from Kikkoman Corp. Using this method, they were able to identify whether an unknown white powder contained viable bacteria within a maximum time of 1.5 hours. The benefit of this approach is that with suitable guidance an untrained person could rapidly identify the risk of a substance at the frontline.³²

1.2.2.5. Mass Spectrometry

The use of Matrix-assisted laser desorption ionization (MALDI-TOF) Mass Spectrometry (MS) and Liquid chromatography tandem mass spectrometry (LCMS) has been widely investigated for detection of BWA's including toxins such as Ricin, BoNT and cholera toxin.³³⁻⁴⁰ By identification of proteins unique to certain BWA's it is possible to rapidly identify bacterial and viral strains. A benefit of this method is that fingerprints for certain agents can be stored in a database. Combined with the speed of this technique it offers rapid identification of a large range of BWA's and CWA's. The major drawbacks of this method are the cost of the equipment involved and the sensitivity to environmental

impurities. While suitable for a laboratory or hospital setting widespread use across police forces and military is prohibitively expensive.

1.3. *B. anthracis*

1.3.1. History

B. anthracis, the causative agent of anthrax, was originally known as Woolsorter's disease owing to its common occurrence in workers classifying and examining wool fleeces. The sheep contracted and carried the bacteria on their coats and workers that handled large quantities of this material were exposed to a large quantity of these endospores.^{41,42}

In the 20th century throughout both the first and second world wars Anthrax was studied as a possible biological warfare agent. Towards the end of the Second World War the UK began extensive research into Anthrax bombs and cattle cakes, which could be dispersed over German cattle farms in an effort to drastically reduce meat supplies as herbivores are particularly susceptible to ingestion of spores. Anthrax was cultivated and successfully tested as a 30 pound bomb in 1942 and a 4 pound bomblet (*i.e.* a small sub-munition many of which would be contained with a cluster munition) in 1943 on Gruinard Island off the coast of Scotland.⁴³ Despite only contaminating approximately 3 acres, the entire island was regarded unsafe and was purchased by the government until it was decontaminated and regarded safe nearly 50 years later.⁴⁴⁻⁴⁷ The decontamination project involved use of herbicide to kill off all flora followed by incineration of the dead vegetation. The island was then flooded with a solution of 5% formaldehyde in seawater at a volume of 50 litres m⁻² over the entire 10 acre island.⁴⁸⁻⁵¹

Following the implementation of the biological and toxic weapons convention in 1975, 170 UN member states have since prohibited the development, production, and stockpiling of biological weapons. Before this treaty the Geneva Protocol 1925 prevented the use of biological weapons in warfare but did not limit their development.²

Despite the implementation of the treaty, in spring 1979 there was a reported outbreak of Anthrax in the city of Sverdlovsk, Russia. According to soviet officials at the time the outbreak was caused by consumption of contaminated meat. However, suspicions arose

as it became apparent that infected individuals were all located in a similar area downwind of a soviet military microbiology facility.^{52,53}

In the months following the September 11th 2001 terror attacks in the US, a 63 year old male died from a case of inhalation Anthrax, the first in the country for 25 years. This was followed by a further 11 cases (5 of which were fatal) of inhalation Anthrax and 7 confirmed cases of cutaneous Anthrax.¹³ The source of these infections was traced to bacterial spores sent maliciously via the postal network to major news corporations and senators by Bruce Edwards Ivins.⁵⁴⁻⁵⁷ Although biological weapons can be used with the aim of causing harm there have been cases where outbreaks or accidental release can cause harm and contamination without intent.^{58,59}

1.3.2. Method of Action

As well as the single main chromosomal DNA, *B. anthracis* also contains shorter strings of DNA known as plasmids. Unlike chromosomal DNA multiple copies of the same plasmid commonly exist within the cell. The virulence plasmids of *B. anthracis* are called pXO1 and pXO2. The plasmid pXO1 is responsible for the production of the components of anthrax toxin which is comprised of three proteins Protective Antigen (PA₈₃; 83 kDa), Edema Factor (EF; 89 kDa) and Lethal Factor (LF; 90 kDa). The plasmid pXO2 is involved in the synthesis of an external capsule that coats the bacteria. Both pXO1 and pXO2 are virulence factors, which contribute to the ability of the bacteria to cause disease.

The mechanism of action of anthrax toxin is shown in Figure 1.5. PA₈₃ binds to receptors on the surface of the eukaryotic cell. As the protein binds a protease cleaves off a 20 kDa unit (PA₂₀) leaving the remaining 63 kDa (PA₆₃) protein bound to the receptor. The bound PA₆₃ then associates with a further 6 units of PA₆₃ forming the heptomeric pore in the process (shown in Figure 1.6). Once the pre-pore is formed up to three of either EF, LF or a combination can bind to the prepore before it undergoes endocytosis, a process by which a portion of the cell wall inverts to encapsulate the pore and surrounding material.

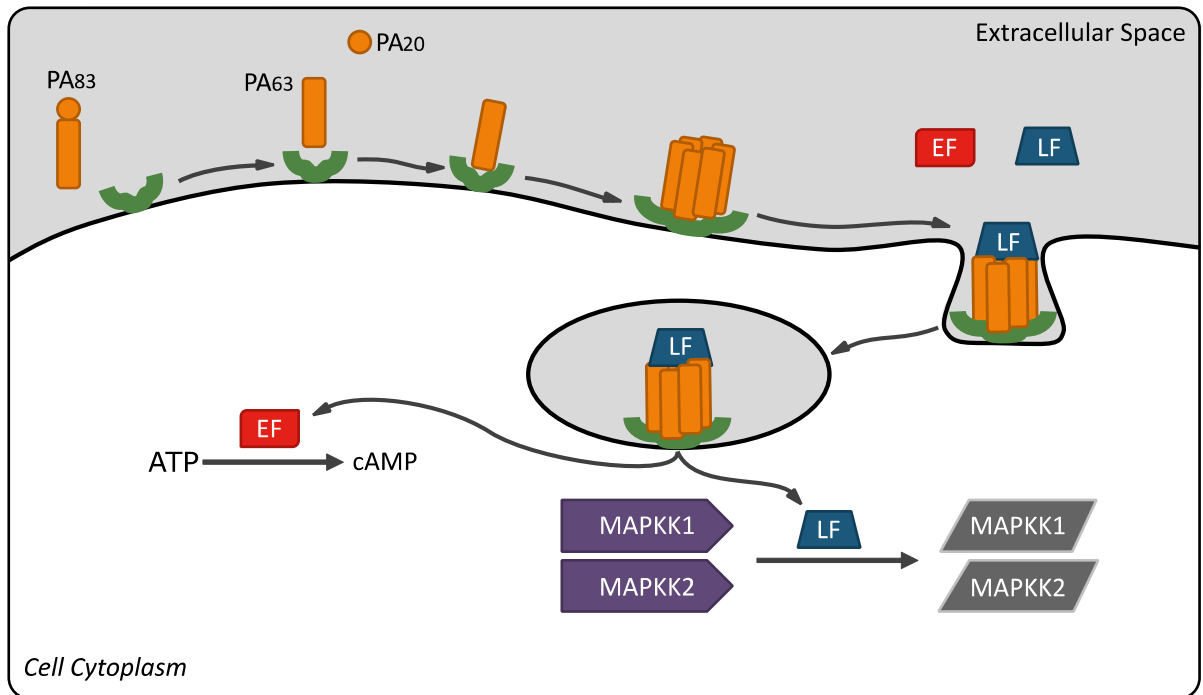


Figure 1.5: Schematic depicting the mechanism of action of anthrax toxin.

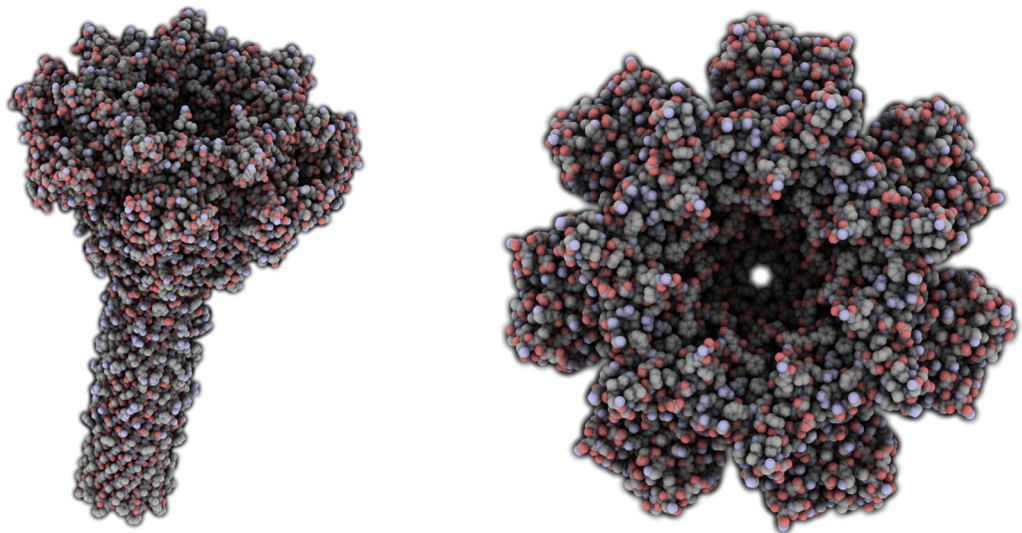


Figure 1.6: CryoEM images of *B. anthracis* protective antigen heptameric pore.^{60,61‡}

Once the endosomal compartment is formed the bound EF and LF are thought to unfold and pass through a 15 Å pore formed by the prepore through the compartment membrane before refolding in the cell cytoplasm and begin causing damage.⁶² The protein EF begins converting ATP into 3'-5'-cyclic adenosine monophosphate (cAMP) which triggers secondary messaging pathways at levels 200 times that of standard.^{63,64}

‡ Images generated using QuteMol⁶¹ from published CryoEM.⁶⁰

Meanwhile LF starts acting as a protease; specifically cleaving part of the mitogen-activated protein kinase kinases (MAPKK1 and MAPKK2). Without PA, EF and LF are unable to enter the cell.

1.3.3. Endospores and Germination

B. anthracis is one of a limited number of bacteria capable of forming endospores. The endospore is a dormant form of the organism in which the majority of water is removed and cell metabolism ceases. Bacteria that can form these structures are capable of surviving thousands of years.⁶⁵

The resilience of the endospore relies on many factors. The spore coat provides resistance to H₂O₂ and enzymes capable of peptidoglycan lysis. The core has been shown to exhibit very low permeability to hydrophilic compounds with sizes greater than 200 g mol⁻¹. Calcium dipicolinate (CaDPA) makes up between 5 and 15% of the endospore by mass.^{66,67} CaDPA is known to provide additional resistance to heat and H₂O₂ but does cause higher sensitivity to UV irradiation as a result of the aromatic structure of the dipicolinate anion.^{68,69} The formation of CaDPA within the spore goes hand in hand with the reduction in water content of the cell from 75 to 80% to between 25 and 50% and as such the majority is ejected from the cell early on in the germination process (see Figure 1.7).⁶⁹ Spores also contain enzymes that upon germination can repair damaged DNA and proteins.⁶⁹

The process of sporulation is well-documented^{65,70-72} and can be broken down into distinctive steps as shown in Figure 1.8. Following separation of the DNA with the cell, internal cleavage of DNA and formation of the forespore it is now observable that the cell has begun sporulation. The forespore is engulfed by the mother membrane. The cortex, a peptidoglycan structural material, begins to form between the two membranes. After the cortex formation, the spore coats are laid down and the spore begins to become more resilient as its water is removed and replaced with CaDPA. Finally, the sporangium containing the endospore is lysed to release the endospore. The process typically takes 6 to 10 hours to complete.^{65,72}

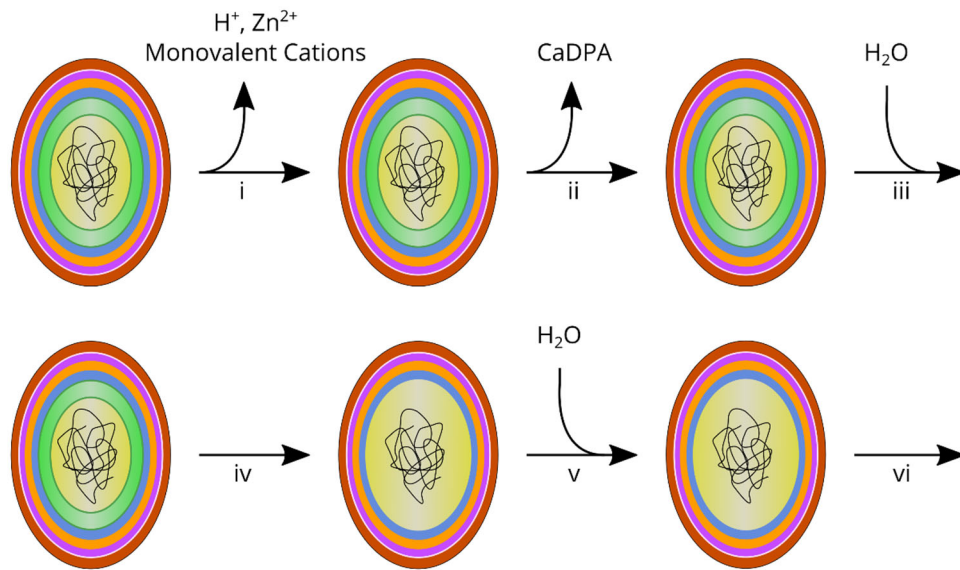


Figure 1.7: Germination process of a *Bacillus* endospore. i) loss of H^+ , Zn^{2+} and monovalent cations. ii) Loss of calcium dipicolinate. iii) Endospore cortex hydration. iv) Hydrolysis of peptidoglycan spore cortex. v) Further uptake of water. vi) Endospore outgrowth to vegetative cell.⁷³⁻⁷⁵

If the *B. anthracis* cell is in its vegetative state, the process of decontamination is made substantially easier as a result of the increase susceptibility of the cells.⁷⁶ It is, therefore, favourable to induce germination in spores before attempting decontamination. The most common way to do this is by application of specific sugars and amino acids.^{17,74}

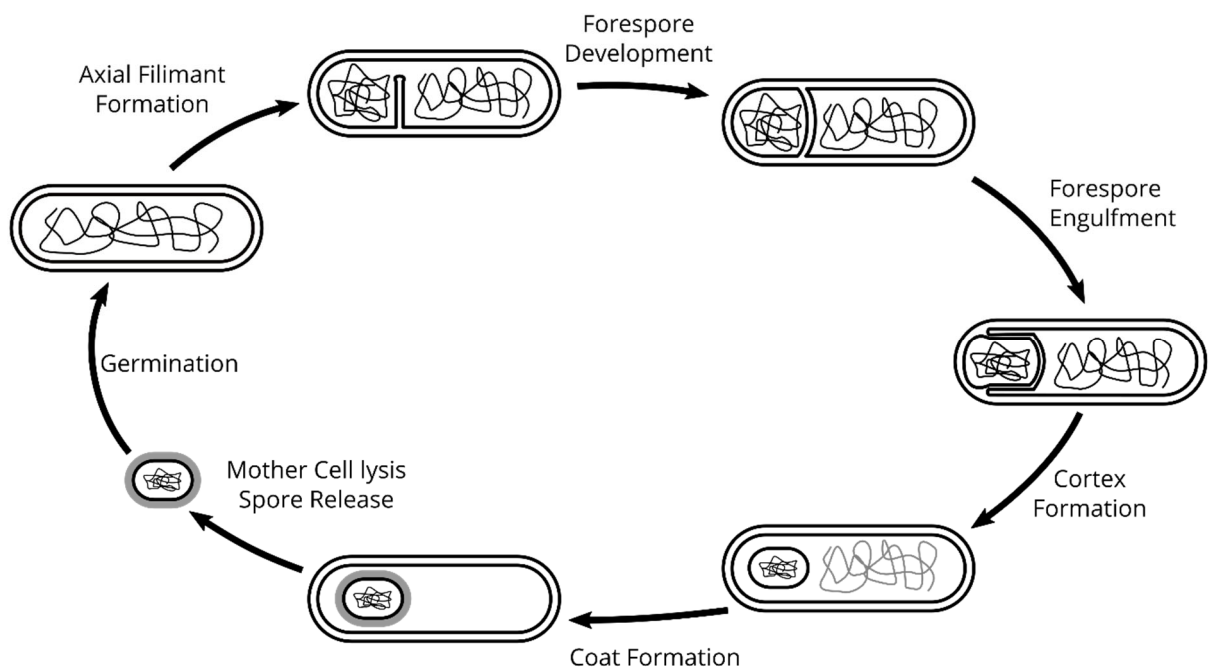


Figure 1.8: Sporulation process of *Bacilli* Bacteria.⁶⁵

1.4. *B. anthracis* Disclosure Agents

Persistent *B. anthracis* endospores in the environment represent a major hazard. In the light of this threat, the development of a disclosure system that can identify and indicate the presence of *B. anthracis* is highly desirable. However, the application process for these sensors can dramatically change their desired characteristics. There is a greater scope of options for sensors designed to be used in a controlled environment, such as a laboratory, compared to those designed to be used in the field. Field-based sensors require much more thought and planning as environmental considerations, product usability and stability are of much greater importance.

1.4.1. Lanthanide DPA Sensors

Inorganic sensors have targeted the major biomarker of *B. anthracis*, calcium dipicolinate (CaDPA). The biomarker accounts for between 5 and 15% of the endospore by mass, thereby making it a perfect candidate for sensing. The first recorded use of DPA as sensor for trivalent terbium.⁷⁷ Despite this, it was a further 22 years before it was realised that the application could be reversed to provide a highly sensitive disclosure agent for bacterial endospores.⁷⁸ Following this realization there was an explosion of research in this area.^{66,79,80} Cable *et al.* explored the use of chelating ligands (see Figure 1.9) which increased the quantum yield as a result of water exclusion which causes non-radiative quenching.⁸¹ As DPA absorbs UV light a non-radiative energy transfer from the ligand to the Tb³⁺ ion.

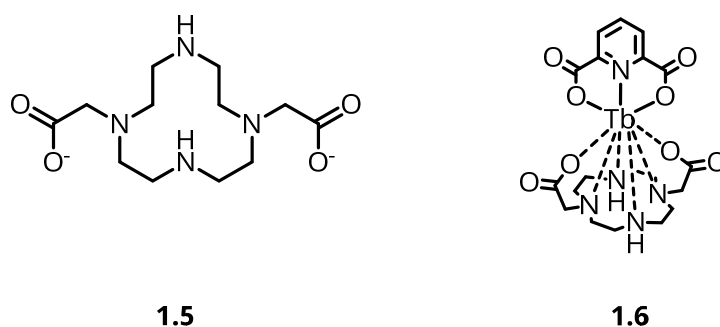


Figure 1.9: Terbium based DPA detector with associated ligand utilised by Cable *et al.*⁸¹

This research approach continues today with significant developments made by incorporating nano-materials into the sensors such as gold nano-particles,⁸² terbium

chelated polyfluorene dots⁸³ and many more.⁸⁴⁻⁸⁸ The sensitivity of these sensors has been tuned and are now capable of detection limits as low as 10 pM.⁸⁹ The combination of graphene quantum dots (GQDs) with a Europium trivalent cation via a covalently coupled EDTA ligand made this sensor capable of fast response times as low as 5.2 seconds.⁸⁹

1.4.2. Organic DPA Sensors

In contrast to the amount of research into inorganic based sensors, there has been relatively very little attention placed on research into organic based *B. anthracis* sensors.

In 2012 Curiel *et al.* published an approach to an organic based DPA sensor shown in Figure 1.10. By targeting the hydrogen bond acceptor nature of the DPA anion and incorporating the fluorescent carbazole moiety they were able to observe a significant change in fluorescence upon DPA binding.

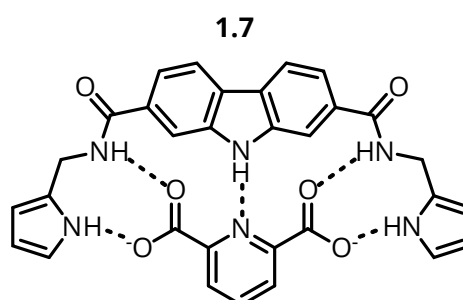


Figure 1.10: Detector developed by Curiel *et al.* showing hydrogen binding to the DPA anion.⁹⁰

Curiel *et al.* showed high selectivity towards the dipicolinate anion over similar structures such as isophthalate. The exceptional binding ability of this detector in DMSO was calculated as more than 10^6 M^{-1} . However, when assessed in a competitive aqueous environment, the association decreased to 35 KM^{-1} (water-acetone (2 % v/v)).

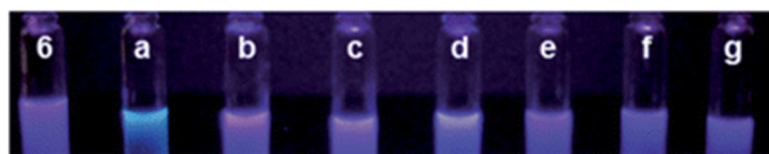


Figure 1.11: Fluorescent response of **1.7** to anions: (a) dipicolinate, (b) phthalate, (c) isophthalate, (d) terephthalate, (e) picolinate, (f) nicotinate and (g) isonicotinate.⁵

⁵ Reproduced from Ref. ⁹⁰ with permission from The Royal Society of Chemistry

1.5. Project Aims and Objectives

The primary aim of this project was to produce a formulation capable of rapid disclosure of surfaces contaminated with *B. anthracis* to enable targeted decontamination similar to FLIR Agentase™ C2 but with BWAs rather than CWAs. This is exemplified in Figure 1.12 where a contaminated surface (left) is sprayed with a formulation that quickly yields a colorimetric response visible to the user (right).

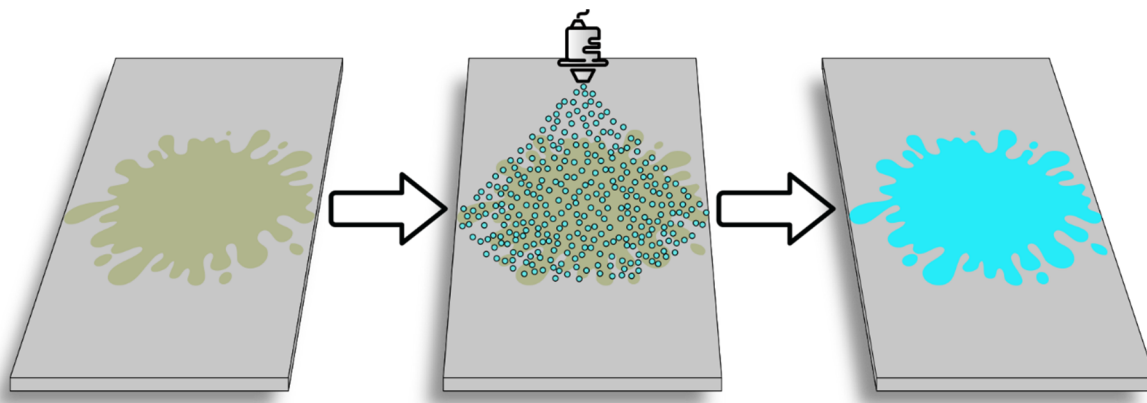


Figure 1.12: Application of disclosure formulation to a contaminated surface and subsequent colorimetric/fluorometric response.

This project is divided into 3 distinct sections of work: i) development of a formulation capable of retaining moisture without restricting germination, ii) synthesis of a disclosure agent capable of indicating the presence of *B. anthracis* and iii) testing products synthesized on a biological simulant to evaluate their use in the field.

Firstly, development of the formulation involves tuning the physical properties of the solution to match the requirements. The solution will need to be non-toxic to ensure the safety of the end-users. High water-solubility will allow for easy dilution on-site which makes distribution and storage much easier. Ideally the endospores will need to be kept moist for a period up to 1 hour to ensure full germination and disclosure. As a result, the water-soluble material will also need to be able to retain high moisture content on a variety of surfaces. Low or minimal cytotoxicity is also important at this stage.

The application of Agentase™ C2 disclosure spray (previously FIDO, see Figure 1.13) produced by FLIR Systems Inc. to a surface contaminated with specific CWAs discloses a threat with a red colorimetric positive response compared to its usual yellow colour.

However, since Agentase™ C2 disclosure spray is sensitive to multiple agents, it can disclose the presence of a threat but not identify the exact nature of the threat. Once the presence of a threat has been identified the specific area of contamination can be sampled and further analysed to give full detection of what agent is present.

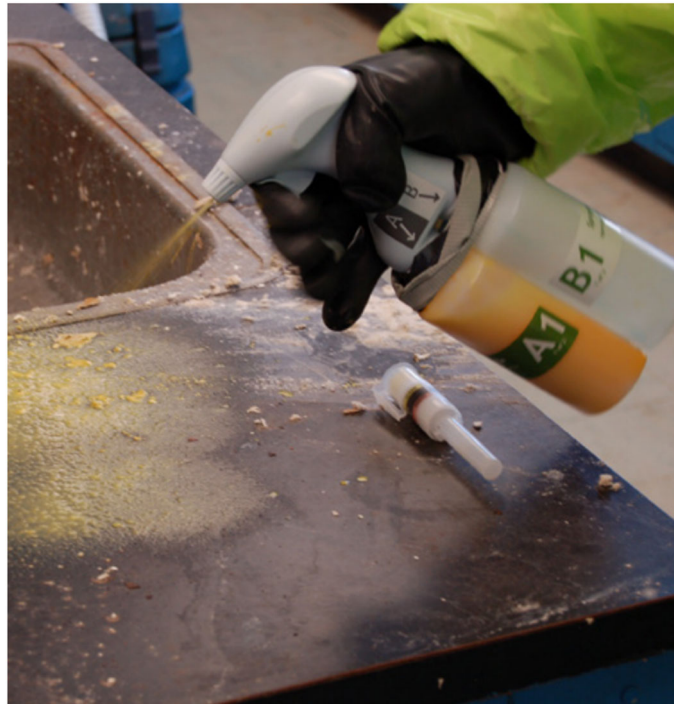


Figure 1.13: Process of application of Agentase™ C2 by FLIR Systems Inc.⁹¹

Analysis of the available options for disclosure of *B. anthracis* suggests the most suitable solution is detection of a biomarker. The DPA biomarker appears to be the strongest candidate because of the high content found in the endospores and its release early in the germination process before metabolic processes are active. However, the most popular method of disclosure of this biomarker involves using heavy metals such as Terbium or Europium. Since the intention is that this product will be freely dispersed in the environment the use of such heavy metals is unacceptable because of their cost and potential toxicity and bioaccumulation.⁹² An alternative to this was to build on work previously conducted by *Curriel et al.*⁹⁰ to determine firstly whether their detector will work in our scenario.

Finally, to determine the effectiveness of the prototype systems targeted in this project, a *B. anthracis* simulant was used. This allowed the *in vitro* determination of the effectiveness of the synthesized materials.

1.6. References

- 1 World Health Organization, *Health Aspects of Chemical and Biological Weapons*, Geneva, 1970.
- 2 Convention on the Prohibition of the Development, Production and Stockpiling of Bacteriological (Biological) and Toxin Weapons and on their Destruction, <http://disarmament.un.org/treaties/t/bwc>, (accessed 22 June 2018).
- 3 S. I. Trevisanato, *Med. Hypotheses*, 2007, **69**, 1371–1374.
- 4 J. I. Martín-Serradilla, A. L. Guerrero-Peral and E. Laherrán, *Med. Hypotheses*, 2008, **71**, 154–155.
- 5 S. Riedel, *Proc. (Bayl. Univ. Med. Cent)*, 2005, **18**, 116–124.
- 6 M. Wheelis, *Emerg. Infect. Dis.*, 2002, **8**, 971–975.
- 7 G. W. Christopher, T. J. Cieslak, J. A. Pavlin and E. M. Eitzen, *JAMA*, 1997, **278**, 412–7.
- 8 H. D. Shukla and S. K. Sharma, *Crit. Rev. Microbiol.*, 2005, **31**, 11–18.
- 9 S. S. Arnon, R. Schechter, T. V Inglesby, D. A. Henderson, J. G. Bartlett, M. S. Ascher, E. Eitzen, A. D. Fine, J. Hauer, M. Layton, S. Lillibridge, M. T. Osterholm, T. O'Toole, G. Parker, T. M. Perl, P. K. Russell, D. L. Swerdlow, K. Tonat and W. G. C. Biodefense, *JAMA-JOURNAL Am. Med. Assoc.*, 2001, **285**, 1059–1070.
- 10 D. M. Gill, *Microbiol. Rev.*, 1982, **46**, 86–94.
- 11 C. Lamanna, *Science*, 1959, **130**, 763–772.
- 12 S. M. Somani and J. A. Romano, *Chemical warfare agents: toxicity at low levels*, CRC Press, 2001.
- 13 N. J. Beeching, D. A. B. Dance, A. R. O. Miller and R. C. Spencer, *BMJ Br. Med. J.*, 2002, **324**, 336–339.
- 14 L. Rose, B. Jensen, A. Peterson, S. N. Banerjee and M. J. Arduino, *Emerg. Infect. Dis. J.*, 2004, **10**, 1023.
- 15 Microbiol - CLED AGAR, <http://www.microbiol.it/en/p-223-cled-agar.html>, (accessed 22 September 2018).

- 16 Z. Lojda, *Histochemie*, 1970, **22**, 347–361.
- 17 A. H. Bishop and C. V Robinson, *J. Appl. Microbiol.*, 2014, **117**, 654–662.
- 18 National Research Council, in *Chemical and Biological Terrorism: Research and Development to Improve Civilian Medical Response*, 1999, pp. 78–96.
- 19 R. M. Atlas, *Bioscience*, 1999, **49**, 465–477.
- 20 The Royal Society, *Measures for controlling the threat from biological weapons*, 2000.
- 21 R. M. Atlas, *ASM News*, 1998, **64**, 383–389.
- 22 J. M. S. Bartlett and D. Stirling, in *PCR Protocols*, Humana Press, New Jersey, 2003, pp. 3–6.
- 23 C. A. Bell, J. R. Uhl, T. L. Hadfield, J. C. David, R. F. Meyer, T. F. Smith and F. R. Cockerill, *J. Clin. Microbiol.*, 2002.
- 24 B. Liedberg, C. Nylander and I. Lunström, *Sensors and Actuators*, 1983, **4**, 299–304.
- 25 N. Ghosh, N. Gupta, G. Gupta, M. Boopathi, V. Pal and A. K. Goel, *Diagn. Microbiol. Infect. Dis.*, 2013, **77**, 14–19.
- 26 N. Ghosh, G. Gupta, M. Boopathi, V. Pal, A. K. Singh, N. Gopalan and A. K. Goel, *INDIAN J. Microbiol.*, 2013, **53**, 48–55.
- 27 H. Im, J. N. Sutherland, J. A. Maynard and S.-H. Oh, *Anal. Chem.*, 2012, **84**, 1941–1947.
- 28 B. A. Adducci, H. A. Gruszewski, P. A. Khatibi and D. G. Schmale, *Biosens. Bioelectron.*, 2016, **78**, 160–166.
- 29 S. Chanteau, L. Rahalison, L. Ralafiarisoa, J. Foulon, M. Ratsitorahina, L. Ratsifasoamanana, E. Carniel and F. Nato, *Lancet*, 2003, **361**, 211–216.
- 30 Y. Du, R. Rosqvist and A. Forsberg, *Infect. Immun.*, 2002, **70**, 1453–60.
- 31 Biothreat Detection IMASS™ Device for rapid testing incidents., <http://www.bbidedetection.com/products/biothreat-detection-imass-device/>, (accessed 16 September 2018).
- 32 Y. Fujinami, M. Kataoka, K. Matsushita, H. Sekiguchi, T. Itoi, K. Tsuge and Y. Seto, *J. Heal. Sci.*, 2004, **50**, 126–132.

- 33 S.-Å. Fredriksson, A. G. Hulst, E. Artursson, A. L. de Jong, C. Nilsson and B. L. M. van Baar, *Anal. Chem.*, 2005, **77**, 1545–1555.
- 34 B. L. van Baar, A. G. Hulst and E. R. Wils, *Toxicon*, 1999, **37**, 85–108.
- 35 H. B. Hines, F. Lebeda, M. Hale and E. E. Brueggemann, *Appl. Environ. Microbiol.*, 2005, **71**, 4478–4486.
- 36 F. Becher, E. Duriez, H. Volland, J. C. Tabet and E. Ezan, *Anal. Chem.*, 2007, **79**, 659–665.
- 37 P. Mouser, M. S. Filigenzi, B. Puschner, V. Johnson, M. A. Miller and S. B. Hooser, *J. Vet. Diagnostic Investig.*, 2007, **19**, 216–220.
- 38 D. H. Na, C. K. Cho, Y. S. Youn, Y. Choi, K. R. Lee, S. D. Yoo and K. C. Lee, *Toxicon*, 2004, **43**, 329–335.
- 39 S. M. Darby, M. L. Miller and R. O. Allen, *J. Forensic Sci.*, 2001, **46**, 1033–42.
- 40 S. G. Ler, F. K. Lee and P. Gopalakrishnakone, *J. Chromatogr. A*, 2006, **1133**, 1–12.
- 41 W. F. Klietmann and K. L. Ruoff, *Clin. Microbiol. Rev.*, 2001, **14**, 364–381.
- 42 D. Thavaselvam and R. Vijayaraghavan, *J. Pharm. Bioallied Sci.*, 2010, **2**, 179–188.
- 43 R. J. Manchee, M. G. Broster, J. Melling, R. M. Henstridge and A. J. Stagg, *Nature*, 1981, **294**, 254–255.
- 44 G. J. Martin and A. M. Friedlander, in *Mandell, Douglas, and Bennett's Principles and Practice of Infectious Diseases*, eds. J. E. Bennett, R. Dolin and D. Blaser, Saunders, Philadelphia, 8th edn., 2015, pp. 2391–2409.
- 45 J. E. Thwaite and H. S. Atkins, in *Medical Microbiology*, eds. D. Greenwood, M. Barer, R. Slack and W. Irving, Churchill Livingstone, Edinburgh, 18th edn., 2012, pp. 237–244.
- 46 C. J. Hilmas, A. M. Katos, P. T. Williams and J. Anderson, in *Handbook of Toxicology of Chemical Warfare Agents*, ed. R. Gupta, Academic Press, San Diego, 1st edn., 2009, pp. 433–459.
- 47 D. P. Clark and N. J. Pazdernik, in *Biotechnology*, eds. D. P. Clark and N. Pazdernik,

- Academic Cell, Boston, 2nd edn., 2016, pp. 687–719.
- 48 Britain's 'Anthrax Island', <http://news.bbc.co.uk/1/hi/scotland/1457035.stm>, (accessed 5 July 2018).
- 49 G. S. Pearson, *ASA Newsl.*, 1990, **01-5**, 86–86.
- 50 E. A. Willis, *Med. Confl. Surviv.*, 2002, **18**, 199–211.
- 51 P. Aldhous, *Nature*, 1990, **344**, 801–801.
- 52 R. C. Spencer, *J. Clin. Pathol.*, 2003, **56**, 182–187.
- 53 M. Meselson, J. Guillemin, M. Hugh-Jones, A. Langmuir, I. Popova, A. Shelokov and O. Yampolskaya, *Science*, 1994, **266**, 1202–1208.
- 54 B. H. Rosenberg, *J. Bioterror. Biodef.*, 2013, 1–8.
- 55 R. Pita and R. Gunaratna, *Int. J. Intell. CounterIntelligence*, 2010, **23**, 61–103.
- 56 D. A. Rasko, P. L. Worsham, T. G. Abshire, S. T. Stanley, J. D. Bannan, M. R. Wilson, R. J. Langham, R. S. Decker, L. Jiang, T. D. Read, A. M. Phillippy, S. L. Salzberg, M. Pop, M. N. Van Ert, L. J. Kenefic, P. S. Keim, C. M. Fraser-Liggett and J. Ravel, in *Proceedings of the National Academy of Sciences*, 2010, pp. 1–6.
- 57 S. P. Velsko, J. J. Osburn, S. K. Sharma and J. D. Ashley, *Electrophoresis*, 2017, **39**, 386–393.
- 58 US orders anthrax review after more live shipments discovered, <http://www.bbc.co.uk/news/world-us-canada-32941062>, (accessed 29 June 2015).
- 59 Drug user dies after anthrax infection, <http://www.theguardian.com/world/2013/mar/08/drug-user-dies-anthrax-infection>, (accessed 29 June 2015).
- 60 J. Jiang, B. L. Pentelute, R. J. Collier and Z. H. Zhou, *Nature*, 2015, **521**, 545–549.
- 61 M. Tarini, P. Cignoni and C. Montani, *IEEE Trans. Vis. Comput. Graph.*, 2006, **12**, 1237–1244.
- 62 J. A. T. Young and R. J. Collier, *Annu. Rev. Biochem.*, 2007, **76**, 243–265.
- 63 S. H. Leppla, *Proc. Natl. Acad. Sci.*, 1982, **79**, 3162–3166.

- 64 M. Wilson, R. McNab and B. Henderson, *Bacterial Disease Mechanisms: An Introduction to Cellular Microbiology*, 2002.
- 65 J. M. Willey, L. M. Sherwood and C. J. Woolverton, *Prescott's Microbiology*, McGraw-Hill Education, New York, 2014.
- 66 A. A. Hindle and E. A. H. Hall, *Analyst*, 1999, **124**, 1599–1604.
- 67 A. Moir, *J. Appl. Microbiol.*, 2006, **101**, 526–530.
- 68 G. Balassa, P. Milhaud, E. Raulet, M. T. Silva and J. C. F. Sousa, *J. Gen. Microbiol.*, 1979, **110**, 365–379.
- 69 W. L. Nicholson, N. Munakata, G. Horneck, H. J. Melosh and P. Setlow, *Microbiol. Mol. Biol. Rev.*, 2000, **64**, 548–572.
- 70 A. Driks, *Microbiol. Mol. Biol. Rev.*, 1999, **63**, 1–20.
- 71 J. Errington, *Nat. Rev. Microbiol.*, 2003, **1**, 117–126.
- 72 P. Stragier and R. Losick, *Annu. Rev. Genet.*, 1996, **30**, 297–341.
- 73 M. Paidhungat and P. Setlow, in *Bacillus subtilis and Its Closest Relatives*, American Society of Microbiology, 2002, pp. 537–548.
- 74 P. Setlow, *Curr. Opin. Microbiol.*, 2003, **6**, 550–556.
- 75 P. T. McKenney, A. Driks and P. Eichenberger, *Nat. Rev. Microbiol.*, 2013, **11**, 33–44.
- 76 P. Setlow, *J. Appl. Microbiol.*, 2006, **101**, 514–525.
- 77 T. D. Barela and A. D. Sherry, *Anal. Biochem.*, 1976, **71**, 351–352.
- 78 D. L. Rosen, C. Sharpless and L. B. McGown, *Anal. Chem.*, 1997, **69**, 1082–1085.
- 79 D. L. Rosen, *Rev. Anal. Chem.*, 1999, **18**, 1–22.
- 80 N. Arnaud, E. Vaquer and J. Georges, *Analyst*, 1998, **123**, 261–265.
- 81 M. L. Cable, J. P. Kirby, K. Sorasaene, H. B. Gray and A. Ponce, *J. Am. Chem. Soc.*, 2007, **129**, 1474–1475.
- 82 M. Zeng, F. Liu, D. Hu, J. Hao, P. Li, L. Wang, Z. Huang and Y. Song, *Anal. Methods*, 2016, **8**, 3892–3898.

- 83 Q. Li, K. Sun, K. Chang, J. Yu, D. T. Chiu, C. Wu and W. Qin, *Anal. Chem.*, 2013, **85**, 9087–9091.
- 84 Y. Zhang, B. Li, H. Ma, L. Zhang and Y. Zheng, *Biosens. Bioelectron.*, 2016, **85**, 287–293.
- 85 Y. Song, J. Chen, D. Hu, F. Liu, P. Li, H. Li, S. Chen, H. Tan and L. Wang, *Sensors Actuators B Chem.*, 2015, **221**, 586–592.
- 86 Y. Wang, Y. Li, W. Qi and Y. Song, *Chem. Commun.*, 2015, **51**, 11022–11025.
- 87 J. Xu, X. Shen, L. Jia, C. Zhang, T. Ma, T. Zhou, T. Zhu, Z. Xu, J. Cao, B. Liu, N. Bi, L. Liu and Y. Li, *Dye. Pigment.*, 2018, **148**, 44–51.
- 88 W. J. Rieter, K. M. L. Taylor and W. Lin, *J. Am. Chem. Soc.*, 2007, **129**, 9852–9853.
- 89 J. Ryu, E. Lee, K. Lee and J. Jang, *J. Mater. Chem. B*, 2015, **3**, 4865–4870.
- 90 D. Curiel, G. Sánchez, M. Más-Montoya, A. Tárraga and P. Molina, *Analyst*, 2012, **137**, 5499.
- 91 Linking Enzyme Detection with Mobile GC/MS Analysis, http://www.flir.co.uk/uploadedFiles/flirGS/Threat_Detection/Chemical_Detection/Mass_Spectrometry/Products/Griffin/Griffin_400/Enzyme-GCMS_AppNote.pdf, (accessed 25 June 2018).
- 92 P. Babula, V. Adam, R. Opatrilova, J. Zehnalek, L. Havel and R. Kizek, *Environ. Chem. Lett.*, 2008, **6**, 189–213.

Chapter 2

Gels and Polyols for *Bacillus anthracis* endospore germination

2.1. Introduction

The environment required to encourage germination of the endospores combined with the unique usage of the final formulation of the desired disclosure system led to a selection of desired chemical, physical and optical properties for the formulation. Humidity is a major factor in endospore germination, and thus the polymer needs to be highly hygroscopic and water soluble.¹⁻³ As a result of the nature of the application, by spray dispersal in the field, care must be taken regarding the potential environmental persistence to ensure that usage does not contaminate land or water supplies. The requirement for a colourimetric response from the disclosure agent necessitates the avoidance of chemical structures that could interfere with this optical property and leads to chemistries that avoid conjugated planar or aromatic systems, which are known to impart strong colours.^{4,5} This selection process decreases the selection to the employment of aliphatic polymers in the disclosure system.

2.1.1. Hydrogelators

Molecular hydrogels represent a potential solution to the formulation issue highlighted in the Project Aims and Objectives section of this thesis (see Chapter 1.5). These materials are found widely in nature in the form of proteins and polysaccharides such as gelatine, agarose and pectin. However, it is much more common in the present day to encounter these materials in synthetic products where their viscoelastic characteristics are particularly desirable. The formation of extended three-dimensional networks throughout a solvent is the foundation of a gel system. In the case of agarose these three-dimensional structures take the form of helical fibrils which aggregate into superhelices with radii of 20-30 nm. These chains are typically made of approximately 800 galactose sugar residues (see Figure 2.1).⁶

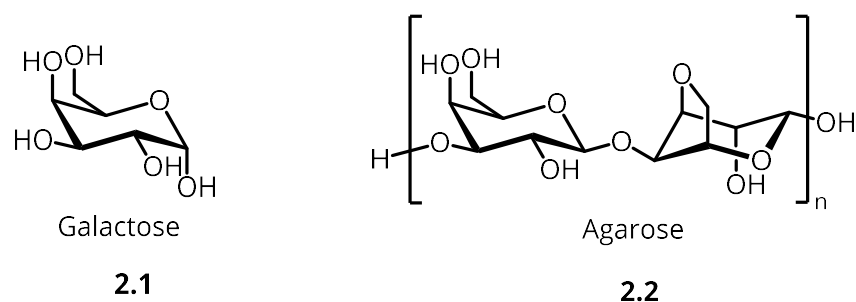
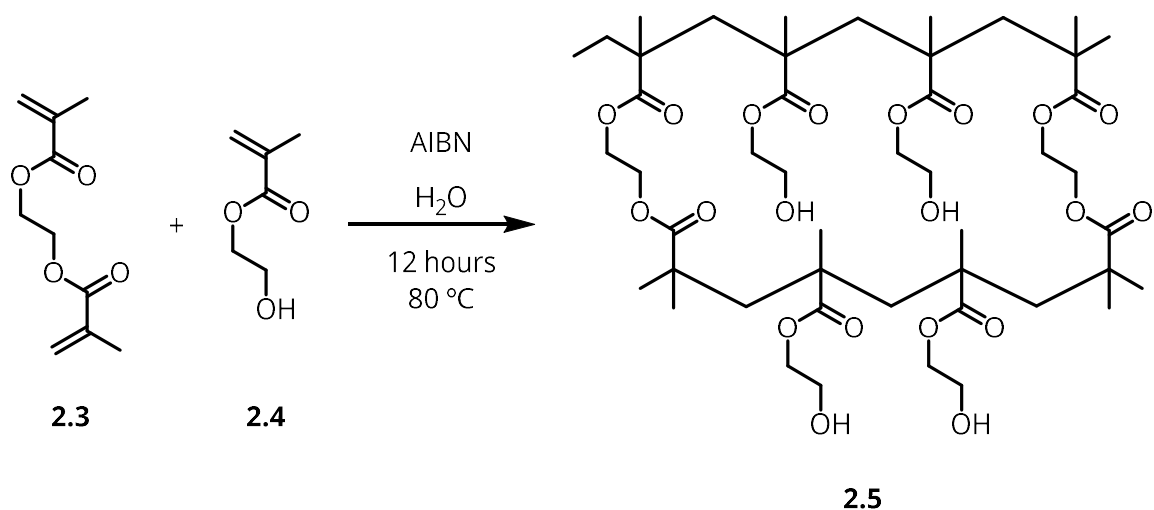


Figure 2.1: Skeletal chemical structures of D-Galactose and Agarose.

In contrast, synthetic polymeric hydrogels have been prepared by addition of crosslinking materials to linear polyols (see Scheme 2.1). One of the earliest examples of this type of material is the polymerisation of (2-hydroxyethyl) methacrylate (HEMA, **2.3**) and ethylene glycol dimethacrylate (EGDMA, **2.4**).⁷



Scheme 2.1: Polymerisation of HEMA and EGDMA.⁸

Hydrogels, both natural and synthetic in origin, have been used for a variety of medical and cellular applications from drug delivery to stem cell scaffolds.⁹ Agar, for example, has been a staple of the modern microbiology laboratory since its first use by Hesse in 1882.¹⁰ An alternative to the macromolecular gelator systems discussed above are materials known as supramolecular hydrogelators. The first material of this kind was thought to be discovered in 1841 by Lipowitz.¹¹ While experimenting with mixtures of uric acid and basic salts Lipowitz observed the formation of a hydrogel. This type of material was neglected until the late 1900s when interest grew after the award of the Nobel prize in Chemistry in 1987 to Cram, Lehn and Pedersen for their seminal studies on supramolecular structures.¹²⁻¹⁴

Many supramolecular gelators are capable of selective gelation in appropriate solvents by means of an induced stimulus. These so-called stimuli responsive gelators are ideal for the method of application for the disclosure system targeted in this study. They can be applied to a surface in the sol state and converted rapidly to the gel once deposited. These types of gelator typically also fall into the category of low molecular weight gelators (LMWG). LMWGs, as opposed to their polymeric counterparts rely on more complex intermolecular interactions to form the rigid structure of the gel rather than steric interactions. A subset of these compounds is a group commonly referred to as 'supergelators' which are capable of forming stable gels at concentrations below 1 wt%.¹⁵ There are numerous examples of LMWG reported in the literature, especially those which are based around moieties prone to hydrogen-bonding such as the urea group.^{16,17} The complementary hydrogen bond donor and acceptor groups present in the urea allows the formation of a linear one dimensional structure (Figure 2.2).

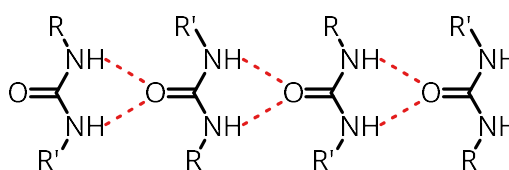


Figure 2.2: Example of supramolecular urea binding motif.

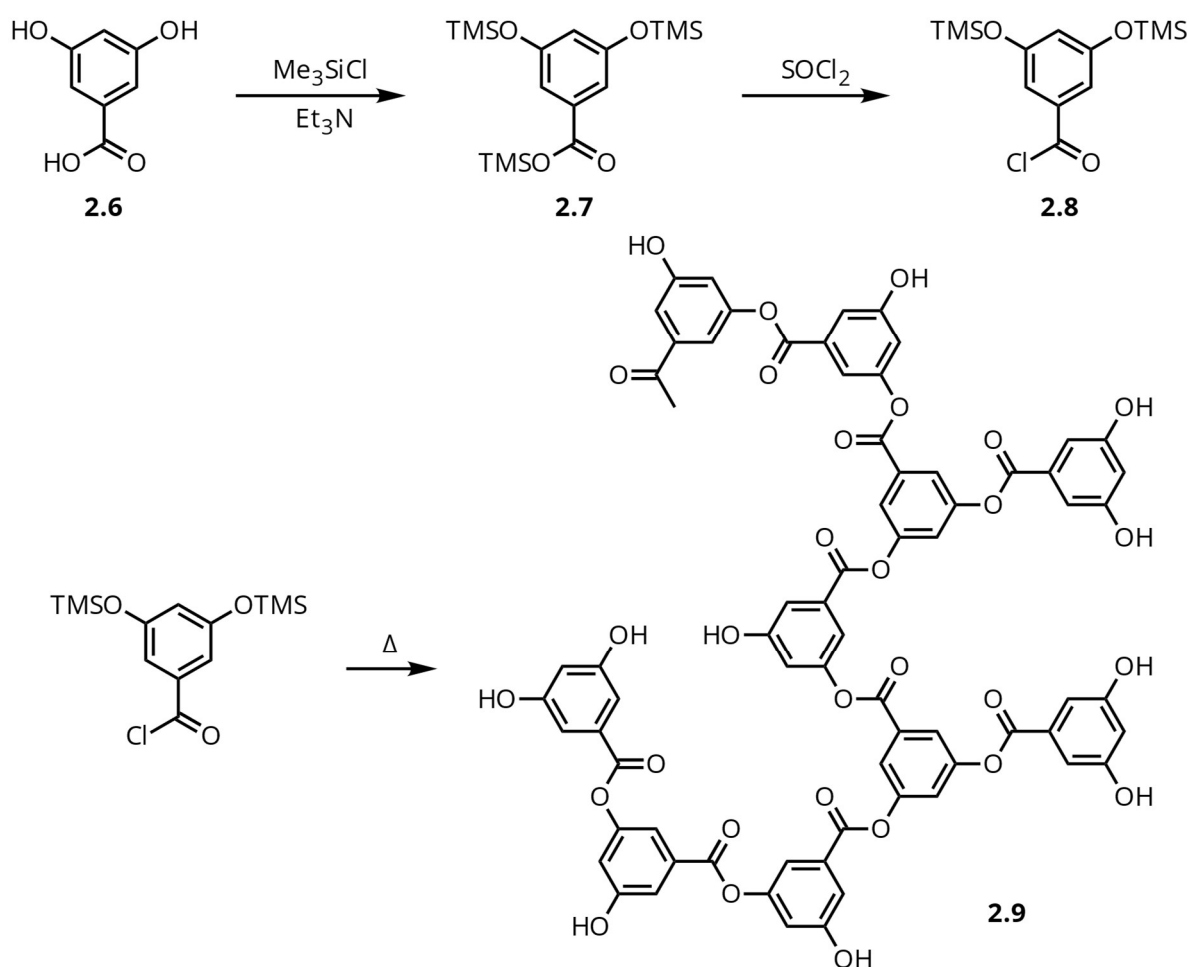
The relatively weak interaction between individual molecules and their low mass of typically less than 1000 Da allows for tuning of the gelation criteria.¹⁸ Stimuli such as UV light, heat, sonication and pH have been used in order to induce gelation.^{19,20}

2.1.2. Polyols

Polyethylene glycol (PEG) polymers have been studied extensively as a result of their biocompatibility and are currently licenced for use as polymer-drug conjugates where the PEG increases drug elimination time. In the context of this study, the non-toxic, non-immunogenic, non-antigenic properties of PEGs reduces concerns should the user come into contact with the disclosure system. High water solubility properties are also very favourable for the desired application as a spray where concentrated solutions could be diluted by the end user.²¹

Despite being proposed by Flory in 1951²² it was not until 27 years later that the morphology of polymers now known as dendritic polymers was initially synthesised by Vögtle *et al.* in 1978.²³ These materials were later studied in depth and optimised by researchers such as Tomalia^{24,25} and Meijer²⁶. At the time these polymers were referred to as ‘cascade molecules’ and were formed by means of a Michael addition of an allyl nitrile to a free amine followed by reduction of the nitrile to another amine.²³ Further studies on these cascade style molecules led to the development of a variety of systems comprising either AB₂ or AB₃ repeat units.^{24,27}

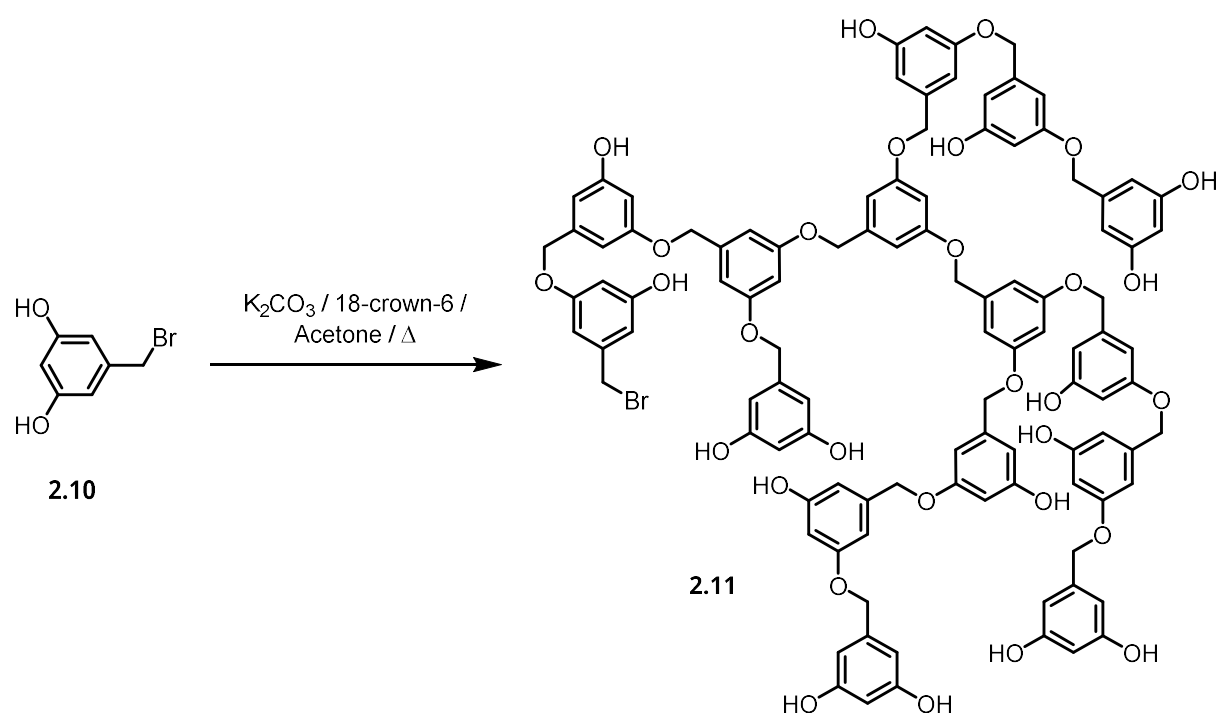
In 1990 Fréchet *et al.* showed the possible one-pot synthesis to hyperbranched polyarylesters (see Scheme 2.2) utilising the thermally labile protecting group trimethylsilyl (TMS). Silyl ether formation of 3,5-hydroxybenzoic acid (**2.6**) followed by conversion of the silyl ester (**2.7**) to an acyl chloride (**2.8**) yields the AB₂ monomer.



Scheme 2.2: Synthesis of AB₂ monomer and subsequent polymerisation of the silyl ether acyl chloride.

Upon heating to temperatures above 190 °C the silyl protecting groups were liberated as trimethylsilyl chloride gas leaving behind the polyester (**2.9**). It was found that higher temperatures yielded lower number average molecular weight (\bar{M}_n) values but the dispersity (\bar{D}_m) was found to be variable from a reasonable 1.9 to 3.8.²⁸

Fréchet *et al.* followed on from this study to develop arylpolyethers using 5-(bromomethyl)-1,3-dihydroxybenzene as the monomer unit. As shown in Scheme 2.3 potassium carbonate was used to deprotonate the acidic phenolic protons which proceed to undergo S_N2 reaction with the bromomethylene from another monomer unit.²⁹ 18-Crown-6 was also used in the reaction to solubilise the potassium salt in order to enhance the efficiency of this process.



Scheme 2.3: Polymerisation of 5-(bromomethyl)-1,3-dihydroxybenzene.

For this project it is preferable to avoid aryl as discussed previously these materials could result in highly coloured material or interfere with the ability of colorimetric and fluorometric sensors to perform. An alternative to these materials is the aliphatic polyester developed by Magnusson *et al.*³⁰ (see Scheme 2.3) The exposure of the monomer 2,2-bis(hydroxymethyl)propionic acid (bis-MPA, **2.12**) to the core unit 1,1,1-tris(hydroxymethyl)propane (**2.13**) in the presence of an acid catalyst such as *p*-toluene sulfonic acid resulted in acid catalysed ester (**2.14**) formation. These materials

were highly branched with a degree of branching of 0.8, much higher than the 0.5 - 0.7 of most literature at the time.

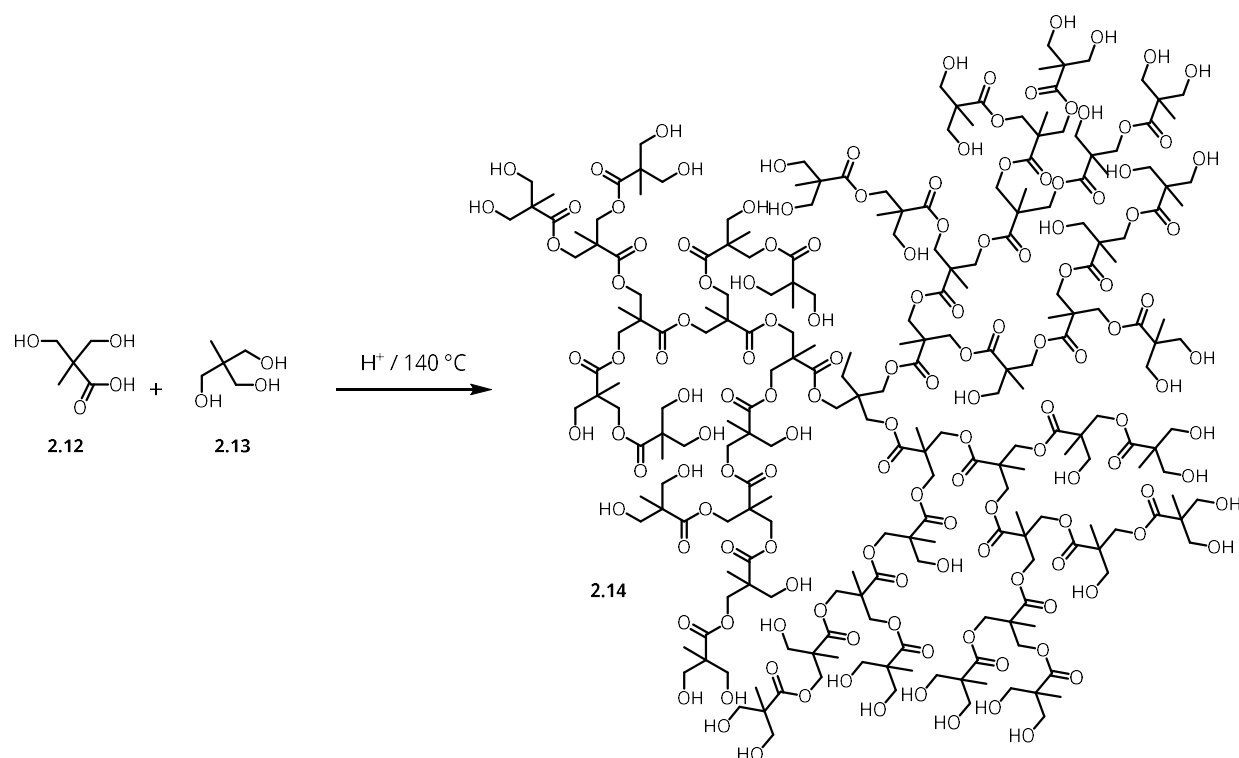


Figure 2.3: Hyperbranched polyesters developed by Hult *et al.*³⁰

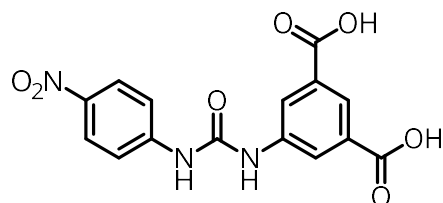
The properties of hyperbranched polymers are particularly favourable for this application, their low viscosity at high molecular weight compared to linear analogues. This allows easy flow of the system over a contaminated area as well as effective surface wetting. The high number of functional groups is desirable as they can be utilised to deliver disclosing or decontamination agents to the required location.³¹

2.2. Results

2.2.1. Hydrogelators

In 2010 Hayes and co-workers published their discovery of a LMWG comprising of a bis-aromatic urea structure (**2.15**)³² shown in Figure 2.4. Attempts were made to investigate and optimise the strength of these gelators by alteration of the type and location of functional groups attached to the phenyl ring.³³ However, structural variations did not afford gelators that could improve upon the very low critical gelation concentration of the *p*-nitro bis-aryl gelator **2.15** of 0.9 mM (0.03 wt%).^{32,34} Fortunately this compound did not

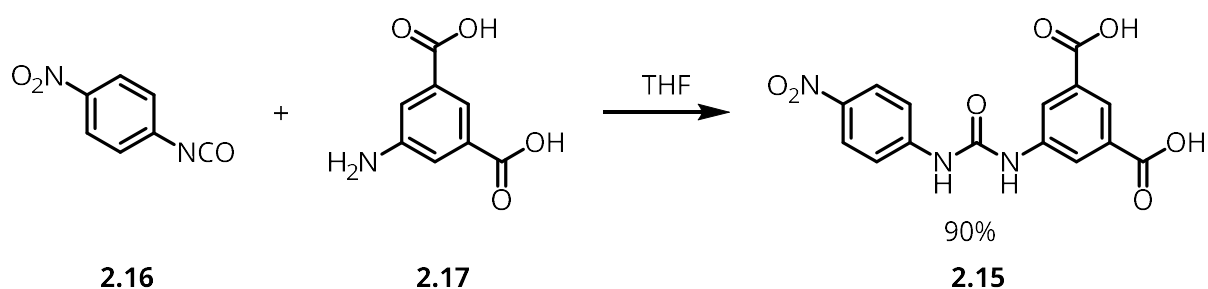
present cytotoxicity properties against a human neuroblastoma cell line at concentrations ranging from 0.1 to 10 μM .³³



2.15

Figure 2.4: Structure of *p*-nitro bis aryl LMWG **2.15**.

The synthesis of **2.15** was carried out using the known procedure previously reported (see Scheme 2.4).³² The rapid coupling of 4-nitrophenyl isocyanate **2.16** and 5-aminoisophthalic acid **2.17** afforded hydrogelator **2.15** in high yield (90%).



Scheme 2.4: Synthesis of hydrogelator **2.15**

The ^1H NMR spectrum of hydrogelator **2.15** (see Figure 2.5) had two singlet resonances at 9.6 and 9.4 ppm, which correlate to the urea nitrogen protons. The greater electron withdrawing nature of the nitro-substituted aromatic results in the observed greater downfield shift of this resonance.

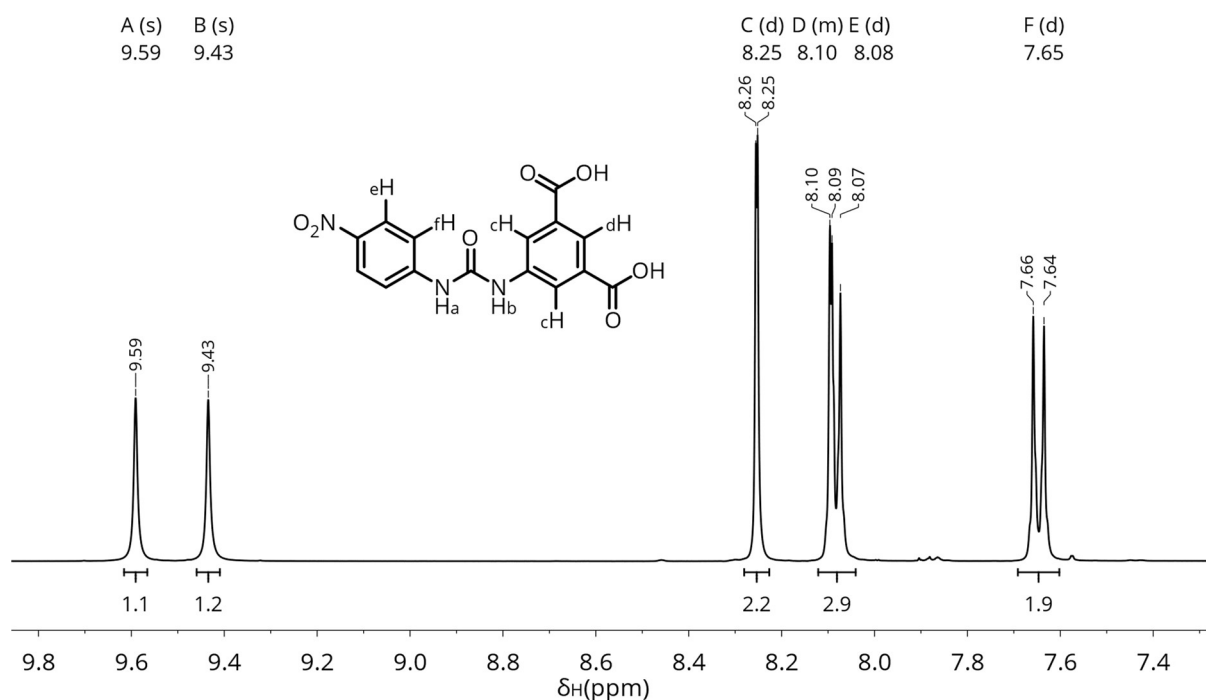


Figure 2.5: ^1H NMR spectrum of **2.15** in DMSO at 295 K.

The hydrogel of **2.15** was formed by dissolving the compound in aqueous sodium hydroxide solution (0.1 M) and then slowly acidified by addition of an equal volume of freshly prepared glucono- δ -lactone solution (0.2 M).³⁵ Gels were prepared at a variety of concentrations and tested by the vial inversion test as shown in Figure 2.6. This is a test employed commonly to show the rigid nature of the gel formed and its ability to hold shape under its own weight.¹⁷



Figure 2.6: a) Structure of glucono- δ -lactone solution. b) Vial inversion test of hydrogelator **2.15** formed using the δ -gluconolactone procedure at different concentrations. (left to right: 0.5, 1, 2, 3, 4, 5 mg mL^{-1}).

The capability of these materials to retain water was assessed by means of a water retention study. The results of this test (Table 2.1) show that in vials the gels retain a large quantity water over the initial 64 hours with loss between 0% and 1%. The experiment was repeated on microscope slides which yielded dramatically different results (see Table 2.2); over 17 hours a 92% of the water was lost. The difference in water retention is thought to be because of the greatly increased surface area combined with decreased shielding that was provided by the walls of the vials initially used.

Vial # \ Hours	0	64	142	475
1	98%	97%	97%	22%
2	98%	97%	97%	22%
3	97%	97%	97%	21%
Average	98±0.0%	97±0.0%	97±0.0%	21±0.1%

Table 2.1: Water retention of gel **2.15** in vials.

Slide # \ Hours	0	17
1	97%	0%
2	97%	7%
3	97%	8%
Average	97±0.1%	5±4%

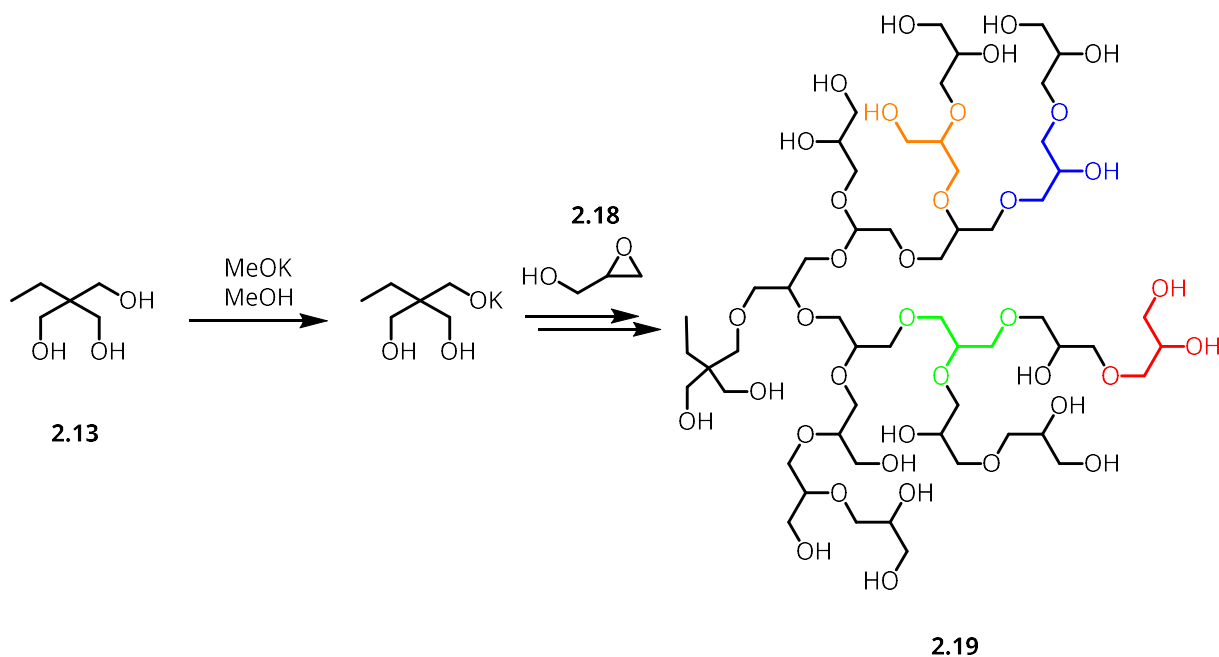
Table 2.2: Water retention of gel **2.15** on glass slides.

These materials were tested for their compatibility with germinating cells as described in depth in Chapter 4.

2.2.2. Hyperbranched Polyglycerol

Following the unsuccessful biological studies conducted on hydrogelator **2.15**, attention was turned to alternative hydrophilic materials that could in theory provide many of the physical properties desired. Following the slow progress since the initial discovery of glycidol polymerisation in 1930 by Rider and Hill,^{36,37} Frey *et al.* in 1999 showed that hyperbranched alkylpolyethers could be accessed by means of anionic ring-opening multibranching polymerisation (ROMBP). Using a method known as slow monomer addition (SMA)³⁸, glycidol was added at a very slow rate to the basic initiator.³⁸ As shown in Scheme 2.5 the alkoxide initiator attacks the epoxide ring of the glycidol (**2.13**). This

forms an ether bond whilst liberating a further alkoxide which can continue the polymerisation. The aliphatic polyethers formed from this synthesis had a number average molecular weight (\bar{M}_n) between 1250 and 6500 and very low dispersity (\mathcal{D}_m) of 1.18 – 1.47. To determine the degree of branching, ^{13}C NMR spectroscopic analysis was employed to identify the different chemical shifts for dendritic, linear 1,3, linear 1,4 and terminal monomer units.³⁸



Scheme 2.5: Polymerisation of glycidol using SMA by Frey *et al.* with highlighted structural units. (red) terminal, (green) dendritic, (orange) linear-1,3 and (blue) linear-1,4.³⁸

To synthesize these materials a similar procedure was used to that of Frey *et al.* with the only modification being the choice of the anion used. The lower cost and greater availability of the sodium methoxide prompted its selection. It was also thought that the sodium methoxide provides the desired deprotonation effect similar to that of potassium methoxide and the use of anhydrous diglyme as a solvent creates an effective dispersion. These materials were initially synthesized by dissolving glycidol in anhydrous diethyl ether and adding this solution to the 95 °C reaction vessel via an addition funnel allowing the residual ether to distil from the vessel as the reaction progressed. This method proved very ineffective as the addition rate was difficult to control and resulted in poor control as a result of variable addition rates. Further practical complications associated with this

process resulted from the variable concentration and temperature as a result of variable distillation rates.

Implementation of the SMA method via syringe pump (see Figure 2.7) led to significantly more repeatable results in good yield (90%). This method yields the clear colourless viscous liquid once neutralized over an Amberlite® IR120 (H) and precipitated twice from methanol into acetone. The final polyglycerol precipitate was then concentrated *in vacuo* and residual solvents were removed by heating to 80 °C at 3 mbar.



Figure 2.7: Mechanical syringe pump used for SMA polymerisation method.

2.2.2.1. Inverse-Gated ^{13}C NMR Spectroscopic analysis.

To determine the degree of polymerisation and branching of these hyperbranched materials an appropriate method to use is a quantitative ^{13}C NMR process known as inverse-gated decoupling. The reasoning behind the use of this specific pulse program is to reduce the enhancement of the signal by the nuclear Overhauser effect (NOE). This effect which is usually beneficial to the collection of standard carbon spectra enhances the signal of proton coupled carbons, as in most molecules carbons relax through the Dipole-Dipole method allowing more complete relaxation of the carbon before re-irradiation. By only switching on proton decoupling during the acquisition phase the build-up of NOE enhancement is greatly reduced (see Figure 2.8). Paramagnetic relaxation agents such as Chromium (III) acetylacetonate can be added to the sample in order to further reduce relaxation. However, these compounds are renowned for increasing line-broadening in acquired spectra. Quaternary carbons are known to possess long relaxation times (T_1). Since the relaxation delay (d_1) is typically set to $5 \times T_1$, the lack of quaternary carbons in polyglycerol allow for more scans in the same period, thereby increasing the signal to noise ratio (S/N).^{39,40}

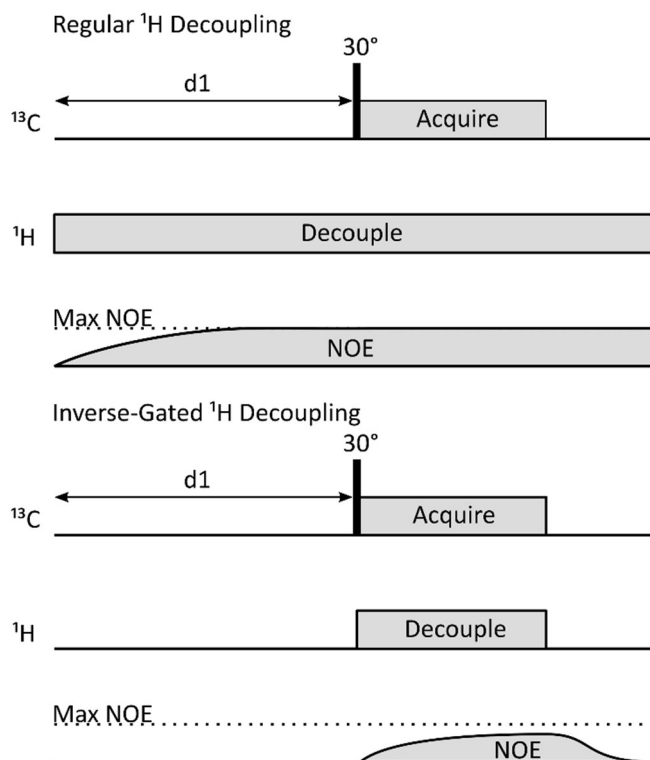


Figure 2.8: Pulse program diagrams for decoupled ^{13}C NMR and inverse-gated decoupling ^{13}C NMR and their respective NOE contributions.

These carbon resonances correlate to distinct structural units within the polymer as characterised by Frey *et al.*³⁸ These units are the linear-1,3, linear-1,4, terminal and dendritic units shown in Figure 2.9. The inverse gated decoupling ^{13}C NMR spectrum of SMA polyglycerol **2.19**_{SMA} affords integrals of the resonances shown in Figure 2.10 that can be used to determine the degree of branching in the polymer. There are two different definitions for the degree of branching the first was defined by Kim (see Equation 2.1) and more recently refined by Frey *et al.* (see Equation 2.2)^{41,42}

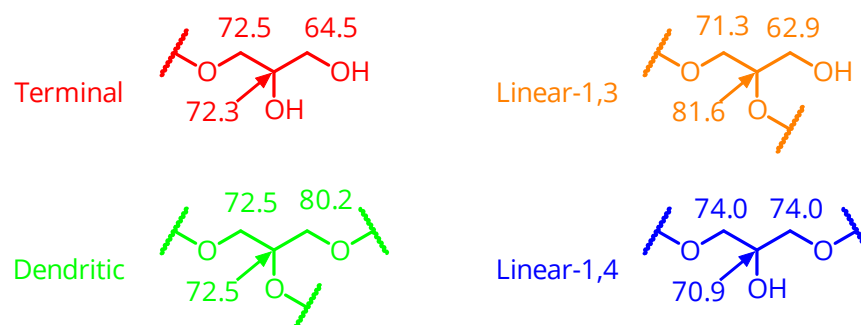


Figure 2.9: The different structural units and associated chemical shifts present in polyglycerol.³⁸

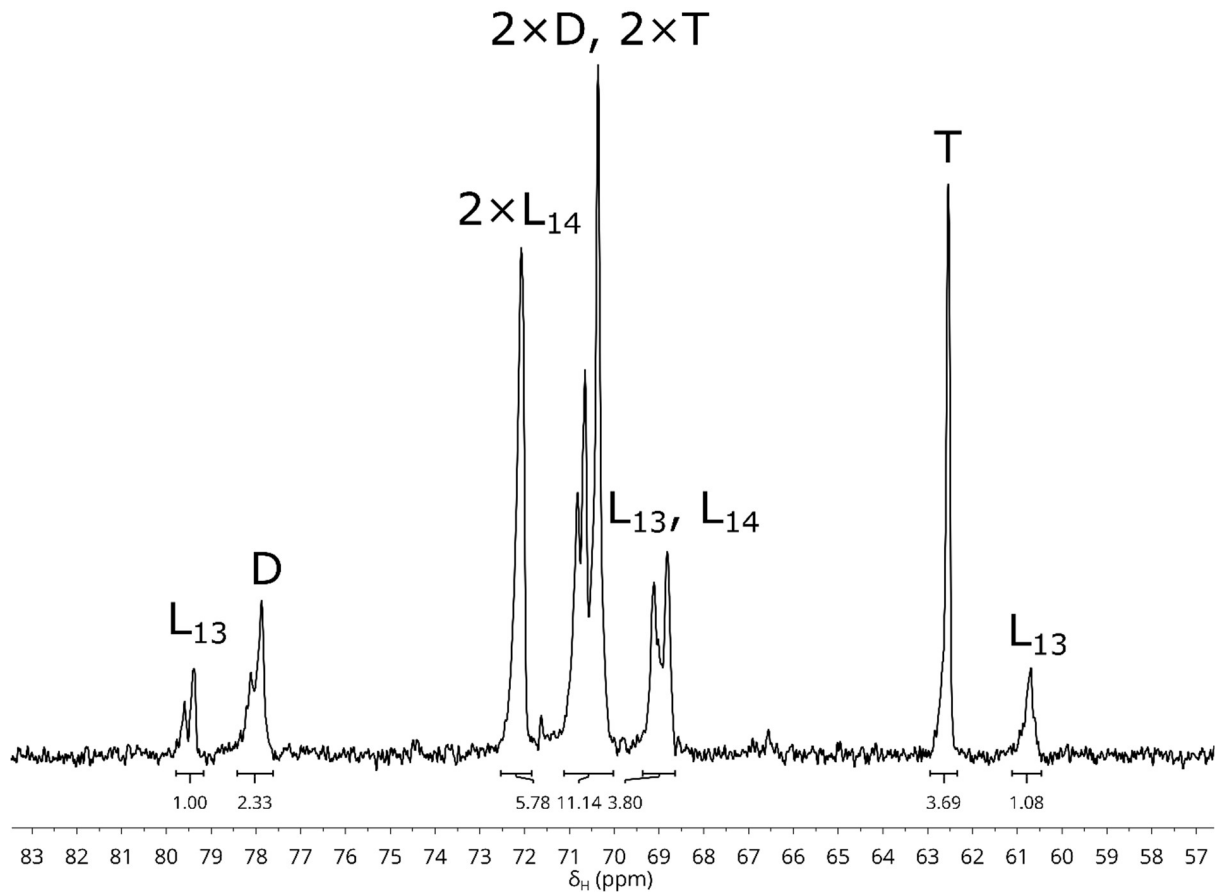


Figure 2.10: Inverse-gated proton decoupled ^{13}C NMR spectra of polyglycerol **2.19**_{SMA} and assigned structural units; D_2O 294K.

$$DB_{kim} = \frac{D + T}{D + T + L_{13} + L_{14}}$$

Equation 2.1: Degree of branching calculation based on ^{13}C NMR spectroscopic analysis as defined by Kim.⁴¹

$$DB_{frey} = \frac{2D}{2D + L_{13} + L_{14}}$$

Equation 2.2: Degree of branching calculation based on ^{13}C NMR spectroscopic analysis as defined by Frey et al.⁴²

Where D = Relative abundance of dendritic units; L_{13} = Relative abundance of Linear-1,3 units; L_{14} = Relative abundance of linear-1,4 units; T = Relative abundance of terminal units. The relative abundance percentages can be resolved by averaging the contributions for each unit from the integral data from the ^{13}C NMR spectra. Using Equation 2.1 and Equation 2.2 with the relative abundances listed in Table 2.3, the values obtained are $DB_{kim} = 0.61$ and $DB_{frey} = 0.55$. The discrepancy between the two values stems from the incorporation of terminal units in Equation 2.1 whereas in Equation 2.2 the terminal units are not counted but dendritic units are counted twice.

Structural Unit	T	L_{13}	L_{14}	D
SMA Relative Abundance	37%	11%	29%	24%

Table 2.3: Relative abundance of structural units based on inverse-gated ^{13}C NMR in polymer **2.19**_{SMA}.

The calculation described by Frey is considered more accurate for higher molecular weight materials. This was noted by Frey *et al.* since the number of dendritic units is equal to the number of terminal units less one, therefore $T = D + 1$. Thus as $D \rightarrow \infty$ it implies that $T \rightarrow \infty$, hence $\frac{D}{T} \rightarrow 1$. This is clearly visible in the $\frac{D}{T}$ ratio for the literature values of polyglycerols (PGly-1 and PGly-4 synthesized by Frey *et al.*) reported by Frey *et al.* shown in Table 2.4.

Structural Unit	\bar{M}_n	T	D	$\frac{D}{T}$ ratio
PGly-1	1245	41%	21%	0.51
PGly-4	6314	32%	28%	0.88

Table 2.4: Comparison of terminal and dendritic units of polyglycerols published by Frey *et al.*³⁸

As well as the degree of branching, the degree of polymerisation (\overline{DP}_n) can be determined using the inverse gated decoupled ^{13}C NMR spectral data. Using Equation 2.3, the calculated \overline{DP}_n for this material was 7.3 giving a monomer/initiator ratio 7:1 which equates to a \bar{M}_n of 588 g mol⁻¹. The term f_c in this equation refers to the functionality of the core initiator. The nature of this method of analysis cannot provide insight into the weight average molecular weight and as such the dispersity cannot be calculated.

$$\overline{DP}_n = \frac{T + L_{13} + L_{14} + D}{T - D} f_c$$

Equation 2.3: Number average degree of polymerisation calculation.

The SMA procedure, while effective, does not permit high throughput or lend itself to scaling and is heavily restricted by the capacity of the syringe pump equipment. In order to probe the necessity of the SMA procedure an alternative method was derived where the glycidol monomer was combined with the initiator in the bulk while maintain the same monomer-initiator ratio to the SMA procedure. This method also allowed for further investigation into the effects of slow monomer addition when using the sodium counter-ion during polymerisation. Unfortunately, since the ring opening process is exothermic this procedure carries a high risk of explosive polymerisation. To mitigate this risk the

temperature of the reaction was slowly increased from ambient over a period of 2 days to 95 °C. Once at this temperature the reaction was continued as described for the SMA product. The appearance of this material differed significantly from that produced via the SMA procedure as is shown in Figure 2.11, the bulk product (**2.19_{BULK}**) possessing a cloudy appearance that became clear upon heating.

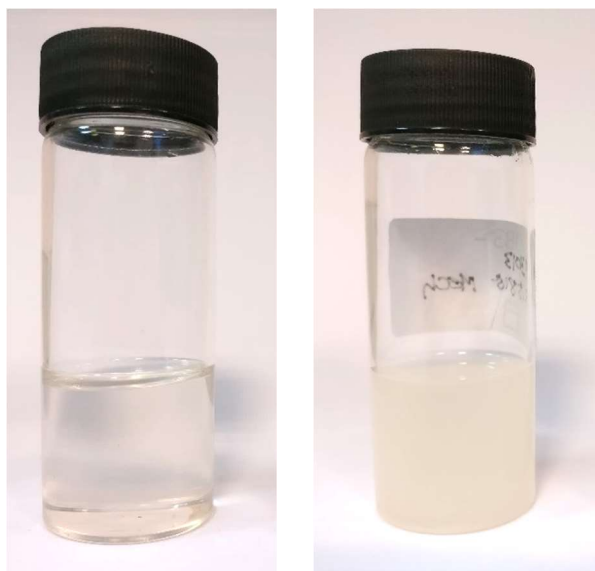


Figure 2.11: Left) Polyglycerol formed by slow monomer addition **2.19_{SMA}**.
Right) Polyglycerol formed by bulk polymerisation **2.19_{BULK}**.

Inverse-gated ^{13}C NMR spectroscopic analysis revealed that the relative abundance of the structural units within the material afforded via the bulk polymerisation approach was dramatically different to that of the material produced using the SMA procedure. In the case of the material afforded via the bulk polymerisation, there was an increased density of linear-1,4 units coupled with a dramatic reduction in the number of dendritic units (see Table 2.5).

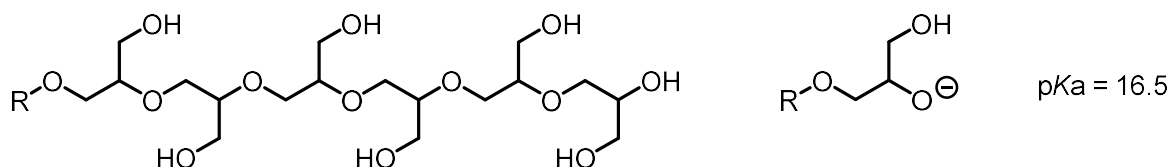
Structural Unit	<i>T</i>	<i>L</i> ₁₃	<i>L</i> ₁₄	<i>D</i>
SMA Relative Abundance	37%	11%	29%	24%
Bulk Relative Abundance	38%	6%	47%	9%

Table 2.5: Relative abundance of structural units based on inverse-gated ^{13}C NMR in the bulk polymer.

It was thought that this difference in structural features could have arisen because of the pKa of the alkoxide favouring the linear-1,4. Once the epoxide undergoes ring opening the resulting secondary alkoxide is slightly more basic than the primary alcohol alternative. The pKa difference of 1 indicates a 10-fold preference for deprotonation of

the primary alcohol. The low temperature also gives the polymer more time to undergo anion exchange to the more thermodynamically favourable product. The dramatic difference between the dendritic and terminal abundances causes significant disparity between the degree of branching equations outlined previously $DB_{kim} = 0.47$ and $DB_{frey} = 0.25$.

Linear 1,3



Linear 1,4

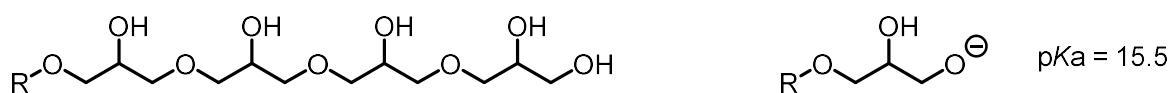


Figure 2.12: Comparison of morphology of linear-1,3 and linear-1,4 chains and their respective anion pKa.

At this point the polyglycerol generated successfully via the SMA procedure was taken forward for biological testing as discussed further in Chapter 4.

2.2.2.2. Gel Permeation Chromatography

To gather further insight into the molecular distribution within the polymer, the use of Gel Permeation Chromatography (GPC) is the most commonly used method for this type of elucidation. It has been noted in the literature that polyglycerols are not analysed easily by this method.³⁸ This is as a result of their extreme branching and interaction with the solvent system. The solvent system and corresponding GPC column is the integral part of this analysis and relies heavily on the polymer not interacting with the column as well as the polymer dissolving fully in the solvent. The solvents available at the time of analysis were tetrahydrofuran (THF) or water. The polyglycerol polymers are insoluble in THF and as such the analysis was carried out in an aqueous environment. The detector originally used for this analysis was a refractive index detector. However, the issue of simply using a refractive index detector against elution volumes is that they are calibrated with linear chain PEG standards. They therefore do not accurately reflect the weights of the comparatively branched structures being analysed. In this case the hyperbranched nature of these polymers restrict their passage through the finer pores of the column resulting

in the reporting of artificially high molecular weights. It was thought that use of a light scattering or viscometer detector would be able to resolve this issue as this method of measurement calculates molecular weight by directly measuring particle size or solution viscosity. However, the common method for calibration of these instruments involves the use of analytical standards that are usually linear polymers. They therefore do not accurately reflect the structure to molecular weight values expected for the hyperbranched materials discussed here. In this case values obtained for the SMA polyglycerol \bar{M}_w ranged from 13000 to 2863000 g mol⁻¹. These values are significantly greater than the values previously derived from the NMR spectroscopic data and as a result of the associated uncertainties with this method of analysis were deemed inaccurate.

2.2.2.3. MALDI-TOF Mass Spectrometric Analysis

An alternative method to GPC analysis that has been used for obtaining molecular weight data on polymers is MALDI-TOF MS. By obtaining individual mass signals and their relative intensities it is possible to determine the \bar{M}_n , \bar{M}_w and \mathcal{D}_m values. This method has been previously utilised for gather the molecular weight data for a variety of materials over a large molecular weight range.⁴³ It is also noted that there is a strong tendency for lower molecular weight materials to perform significantly better in MALDI-TOF MS. This results from the parameters used to ionise the matrix, with high laser powers resulting in increased skew and low laser powers resulting in poor sensitivity and signal distortion.⁴⁴ This manifests as a positive skew of the apparent mass distribution.

The obtained mass spectrum for the SMA polyglycerol (see Figure 2.13) exhibits an extensive positive skew. There is some evidence for this occurring in polyglycerols and the increased presence of this skew could be because of the reactivity of the initiator being less than that of the propagating chain. Therefore, chains that initiate earlier than others can reach higher molecular weights. Combined with the preference for lower molecular weight materials to effectively ionise during MALDI led to the over expression of lower molecular weights.⁴³

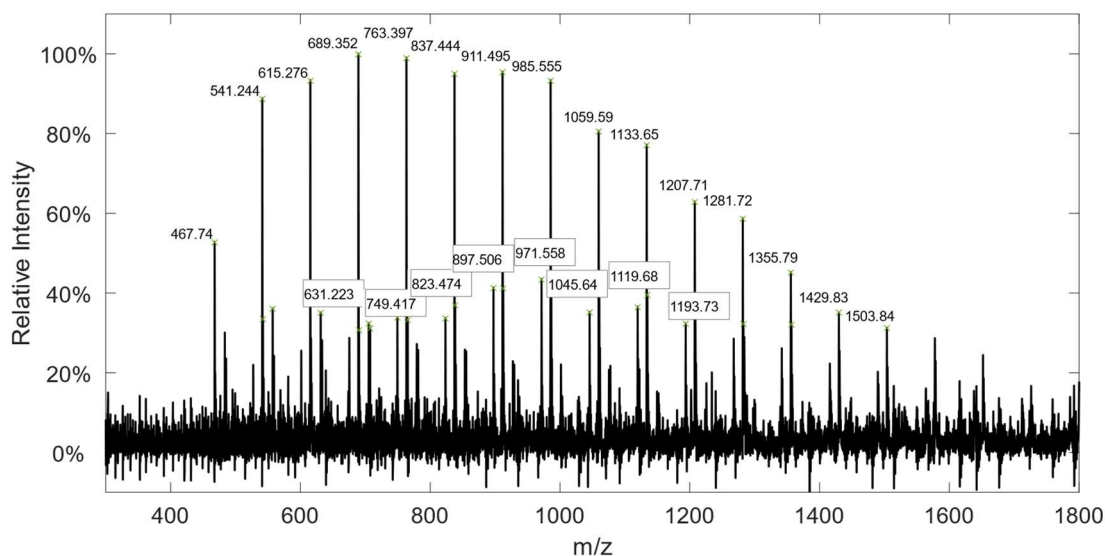


Figure 2.13: MALDI-TOF Mass Spectrum of SMA polyglycerol **2.19_{SMA}** (HCCA matrix).

Unfortunately, the major series in the observed spectrum did not match the expected values for the polyglycerol **2.19_{SMA}**, though the expected values were visible at less than half the relative abundance indicating that the desired hyperbranched polymer was present in the sample.

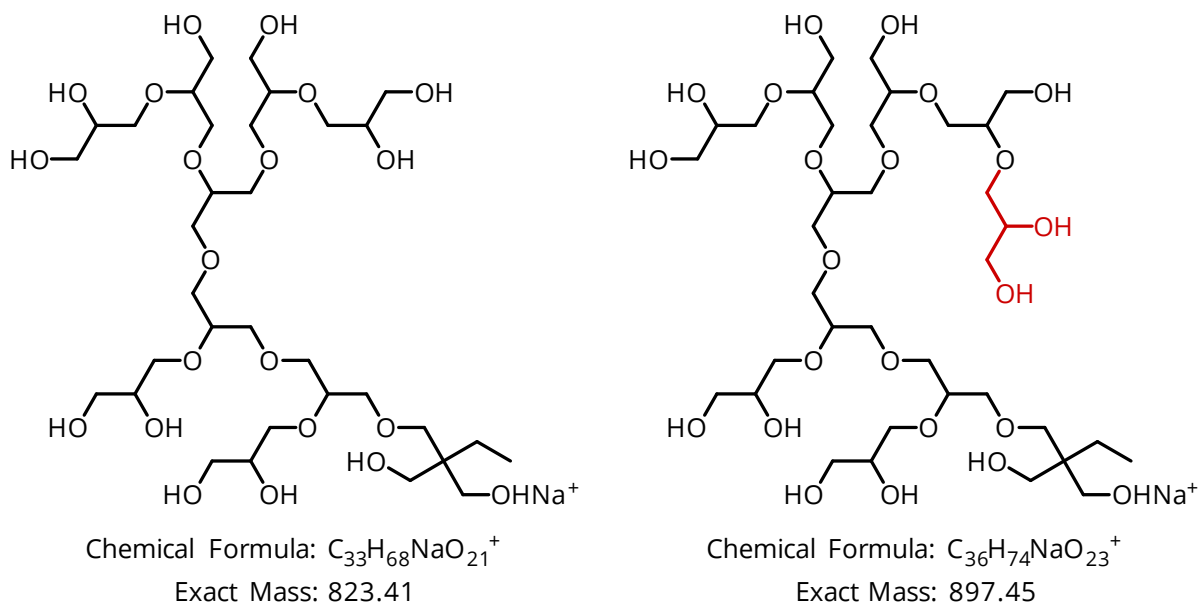


Figure 2.14: Branched structures of SMA polyglycerol with exact masses.

The occurrence of this unknown signal that formed the major series was originally thought to be caused by fragmentation of the polymer causing loss of a mass equal to 134 Da (see Figure 2.15).

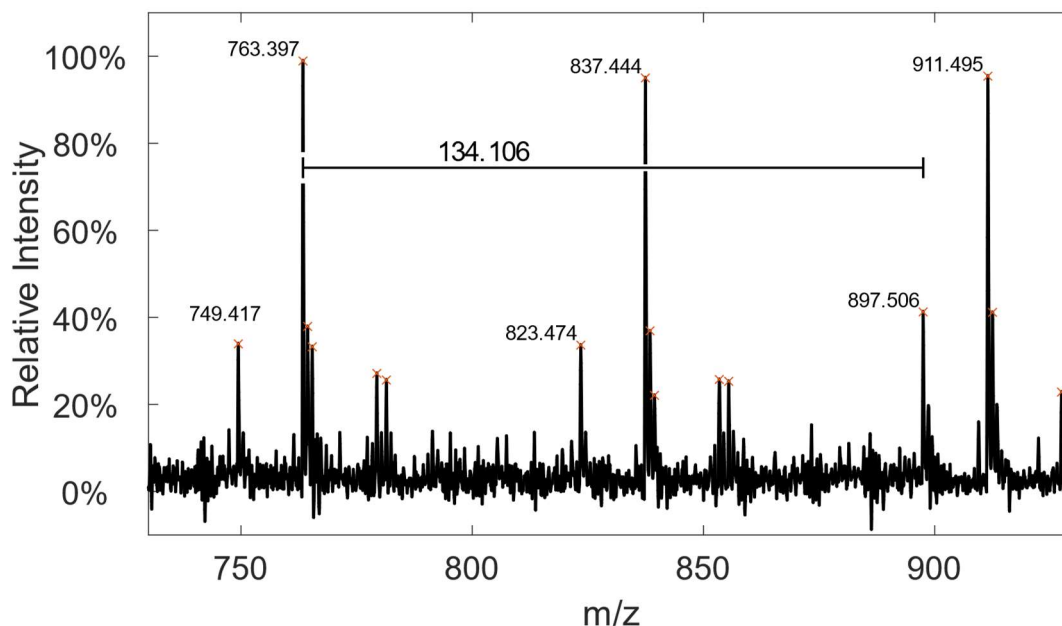


Figure 2.15: MALDI-TOF Mass Spectrum of SMA polyglycerol **2.19_{SMA}** showing the 134 Da shift to the cyclic branched structure (HCCA matrix).

However, on closer inspection it became apparent that these masses correlated exceedingly well with the cyclic products shown in Figure 2.16. While it had been noted originally by Frey *et al.* that it was possible to form these cyclic species from rapid monomer addition the use of the syringe pump was thought to have mitigated this risk. The use of the sodium counterion during the polymerisation could be the significant factor in the formation of this unintended product. It has been previously noted that most polymerisations based on 'ab_n' monomers possess the ability to form cyclic structures.⁴⁵ While the discoveries published by Kricheldorf and Eggerstedt were initially restricted to polyesters, upon further examination it was found that this effect is visible for a wide array of 'ab_n', 'a_n + b_n' and 'a—b' polymers.^{46–48}

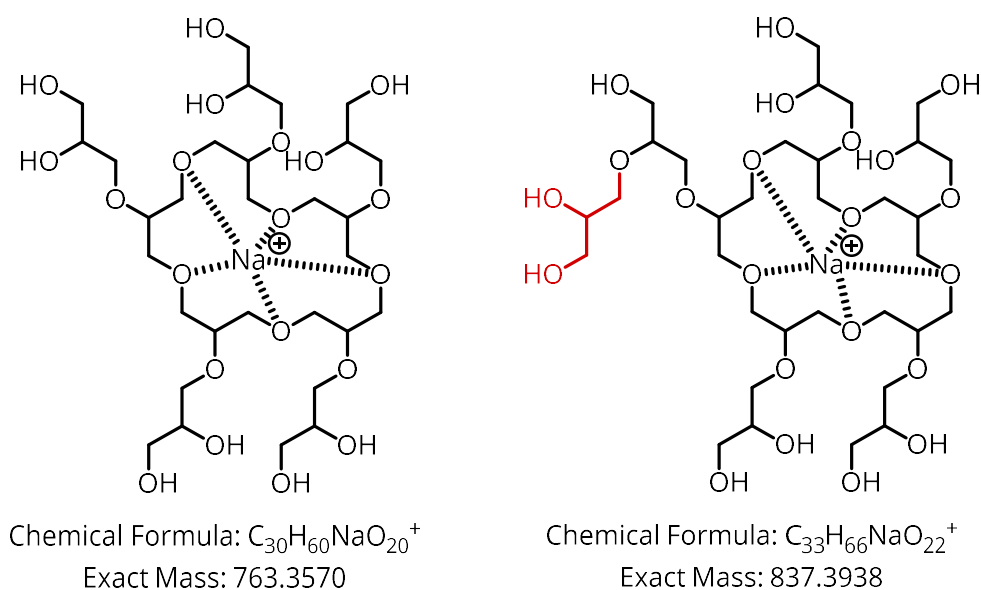


Figure 2.16: Cyclic branched structures of SMA polyglycerol with exact masses.

The known smaller ionic radii of the sodium ion contributes to its harder nature and ensuing slightly lower reactivity (see Figure 2.17).⁴⁹ However, as rapid monomer addition was suggested as a cause it is possible that the lower reactivity of the initiator needs to be countered by further decreasing the addition rate of the glycidol monomer. It has been noted that potassium cations bind more strongly to all sizes of crown ethers than sodium.⁵⁰⁻⁵² The exception to this observation appears to be small crown ethers with 4 oxygens (12C4 – 15C4) where the smallest alkali metals are preferred.⁵³ It has also been found that the smaller concentrated charge of the sodium cation preferentially binds the charged donor groups. Based on these observations it can be postulated that the potassium cations are more effectively chelated by the diethylene glycol dimethyl ether solvent whereas the sodium cation binds more preferentially to the alkoxide active chain end thus encouraging templating and favouring macrocycle formation.^{54,55}

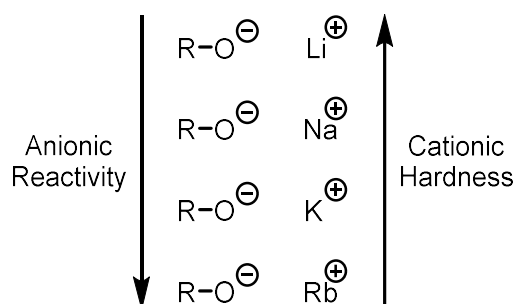


Figure 2.17: Comparison of reactivity of alkoxides based on their associated counterion.⁴⁹

However, despite the formation of these unintended cyclic products biological testing had already been carried out to determine their suitability and found they yielded positive results (discussed in depth in Chapter 4). Ultimately it is not essential for the application targeted that these materials are completely hyperbranched, but this may be an important factor should specific morphologies be desired in the future.

The relative abundances (N_i) of each mass signal (M_i) obtained from the MALDI-TOF mass spectra can be used to calculate the molecular weight values using Equation 2.4 and Equation 2.5.

$$\bar{M}_n = \frac{\sum N_i M_i}{\sum N_i}$$

Equation 2.4: Number average molecular weight

$$\bar{M}_w = \frac{\sum N_i M_i^2}{\sum N_i M_i}$$

Equation 2.5: Weight average molecular weight

The SMA polyglycerol contains cyclic and branched components, however, since these are combined in the material values from the signals of sodium adducts for both morphologies will be considered. The material gives \bar{M}_n of 956.1 Da, an \bar{M}_w of 1051.3 and a \mathcal{D}_m of 1.10. These values are significantly closer to the values obtained *via* NMR compared to those obtained *via* GPC corroborating the evidence in support of these masses. However, the bulk polyglycerol **2.19**_{BULK} exhibits no formation of the hyperbranched structure as is shown in Figure 2.18 by the sole presence of the sodium and potassium adducts of the cyclic systems. Using the sodium adduct masses, the values for \bar{M}_n , \bar{M}_w and \mathcal{D}_m were found to be 809.0 Da, 1000.0 Da and 1.24 respectively which are similar to those found for the SMA polyglycerol. The higher presence of cyclic structures within the bulk polymerised material is most likely a result of the lower reaction temperatures and extended reaction time combined with the templating effect noted previously.⁵⁶ The low temperatures reduce the reaction rate allowing the competing proton transfer process to become more significant resulting in greater prevalence of the cyclic structures.

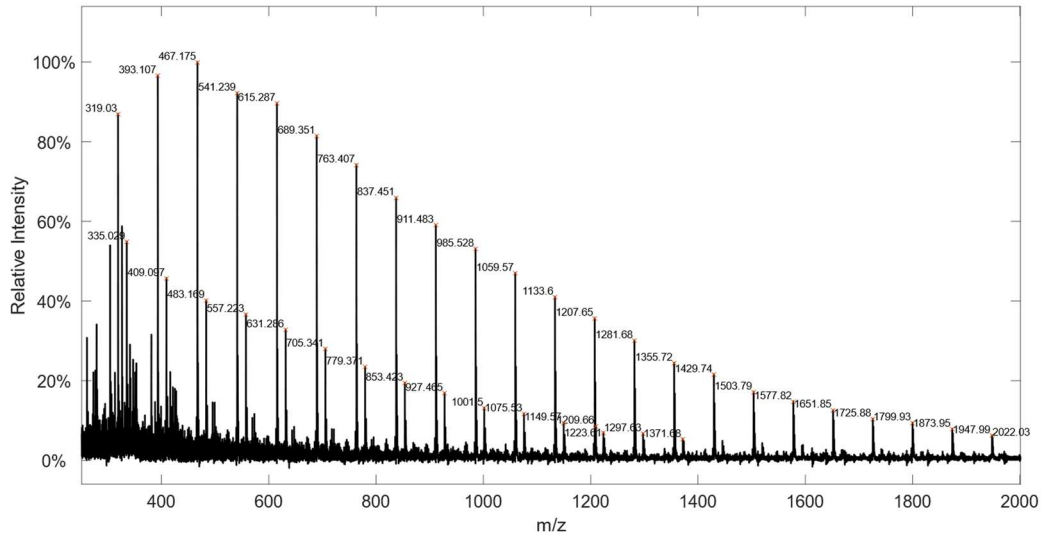


Figure 2.18: MALDI-TOF mass spectrum of cyclic structures of bulk polyglycerol.

2.2.2.4. Viscometry

Unlike the hydrogels presented earlier, the polyglycerols described here do not exhibit a sol-gel transition under the concentration regimes used in these studies. Their capability to reduce evaporative loss and adhere to a surface stems from the number of branched pendant hydroxyl groups. A distinctive side-effect from these branched functionalities is their ability to form intermolecular hydrogen bonds and chain entanglement resulting in increased viscosity. The viscometry apparatus used was an automated measurement system comprising of a modified Ubbelohde viscometer shown in Figure 2.19. The automated system utilises a vacuum and laser timing gates to accurately measure the flow rate through the capillary within the viscometer and provide repeatable measurements. This gives kinematic viscosity values in units of cSt for the polymer solution (η) and its carrier solvent which is water (η_0).



Figure 2.19: Left) Ubbelohde Viscometer Right) Automated measurement system.

The system was calibrated to the known constants for water at 25 °C before taking measurements of the polymer solution.^{57,58}

Solution	20% w/v Solution (η)(cSt)	Water (η_0)(cSt)
Kinematic viscosity	1.49	0.89

Table 2.6: Comparison of kinematic viscosity of water and polymer-water 20% solution.

$$\eta_{rel} = \frac{\eta}{\eta_0}$$

Equation 2.6: Calculation for relative viscosity.

The relative viscosity for this material $\eta_{rel} = 1.67$ is a unitless ratio between a solution of compound and its solvent. This shows that there is a significant increase in the viscosity of the polymer solution over that of neat solvent which will improve surface adherence.

$$\eta_{inh} = \frac{\ln \eta_{rel}}{c}$$

Equation 2.7: Calculation for inherent viscosity.

The inherent viscosity of the polymer was calculated to be $\eta_{in} = 0.0258 \text{ dL g}^{-1}$ which appears to match the observable properties of the material. Comparatively, the linear polyethylene glycol with an \bar{M}_n of 1000 exhibits a kinematic viscosity of 17.4 cSt but at the much greater temperature of 100°C.

2.2.2.5. Thermal analysis

Differential scanning calorimetry (DSC) was used to identify the thermal characteristics of the polyglycerols showing the thermoreversible nature of the material over the range -95 to 200 °C as well as the glass transition temperature (T_g) of the SMA polyglycerol at -28.1 °C. The thermogravimetric analysis of this material shows its high stability with the onset of degradation not occurring until 375 °C with maximum degradation occurring at 410 °C (see Figure 2.20). This high temperature stability suggests that these materials are capable of withstanding sterilisation within an autoclave. While this is not essential for the experimental processes being used in this work it is beneficial should a sterile commercial product be desired.

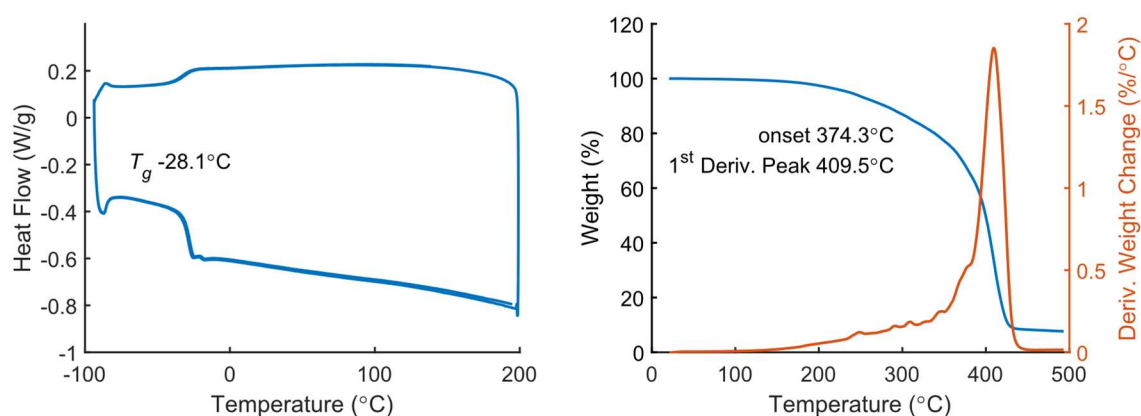


Figure 2.20: Left) DSC analysis of SMA polyglycerol Right) TGA analysis of SMA polyglycerol **2.19_{SMA}**.

Comparatively the T_g of the bulk polyglycerol lies at a slightly higher value of -15.0 °C (see Figure 2.21). The original synthesis conducted by Frey *et al.* produced materials with glass transition temperatures between -19 and -25 °C which is close to the values obtained in this study.³⁸

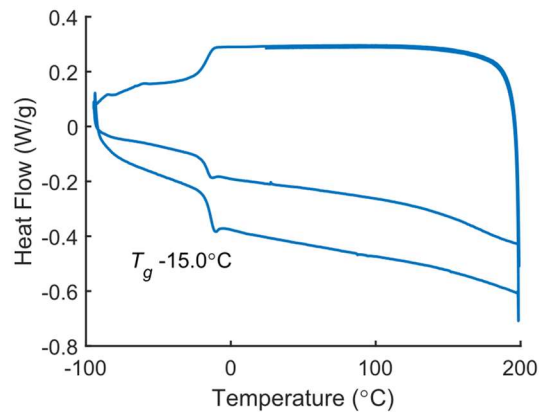


Figure 2.21: DSC analysis of polyglycerol synthesized via the bulk procedure **2.19_{BULK}**.

2.2.2.6. Rheology

A parallel plate rheometer was used to examine the physical state of the polyglycerol polymer produced via the SMA route. Utilising a temperature sweep method provides further insight into the materials physical state. This method is commonly used to identify the viscoelastic properties of a material. The crossing point of G' and G'' indicates the visco-elastic region. These materials show no such crossing point over the greater than ambient temperatures covered and instead appears to show consistent divergence of the curves (see Figure 2.22). This is typical of a material that has already undergone all physical state changes and is simply becoming less viscous as the temperature increases. This region is also known as the terminal phase. This is expected at these temperatures with this amorphous material as there will not be any further structural changes this far above the T_g . However, this data does show the clear thermoreversible nature of the physical properties of the material.

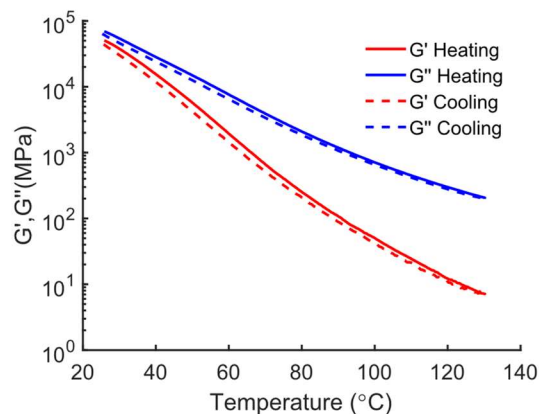
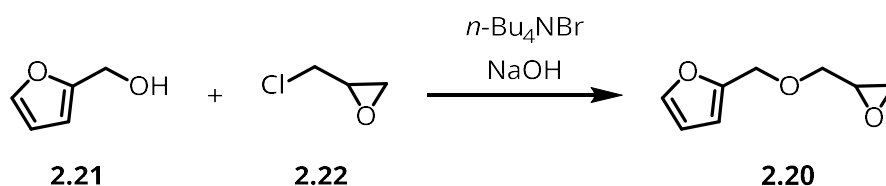


Figure 2.22: Rheometric analysis of SMA Polyglycerol **2.19_{SMA}** showing the G' and G'' at various temperatures.

2.2.3. Glycidyl FGE copolymer

The SMA polyglycerols described thus far provide an excellent branched backbone to which can be attached bioactive components such as sensors and cleavable decontamination groups. However, in order to preserve the hydroxyl functionality as much as possible orthogonal reactive groups could be used. These would enable facile further modification of the polymer without unwanted loss of the high hydroxyl functionality. Installation of the pendant furfuryl alcohol groups allows for this via the well-known Diels-Alder thermoreversible reaction. The benefit of this method is that these reactions are typically conducted in very mild conditions and at low temperatures which allows for sensitive or less stable functional compounds to be attached to the polymer backbone without fear of degradation or damage to these materials.

The ideal method of introducing this functionality is addition of the alternative monomer during polymerisation. To enable this the monomer furfuryl glycidyl ether (FGE, **2.20**) was synthesized from furfuryl alcohol (**2.21**) and epichlorohydrin (**2.22**).



Scheme 2.6: Synthesis of FGE **2.20**.

This reaction is carried out solvent free with excess sodium hydroxide and tetra-*n*-butylammonium bromide as a phase transfer catalyst. Once extracted the product can be distilled from the crude orange/brown solution at 75 – 82 °C (3.1 mbar) yielding a clear colourless oil in good yield (79%).

The ¹H NMR spectrum shown in Figure 2.23 for FGE **2.20** is further complicated by the stereogenic centre at substituted epoxide position 9. This chiral centre induces different chemical shifts to the vicinal protons 10 and 8 that in turn induces complex splitting to all these resonances such as position 9.

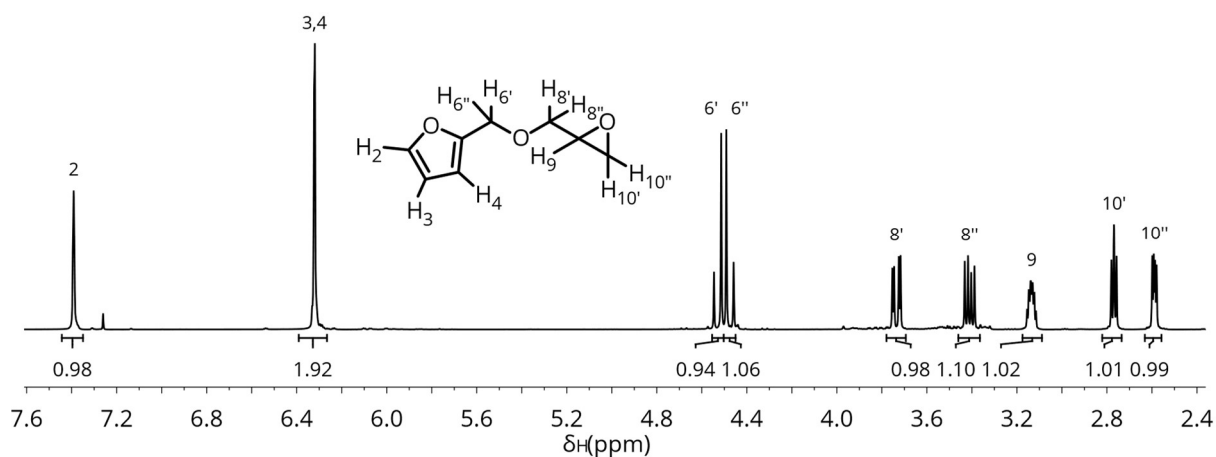
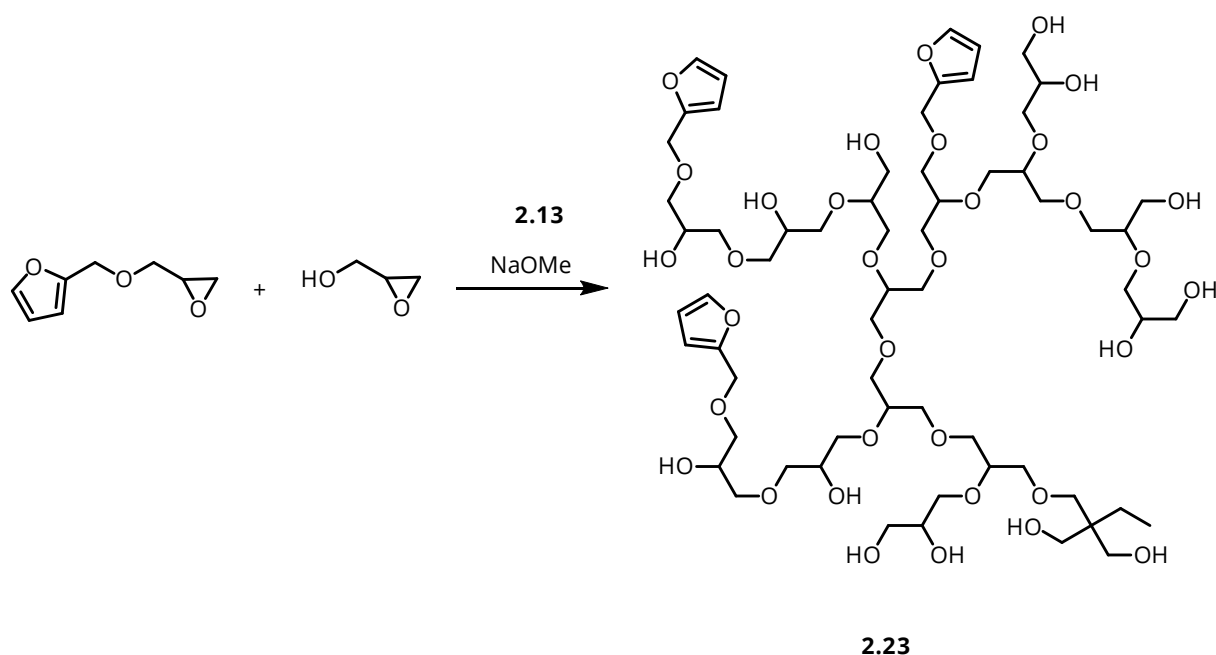


Figure 2.23: ^1H NMR spectrum of FGE **2.20**.

Fortunately, FGE **2.20** was found to be miscible with the glycidol monomer which enables both monomers to be combined and introduced via the slow monomer addition method which ensures the relative concentration of the monomers remains the same throughout.



Scheme 2.7: Synthesis of Glycidyl FGE copolymer **2.23** by SMA.

Solutions of various weight percentages of the monomers glycidol **2.18** and FGE **2.20** were used to synthesize the polymers. The inverse gated ^{13}C NMR spectrum of the reveals the presence of additional resonances at 151, 144, 111, 110 and 64 ppm which all give integrals proportional to one carbon. These additional resonances correspond to the values found for the FGE monomer and indicate its inclusion in the polymer since there is no observable carbon resonances for the unreacted epoxide.

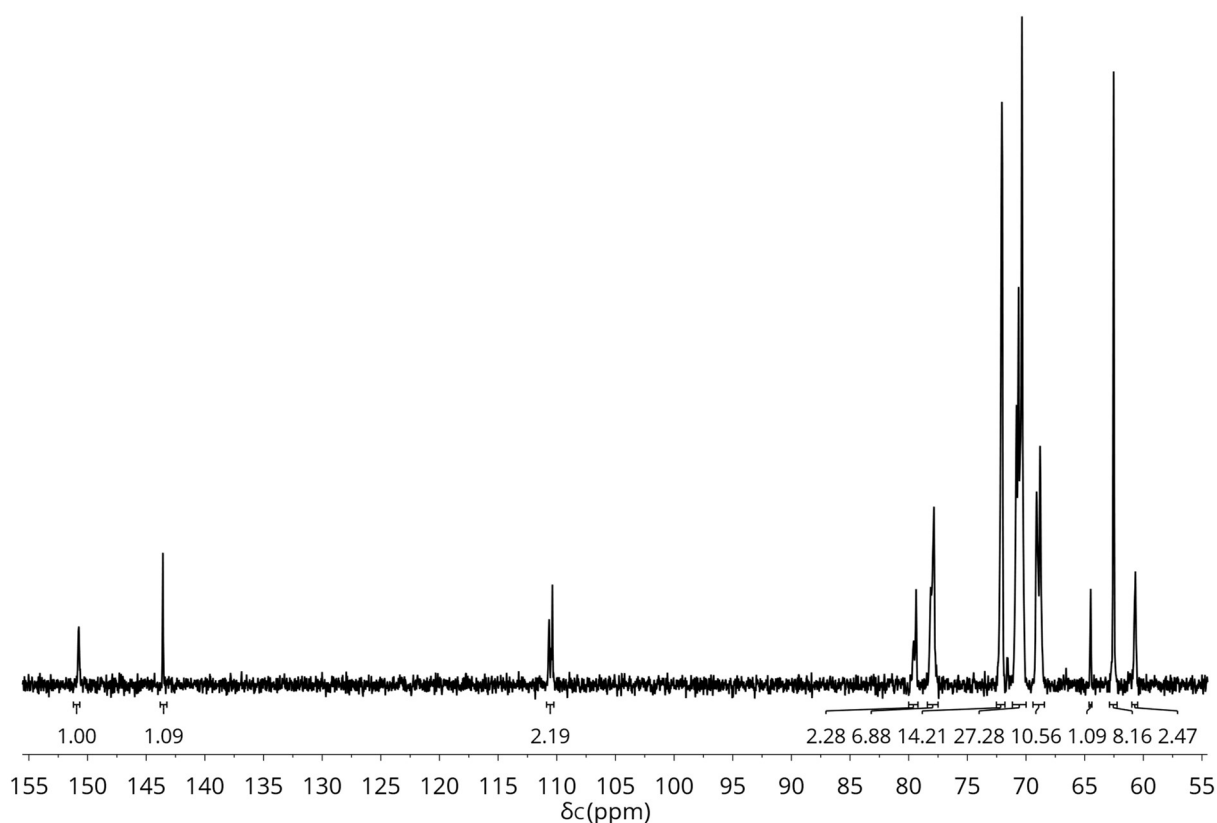


Figure 2.24: Inverse gated ^{13}C NMR spectrum of glycidyl FGE copolymer; D_2O , 294 K.

The DSC analysis of the 20% w/w FGE copolymer (**FGE20**) showed a similar T_g to the previous polyglycerols tested (see Figure 2.25). The value of -17.9°C lies between the values obtained for the SMA and bulk polyglycerol methods of -28.1°C and -15.0°C , respectively.

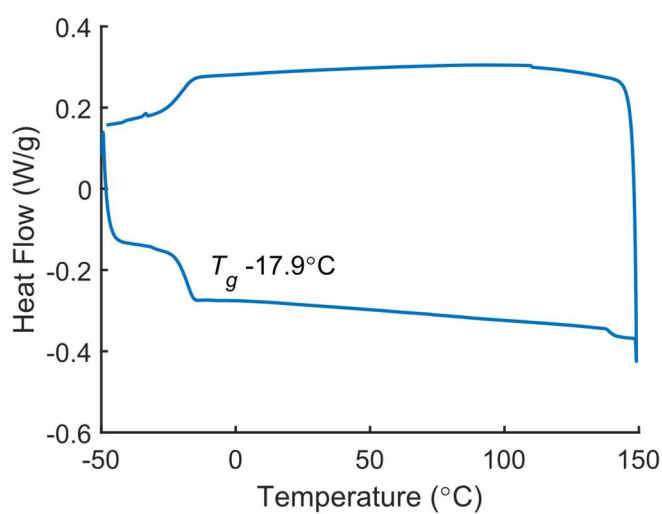


Figure 2.25: DSC thermogram of **FGE20**.

2.2.3.1. MALDI-TOF MS Analysis of FGE Copolymer

Introducing a second monomer increases the complexity of the MALDI-TOF spectrum significantly. For example, mass spectrometric analysis of the polyglycerols previously synthesized revealed mass ions corresponding to cyclic and branched structures for each of the monomer addition approaches used. If it is assumed that polymerisations would occur in a similar fashion, a degree of polymerisation between 6 and 26 could be expected giving rise to a mass spectrum containing up to 42 signals. On top of this data, the presence of mass ions corresponding to the proton, sodium and potassium adducts of the oligomers would lead to tripling the number of signals to 138. However, once a second monomer is introduced there is now the opportunity to have a variable number of glycidol units and a variable number of FGE units thereby raising the number of signals by this factor.

$$\text{Number of signals} = \text{Glycidol units} \times \text{FGE units} \times \text{Adducts} \times \text{Structure}$$

Equation 2.8: Theoretical number of signals produced by the complex mixture arising from the copolymer

If it is assumed the number of FGE units within the polyglycerol can vary between 0 and 12 this give a factor of 13 which results in the number of signals of the exact masses for this example of 1638. This is then further complicated by additional isotopic masses which typically give 1-2 extra signals for every exact mass signal. This complexity can be easily observed in the mass spectrum shown in Figure 2.26.

As a direct result of this complexity the molecular weight data was unable to be calculated with certainty as each signal could not be directly attributed to a specific oligomer structure. Despite this issue, by using every signal above a threshold of 3.5% (the same threshold used in the expansion shown in Figure 2.26) the calculated values for \bar{M}_n of 633.3 Da, an \bar{M}_w of 868.4 and a \bar{D}_m of 1.37 were generated. These values are much lower than expected, most likely as a result of the large amount of noise in the lower region of the spectrum. This could also be enhanced by the positive skew effect discussed previously leading to lower molecular weight molecules overexpressing compared to the larger masses.⁴³

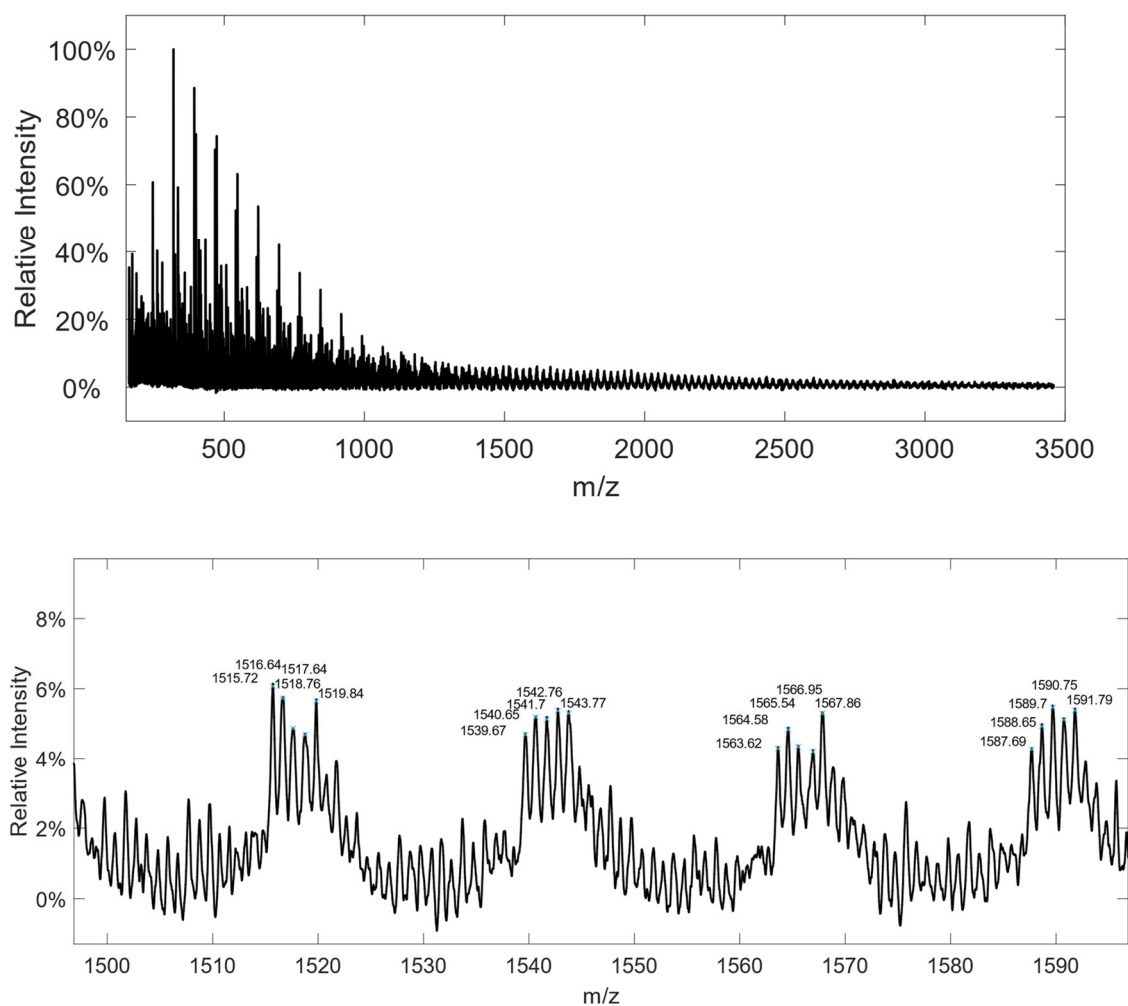


Figure 2.26: Top) MALDI-TOF mass spectrum of **FGE20**
Bottom) Expansion of MALDI-TOF mass spectrum of **FGE20**

The complexity of assigning these signals is very apparent when comparing the obtained spectrum and the synthetic spectrum comprising of the expected mass signals for various combinations of monomers, adducts and structures (see Figure 2.27). These values have been condensed in Table 2.7 where the observed mass is directly compared to potential similar exact masses. Where no value could be identified the signal was deemed to be an isotopic signal.

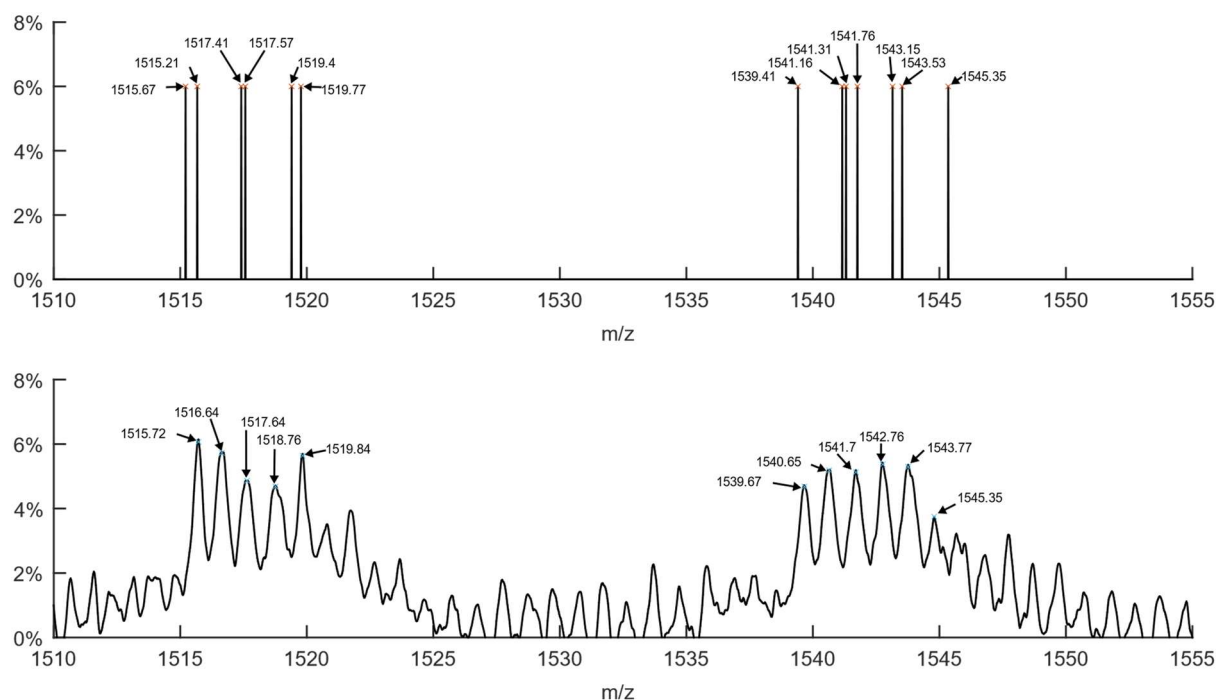


Figure 2.27: top) synthetic mass spectrum of potential masses arising from different copolymers. bottom) obtained MALDI mass spectrum of **FGE20**.

Obtained (Da)	Composition	Adduct	Structure	Predicted (Da)
1515.72	Gly ₁₆ FGE ₂	Na	Cyclic	1515.67
	Gly ₃ FGE ₈	H	Hyperbranched	1515.21
1516.64	<i>Isotope of above signal</i>			
1517.64	Gly ₈ FGE ₆	H	Cyclic	1517.41
	Gly ₁₄ FGE ₂	K	Hyperbranched	1517.57
1518.78	<i>Isotope of above signal</i>			
1519.84	Gly ₁₄ FGE ₅	Na	Hyperbranched	1519.40
	Gly ₂₀	K	Cyclic	1519.77
1539.67	Gly ₈ FGE ₆	Na	Cyclic	1539.41
1540.65	<i>Isotope of above signal</i>			
1541.70	FGE ₁₀	H	Cyclic	1541.16
	Gly ₆ FGE ₆	H	Hyperbranched	1541.31
	Gly ₁₉	K	Hyperbranched	1541.76
1542.76	<i>Isotope of above signal</i>			
1543.77	FGE ₉	Na	Hyperbranched	1543.15
	Gly ₁₂ FGE ₄	K	Cyclic	1543.52
1545.35	Gly ₆ FGE ₇	Na	Cyclic	1545.35

Table 2.7: Observed and Predicted Signals and their components.

2.2.3.2. Dynamic Light Scattering

While dissolving the **FGE20** copolymer in water, an interesting lower critical solution temperature (LCST) effect was observed upon heating (see Figure 2.28). This effect was not observed for the 10% FGE w/w copolymer solution.

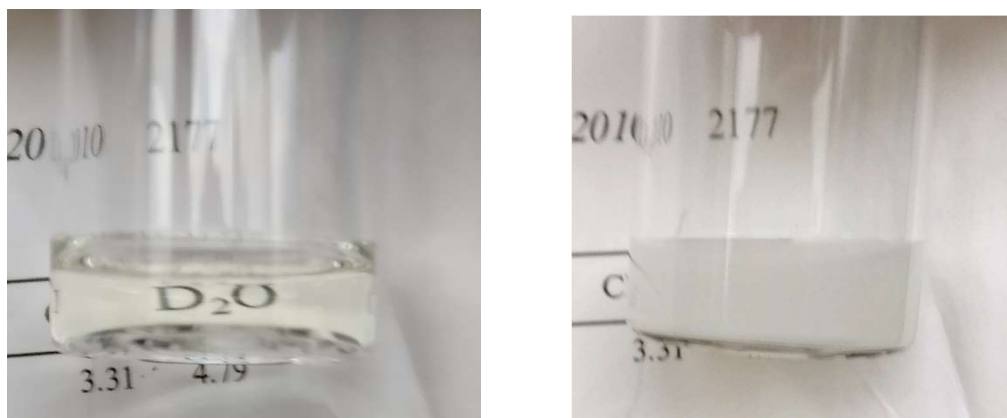
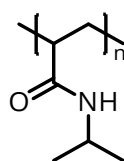


Figure 2.28: Left) 20 °C solution of **FGE20** in water Right) 45 °C solution of polyglycerol in water.

This LCST effect of polymers in aqueous solutions has been studied extensively, in particular the polymer poly(*N*-isopropylacrylamide) (PnIPAM, **2.24**) (see Figure 2.29).⁵⁹ This effect was first described for PnIPAM aqueous solutions in 1968 by M. Heskins and Guillet.⁶⁰ However, this effect has only recently come to light in the case of polyglycerols but only in those that have been functionalised post-polymerisation at the chain ends.⁶¹ This distinction is vital as the FGE copolymers shown here can have furfuryl functionality throughout the polymeric structure rather than only at the terminal units.



2.24

Figure 2.29: Structural repeat unit of PnIPAM.

The LCST behaviour of copolymer **2.23** was investigated by means of Dynamic Light Scattering (DLS). This method of analysis generates data on the size of observable particles with a solution. Using a temperature ramp to take these measurements with respect to temperature gives the waterfall plot shown in Figure 2.30. This shows the observable particle size in solution remains relatively stable at 200 nm until a temperature

of 32 °C was reached at which point it increases ten-fold to *ca.* 2000 nm. The balance of hydrophilic and hydrophobic groups leads the observed LCST effect. As has been noted with PnIPAM as the temperature of the solution increases the hydrophobic segments associate. This causes intra- and intermolecular aggregation leading to collapse of the individual polymer chains (microphase separation) and precipitation of the polymer (macrophase separation).⁵⁹ LCST measurements are typically recorded on the heating ramp to combat hysteresis that has been shown by slower redissolution times compared to initial cloud formation. The **FGE20** copolymer solutions tested here were observed to undergo reversible demixing and remixing over a period of minutes. However, it has been shown for certain PnIPAM solutions that heating just above the LCST allows for much faster remixing (seconds) than annealing at high temperatures (>1 day).⁶²

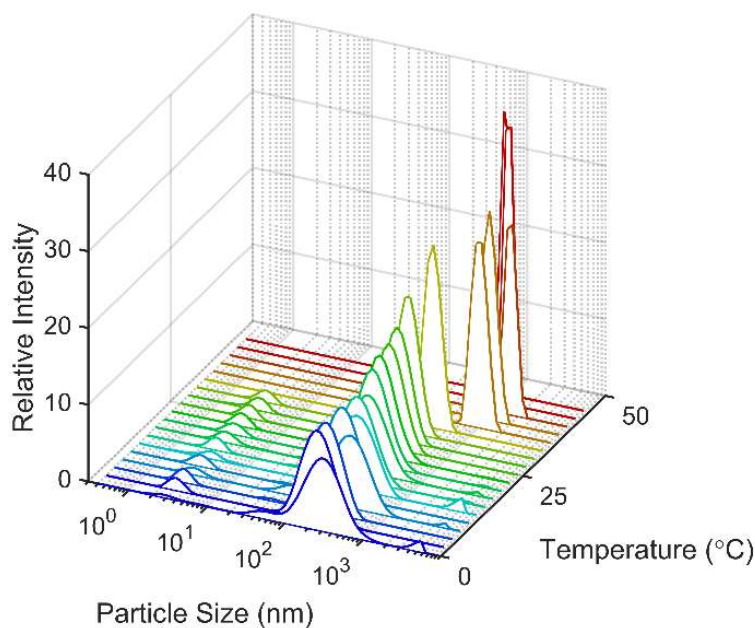


Figure 2.30: DLS analysis - temperature ramp of FGE 20% in water.

This data can be extended further by taking temperature ramp measurements at various concentrations. To combine this data the waterfall plot data is reduced to a 2-dimensional dataset and assigned its respective concentration. These new datasets can then be combined by taking the smoothed peak maxima, interpolated and plotted on a contour map showing changing particle size with respect to concentration and temperature (see Figure 2.31). There is a visible positive correlation of increasing temperature to particle size and increasing concentration to particle size.

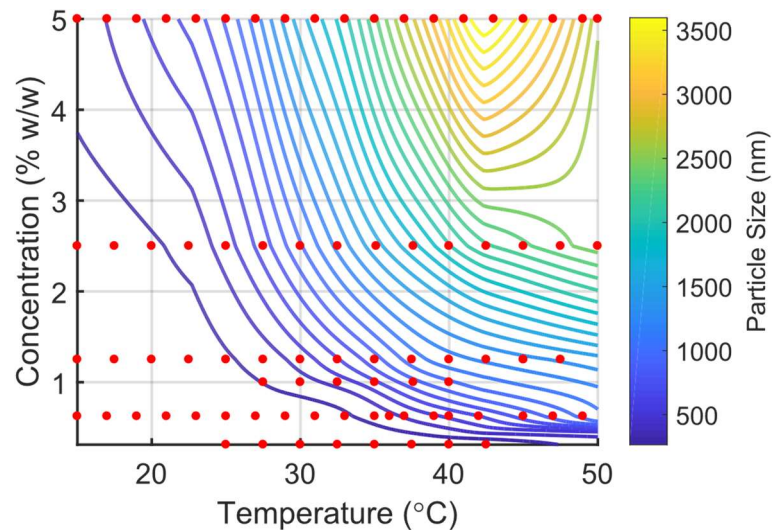


Figure 2.31: Contour plot of particle size vs. concentration vs. temperature. (Individual measurements are marked by a red circle.)

Taking this further, the derivative can be used to identify the steepest slope of the curve which in turn gives the midpoint of the curve and can be used to identify the cloud point temperature of the solution. By taking the derivative of the slope in the temperature dimension another contour plot is obtained whereby the peak/ridge maxima shows the cloud point at specific concentrations (see Figure 2.32). This reinforces the observed shift noted in the previous contour plot. In this case the units can be thought to be arbitrary as they merely indicate the midpoint of the slope, in this case the actual units are $\text{nm} (\text{wt}\%)^{-1} \text{ } ^\circ\text{C}^{-1}$.

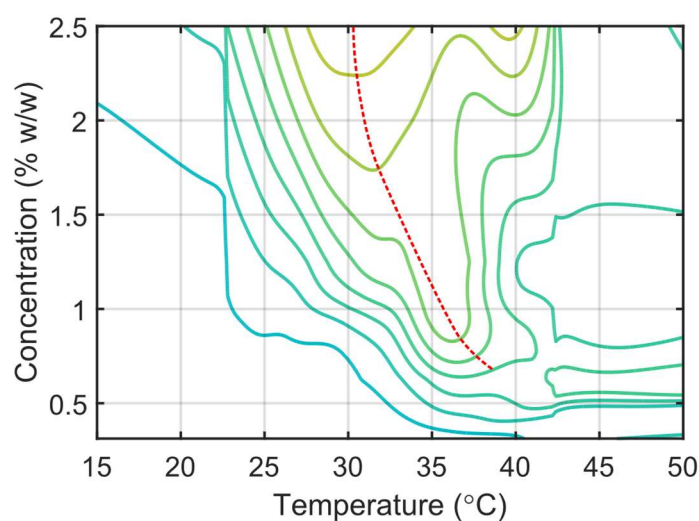


Figure 2.32: Contour plot of derivative of particle size vs. concentration vs temperature. (Observable trend measurement outlined in red)

The potential exploitation of the LCST properties of the **FGE20** solution were tested by attempting filtration of the solution. By heating the solution above its LCST then passing the solution through a 0.2 μm filter, the solution no longer has an observable LCST. This is most likely a result of the more heavily FGE functionalized material taking the largest part in LCST formation being removed as a result of its size at the elevated temperatures. Once removed the remaining solution can no longer form these larger structures as it lacks the required functionality.

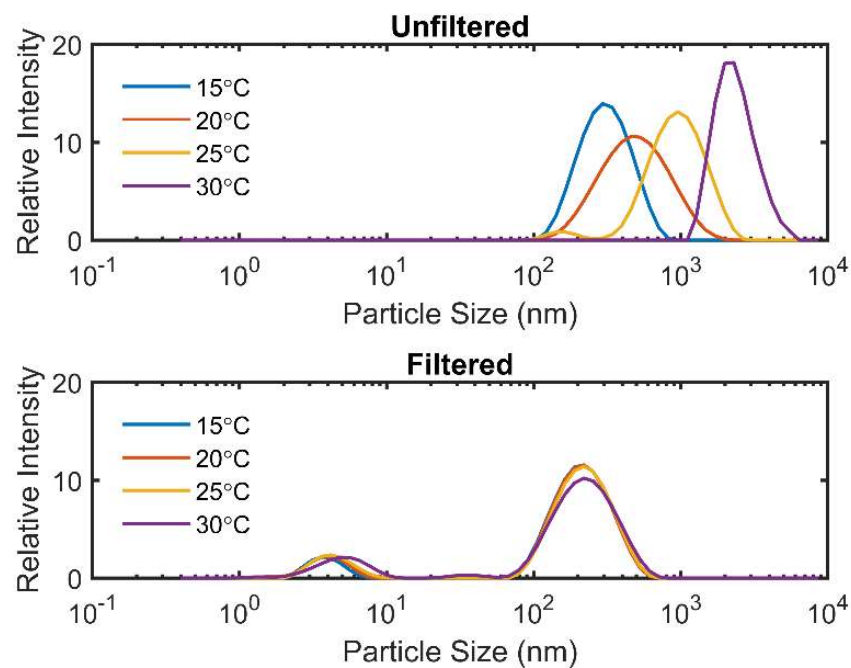


Figure 2.33: Comparison of Unfiltered and Filtered solutions of **FGE20** in water 1.25% w/v.

The results obtained from the DLS analysis clearly show the formation of particles within the solution at elevated temperatures. These self-assembled globules of FGE polyglycerol copolymer can be removed from the solution by filtration through 0.2 μm membrane filter.⁵⁹

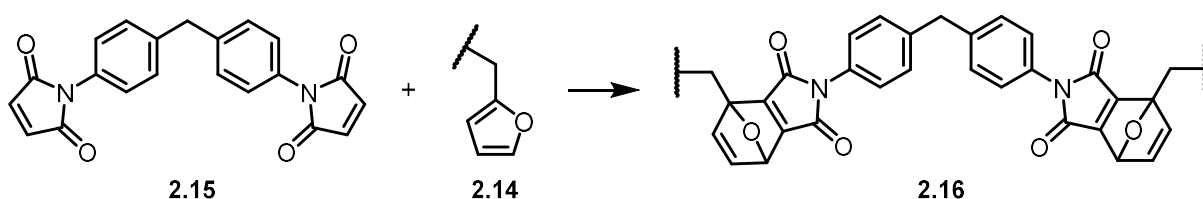
2.3. Conclusion and Future Work

The hydrogelator **2.15** was synthesized and found to be very promising with regards to its ability to retain moisture over an extended period. However, this work was ceased following the discovery of its unintended inhibitory on the germination of the biological simulant, as discussed in greater detail in Chapter 4.

Hyperbranched and cyclic polyglycerols have been synthesized using multiple variations on the procedure originally reported³⁸ by Frey *et al.* These included the use of sodium as the counter-ion to the alkoxides during polymerisation which resulted in an increased yield of cyclic polyglycerols compared to materials reported by Frey *et al.* While this unintended product would usually cause issues for the future use of the material in this case, as is discussed in detail in Chapter 4, the mixed material was very suitable for future testing. A bulk polymerisation method was also investigated which resulted in formation of predominantly cyclic structures thought to be caused by a preferential templating effect of the sodium cations over the potassium cations used by Frey *et al.*^{63,64}

These materials exhibit ideal physical properties to the originally discussed requirements. Their water solubility offers rapid preparation of formulations, the relatively low reactivity of the hydroxyl functionality makes these materials particularly stable as evident from the TGA analysis which showed these materials can endure the temperatures found within an autoclave meaning they could easily be prepared as an aseptic solution.

Following the synthesis of polyglycerol modifications were introduced to yield orthogonal reactivity within the polymer with the potential to be exploited to functionalise the material further or introduce thermoreversible cross-linking compounds such as bismaleimide **2.15** (see Scheme 2.8).



Scheme 2.8: Diels-Alder cross-linking reaction.

It was noted that the furfuryl functionalised polyglycerols exhibited interesting LCST characteristics in water. This characteristic has only been observed previously with linear aliphatic modifications to the polyglycerol found by Liu and Chen *et al.* in late 2017.⁶¹ DLS analysis was used to investigate this phenomenon and understand its apparent relationship with concentration.

The modified polyglycerols reported by Liu and Chen *et al.* were formed by functionalisation of polyglycerol post-polymerisation by carbonyl diimidazole (CDI) coupling on a milligram scale (≤ 300 mg polyglycerol). These results represent a proof of concept approach whereby very small quantities of material can be produced with the observable LCST effect. Conversely, the results described herein show an approach that can produce a similar observable LCST effect at much larger scale (c .50 g) by means of a process that is more suitable for industrial scaling. In addition to this is the ability of the furfuryl groups to act as functionalizable handles to provide further modification without reduction of the number of hydroxyl groups. Conversely, The materials described previously by Liu and Chen *et al.* are only functionalised with aliphatic chains providing no further reactivity.

The foundation this work has laid can be built on by synthesis of the furfuryl polymers while investigating the potential alternative morphologies arising from the use of different cations, such as potassium, rubidium or caesium, during polymerisation. Variation of the alkali metal has been shown to produce differing templating effects as well as the use of more highly charged cations such as Ca^{2+} .^{54,55} While cyclic structures are not a hinderance for this application, the synthesis of purely hyperbranched structures may exhibit differing or more tuneable LCST properties. This design functionality can be built on further by modifying the method of addition of the comonomer FGE either serially or in parallel to the glycidol.

2.4. Experimental

2.4.1. General Experimental

^1H and ^{13}C NMR spectra were recorded at 400 and 100 MHz, respectively using either a Bruker Nanobay 400 or Bruker DPX 400 spectrometer and referenced to the residual ^1H signals of deuterated chloroform (CDCl_3) at 7.26 ppm, deuterated dimethyl sulfoxide (d_6 -DMSO) at 2.50 ppm or TMS at 0.00 ppm. All NMR spectra were analysed using MestReNova 11. Infrared (FTIR) spectra obtained using a Perkin Elmer 1720-X IR-Fourier Transform spectrometer fitted with a diamond ATR crystal and analysed using Omnic and MATLAB. DSC and TGA thermogram data were collected on a TA instruments TA-Q2000 DSC and TA-TGA Q50, respectively and analysed by TA Universal Analysis and MATLAB. MALDI-TOF mass spectrometric data was collected on a Bruker Ultraflex operating in positive ion mode using α -cyano-4-hydroxycinnamic as the matrix (saturated solution in TA30) with analyte concentration of 1 mg mL^{-1} and analysed by MATLAB. Mass spectrometric data was also collected by ESI analysis on a Thermo Scientific LTQ-Orbitrap XL mass spec using the Orbitrap detector operating at 100 K resolution, in positive ion mode. Mass tolerance of matching to proposed compound was limited to 5 ppm. DLS data was collected on a Malvern Zetasizer Nano ZS taking a minimum of 15 scans per run and 5 runs per temperature increment and analysed by MATLAB. Water retention studies were conducted with 1 mL of gel per sample at 5 mg mL^{-1} hydrogelator with water loss recorded by 4 d.p. analytical balance. The syringe pump used was a Treonic IP4 set to 5 mL hour^{-1} . Viscosity values were obtained from a SI Analytics AVS[®] 470 using an Ubbelohde viscometer at 25 °C.

2.4.2. General procedure for initiator preparation

1,1,1-Tris(hydroxymethyl)propane (1.2 g, 8.94 mmol) was added sodium methoxide (160 mg, 2.95 mmol) in methanol (10 mL). The solution was concentrated by heating until void of solvent giving a white solid (1.36 g, > 99%).

2.4.3. General procedure for SMA polymer synthesis (**2.19_{SMA}**)

Initiator was prepared using the general procedure (2.4.2) and added to a reaction vessel. Anhydrous diglyme (30 mL) was then added to the reaction vessel and the solution was

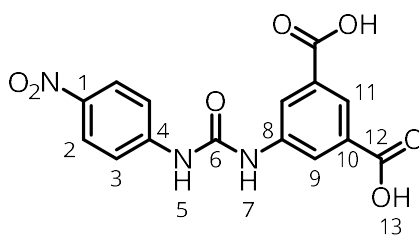
heated to 95 °C. Monomer (50 g) was added dropwise at a rate of 5 mL per hour. The reaction was left for 18 hours then diluted with methanol (150 mL) and neutralised over Amberlite® IR120 (H) column then precipitated twice into acetone. The supernatant was decanted, and the resulting precipitate was dissolved in methanol, concentrated *in vacuo* and the heated to 80 °C at 3 mbar to yield a clear amorphous viscous resin (45 g, 90%).

2.4.4. General procedure for Bulk polymer synthesis (**2.19_{BULK}**)

Initiator was prepared using the general procedure (2.4.2) and added to a reaction vessel. Anhydrous diglyme (30 mL) was then added to the reaction vessel followed by glycidol (50 g). The reaction was heated at 30 °C for 18 hours then slowly raised to 95 °C over 48 hours. After this the solution was diluted with methanol (150 mL) and neutralised over Amberlite® IR120 (H) column then precipitated twice into acetone. The supernatant was decanted, and the resulting precipitate was dissolved in methanol, concentrated *in vacuo* and the heated to 80 °C at 3 mbar to yield a cloudy amorphous viscous resin (39 g, 78%).
 $\nu_{\max}(\text{ATR, cm}^{-1})$ 3350 (O-H), 2871 (C-H), 1067 (C-O), δ_{H} (400 MHz, D₂O) 3.85 – 3.18 (m) ppm;
 δ_{C} (100 MHz, D₂O) 79.6, 79.4, 77.9, 72.1, 72.0, 70.8, 70.7, 70.6, 70.4, 70.4, 69.1, 68.8, 62.6, 62.5, 60.7. ppm;

Batch	\bar{M}_w	\bar{M}_n	D_m	DB_{frey}
2.19_{SMA/1}	1000	920	1.09	0.54
2.19_{SMA/2}	1050	960	1.10	0.55
2.19_{SMA/3}	950	860	1.10	0.53
2.19_{SMA/4}	1270	1110	1.15	0.57
2.19_{BULK/1}	750	600	1.25	0.71
2.19_{BULK/2}	850	770	1.15	0.69
2.19_{BULK/3}	940	870	1.09	0.70
2.19_{BULK/4}	1000	810	1.24	0.71

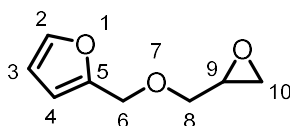
Table 2.8: Molecular weight data for polymers from different batches.

2.4.5. 5-(3-(4-nitrophenyl)ureido)isophthalic acid (**2.15**)

Synthesized in accordance with the procedure described by Hayes and co-workers.^{32,34}

A solution of 4-nitrophenyl isocyanate (0.64 g, 3.9 mmol) in 50 mL of dry THF was added dropwise over a solution of 5-aminoisophthalic acid (0.78 g, 4.3 mmol) in 50 mL of dry THF. The mixture was stirred at room temperature for 4 h and then concentrated in vacuo. The resulting yellow solid was treated with 50 mL of 1 M aqueous NaOH and the insoluble material removed by filtration. The red solution was treated with aqueous HCl to obtain a yellow gel. The gel phase was filtered, washed with distilled water and finally the solvent was evaporated under vacuum to yield 5-(3-(4-nitrophenyl)ureido)isophthalic acid **2.15** as a yellow solid. (1.15 g, 85%), $\nu_{\max}(\text{ATR, cm}^{-1})$ 3352 (N-H), 3083 (O-H), 1710 (C=O), 1615 (C=O), 1600 (C=O), 1324 (NO₂), 1300 (NO₂), δ_{H} (400 MHz, DMSO-d₆) 13.29 (2 H, s, **13**), 10.32 (1 H, s, **5**), 10.09 (1 H, s, **7**), 8.33 (2 H, d, J 1.5, **9**), 8.23 (2 H, d, J 9.0, **3**), 8.13 (1 H, t, J 1.5, **11**), 7.74 (2 H, d, J 9.0, **2**), δ_{C} (100 MHz, DMSO) 166.5 (**12**), 152.2 (**6**), 146.2 (**4**), 141.1 (**1**), 139.9 (**8**), 131.8 (**10**), 125.2 (**3**), 123.6 (**11**), 122.6 (**9**), 117.4 (**2**), m/z expected 346.0597 found 346.0669 [M+H]

2.4.6. Furfuryl Glycidyl Ether



Modified from procedure reported by Hyaric *et al.*⁶⁵

Sodium hydroxide (25 g), (\pm)-epichlorohydrin (16 mL, 204 mmol) and tetra-*n*-butylammonium bromide (0.8 g, 2.48 mmol) were combined and cooled to 20°C. Furfuryl alcohol (4.42 mL, 51 mmol) was added dropwise with vigorous stirring while maintaining a temperature below 20 °C. After 18 hours water was added, and the product was extracted with diethyl ether (3×100 mL). The organic fraction was dried over anhydrous

MgSO₄, filtered and then concentrated *in vacuo* before distillation under reduced pressure to yield the product as a clear colourless oil (6.82 g, 87%), bp 75-82 °C (3.1 mbar), ν_{\max} (ATR, cm⁻¹) 2997 (C-H), 1503 (furan ring), 1248 (epoxide), 1154 (C-O), 884 (epoxide), δ_{H} (400 MHz, CDCl₃) 7.39 (1 H, m, **2**), 6.32 (2 H, m, **2+3**), 4.53 (1 H, d, *J* 13.0, **6**), 4.47 (1 H, d, *J* 13.0, **6'**), 3.74 (1 H, dd, *J* 11.5, 3.0, **8**), 3.41 (1 H, dd, *J* 11.5, 6.0, **8'**), 3.13 (1 H, ddt, *J* 6.0, 4.0, 3.0, **9**), 2.77 (1 H, dd, *J* 5.0, 4.0, **10**), 2.59 (1 H, dd, *J* 5.0, 3.0, **10'**) ppm; δ_{C} (100 MHz, CDCl₃) 151.4 (**5**), 143.0 (**2**), 110.4 (**4**), 109.7 (**3**), 70.6 (**8**), 65.1 (**6**), 50.8 (**9**), 44.3 (**10**) ppm; FTMS-ESI (EI POS) *m/z* expected 177.0630 found 177.0526 [M+Na];

2.5. References

- 1 B. Setlow, E. Melly and P. Setlow, *J. Bacteriol.*, 2001, **183**, 4894–9.
- 2 P. Setlow, *J. Appl. Microbiol.*, 2006, **101**, 514–525.
- 3 P. Setlow, *Curr. Opin. Microbiol.*, 2003, **6**, 550–556.
- 4 P. M. Beaujuge and J. R. Reynolds, *Chem. Rev.*, 2010, **110**, 268–320.
- 5 D. N. Batchelder, *Contemp. Phys.*, 1988, **29**, 3–31.
- 6 J. Sambrook and D. W. Russel, *Molecular Cloning: A Laboratory Manual*, Cold Spring Harbor Protocols, 3rd edn., 2001.
- 7 O. Wichterle and D. Lím, *Nature*, 1960, **185**, 117–118.
- 8 B. Podkościelna, A. Bartnicki and B. Gawdzik, *Express Polym. Lett.*, 2012, **6**, 759–771.
- 9 R. V Ulijn, N. Bibi, V. Jayawarna, P. D. Thornton, S. J. Todd, R. J. Mart, A. M. Smith and J. E. Gough, *Mater. Today*, 2007, **10**, 40–48.
- 10 J. M. Willey, L. M. Sherwood and C. J. Woolverton, *Prescott's Microbiology*, McGraw-Hill Education, New York, 2014.
- 11 A. Lipowitz, *Justus Liebigs Ann. Chem.*, 1841, **38**, 348–355.
- 12 D. M. Zurcher and A. J. McNeil, *J. Org. Chem.*, 2015, **80**, 2473–2478.
- 13 N. M. Sangeetha and U. Maitra, *Chem. Soc. Rev.*, 2005, **34**, 821–836.
- 14 Nobel Media AB, The Nobel Prize in Chemistry 1987, http://www.nobelprize.org/nobel_prizes/chemistry/laureates/1987/, (accessed 3

- August 2018).
- 15 R. G. Weiss and P. Terech, *Molecular Gels*, Springer, Dordrecht, 2006.
 - 16 M. Yamanaka, *J. Incl. Phenom. Macrocycl. Chem.*, 2013, **77**, 33–48.
 - 17 R. G. Weiss and P. Terech, *Molecular Gels*, Springer, Dordrecht, 2006.
 - 18 Y.-T. Tang, X.-Q. Dou, Z.-A. Ji, P. Li, S.-M. Zhu, J.-J. Gu, C.-L. Feng and D. Zhang, *J. Mol. Liq.*, 2013, **177**, 167–171.
 - 19 E. R. Draper and D. J. Adams, *Chem*, 2017, **3**, 390–410.
 - 20 X. Yang, G. Zhang and D. Zhang, *J. Mater. Chem.*, 2012, **22**, 38–50.
 - 21 F. M. Veronese and G. Pasut, *Drug Discov. Today*, 2005, **10**, 1451–8.
 - 22 P. J. Flory, *J. Am. Chem. Soc.*, 1952, **74**, 2718–2723.
 - 23 E. Buhleier, W. Wehner and F. Vögtle, *Synthesis (Stuttg.)*, 1978, **1978**, 155–158.
 - 24 D. A. Tomalia, H. Baker, J. Dewald, M. Hall, G. Kallos, S. Martin, J. Roeck, J. Ryder and P. Smith, *Polym J*, 1985, **17**, 117–132.
 - 25 A. B. Padias, H. K. Hall, D. A. Tomalia and J. R. McConnell, *J. Org. Chem.*, 1987, **52**, 5305–5312.
 - 26 J. F. G. A. Jansen, E. M. M. de Brabander-van den Berg and E. W. Meijer, *Science (80-)*, 1994, **266**, 1226–1229.
 - 27 G. R. Newkome, Z. Yao, G. R. Baker and V. K. Gupta, *J. Org. Chem.*, 1985, **50**, 2003–2004.
 - 28 C. J. Hawker, R. Lee and J. M. J. Fréchet, *J. Am. Chem. Soc.*, 1991, **113**, 4583–4588.
 - 29 K. E. Uhrich, C. J. Hawker, J. M. J. Fréchet and S. R. Turner, *Macromolecules*, 1992, 4583–4587.
 - 30 E. Malmström, M. Johansson and A. Hult, *Macromolecules*, 1995, **28**, 1698–1703.
 - 31 C. Gao and D. Yan, *Prog. Polym. Sci.*, 2004, **29**, 183–275.
 - 32 F. Rodriguez-Llansola, B. Escuder, J. F. Miravet, D. Hermida-Merino, I. W. Hamley, C. J. Cardin and W. Hayes, *Chem. Commun.*, 2010, **46**, 7960–7962.

- 33 B. C. Baker, C. L. Higgins, D. Ravishankar, H. M. Colquhoun, G. C. Stevens, F. Greco, B. W. Greenland and W. Hayes, *ChemistrySelect*, 2016, **1**, 1641–1649.
- 34 D. M. Wood, B. W. Greenland, A. L. Acton, F. Rodríguez-Llansola, C. A. Murray, C. J. Cardin, J. F. Miravet, B. Escuder, I. W. Hamley and W. Hayes, *Chemistry*, 2012, **18**, 2692–9.
- 35 D. J. Adams and P. D. Topham, *Soft Matter*, 2010, **6**, 3707–3721.
- 36 T. H. Rider and A. J. Hill, *J. Am. Chem. Soc.*, 1930, **52**, 1521–1527.
- 37 M. Schömer, C. Schüll and H. Frey, *J. Polym. Sci. Part A Polym. Chem.*, 2013, **51**, 995–1019.
- 38 A. Sunder, R. Hanselmann, H. Frey and R. Mülhaupt, *Macromolecules*, 1999, **32**, 4240–4246.
- 39 J. W. Akitt and B. E. Mann, *NMR and chemistry: an introduction to modern NMR spectroscopy*, CRC Taylor & Francis, London, 4th edn., 2000.
- 40 R. J. Abraham, J. Fisher and P. Loftus., *Introduction to NMR spectroscopy*, Wiley, Chichester, 1988.
- 41 Y. H. Kim, *Macromol. Symp.*, 1994, **77**, 21–33.
- 42 D. Hölter, A. Burgath and H. Frey, *Acta Polym.*, 1997, **48**, 30–35.
- 43 D. Yu, N. Vladimirov and J. M. J. Fréchet, *Macromolecules*, 1999, **32**, 5186–5192.
- 44 W. Yan, J. A. Gardella and T. D. Wood, *J. Am. Soc. Mass Spectrom.*, 2002, **13**, 914–920.
- 45 H. R. Kricheldorf, *Macromol. Rapid Commun.*, 2007, **28**, 1839–1870.
- 46 H. R. Kricheldorf and S. Eggerstedt, *Macromol. Chem. Phys.*, 1999, **200**, 1284–1291.
- 47 H. R. Kricheldorf, D. Langanke, A. Stricker and H. J. Räder, *Macromol. Chem. Phys.*, 2002, **203**, 405–412.
- 48 C. Wutz and H. R. Kricheldorf, *Macromol. Theory Simulations*, 2012, **21**, 266–271.
- 49 K. J. Msayib and C. I. F. Watt, *Chem. Soc. Rev.*, 1992, **21**, 237–243.
- 50 G. W. Gokel and J. A. Semlyen, *Crown Ethers and Cryptands*, Wiley, Chichester, New

- York, 1996.
- 51 G. W. Liesegang, M. M. Farrow, F. Arce Vazquez, N. Purdie and E. M. Eyring, *J. Am. Chem. Soc.*, 1977, **99**, 3240–3243.
- 52 J.-M. Lehn, J. Simon and J. Wagner, *Angew. Chemie Int. Ed. English*, 2018, **12**, 578–579.
- 53 R. A. Bartsch, B. P. Czech, S. I. Kang, L. E. Stewart, W. Walkowiak, W. A. Charewicz, G. S. Heo and B. Son, *J. Am. Chem. Soc.*, 1985, **107**, 4997–4998.
- 54 L. Mandolini and B. Masci, *J. Am. Chem. Soc.*, 1977, **99**, 7709–7710.
- 55 G. Ercolani, L. Mandolini and B. Masci, *J. Am. Chem. Soc.*, 1981, **103**, 2780–2782.
- 56 G. W. Gokel and J. A. Semlyen, *Crown Ethers and Cryptands*, Wiley, Chichester, New York, 1996.
- 57 Anton Paar, Viscosity of Water – viscosity table and viscosity chart, <https://wiki.anton-paar.com/en/water/>, (accessed 20 August 2018).
- 58 M. L. Huber, R. A. Perkins, A. Laesecke, D. G. Friend, J. V. Sengers, M. J. Assael, I. N. Metaxa, E. Vogel, R. Mareš and K. Miyagawa, *J. Phys. Chem. Ref. Data*, 2009, **38**, 101–125.
- 59 V. Aseyev, H. Tenhu and F. M. Winnik, eds. A. H. E. Müller and O. Borisov, Springer Berlin Heidelberg, Berlin, Heidelberg, 2011, pp. 29–89.
- 60 M. Heskins and J. E. Guillet, *J. Macromol. Sci. Part A - Chem.*, 1968, **2**, 1441–1455.
- 61 Y. Zhang, R.-C. Wang, H.-J. Liu and Y. Chen, *Soft Matter*, 2017, **13**, 8136–8143.
- 62 K. Van Durme, G. Van Assche and B. Van Mele, *Macromolecules*, 2004, **37**, 9596–9605.
- 63 L. Mandolini and B. Masci, *J. Am. Chem. Soc.*, 1977, **99**, 7709–7710.
- 64 G. Ercolani, L. Mandolini and B. Masci, *J. Am. Chem. Soc.*, 1981, **103**, 2780–2782.
- 65 C. G. de Almeida, S. G. Reis, A. M. de Almeida, C. G. Diniz, V. L. da Silva and M. Le Hyaric, *Chem. Biol. Drug Des.*, 2011, **78**, 876–880.

Chapter 3

Organic based *Bacillus anthracis* disclosure agent.

3.1 Introduction

Rapid disclosure of bioweapons such as *B. anthracis* is vital for the successful decontamination of surfaces and treatment of infected victims. Currently available methods of disclosure have many practical drawbacks that limit their use in the field for identifying a hazard that covers a large area. The most effective disclosure agents for *B. anthracis* are based on lanthanides such as terbium and europium, which are expensive and could also pose long-term health risks and environmental damage.

The common link between all the methods discussed is the particular biomarker that they target. Calcium dipicolinate (CaDPA) makes up between 10 and 15% of the dry weight of the spore and has been successfully utilised as the key biomarker.^{1,2} Ideally for field dispersal the selected disclosure agent needs to be non-toxic or capable of undergoing degradation in the environment. This limitation eliminates most inorganic based methods as these can persist in the environment and cause lasting harm to plants and animals.³

3.1.1 Calcium dipicolinate-based sensors

The novel approach published by Curiel *et al.* to an organic based dipicolinate (DPA) sensor targeted the hydrogen bond acceptor nature of the DPA anion as shown in Figure 3.1. The incorporation of the fluorescent carbazole moiety provided an observable significant change in fluorescence upon DPA binding.⁴

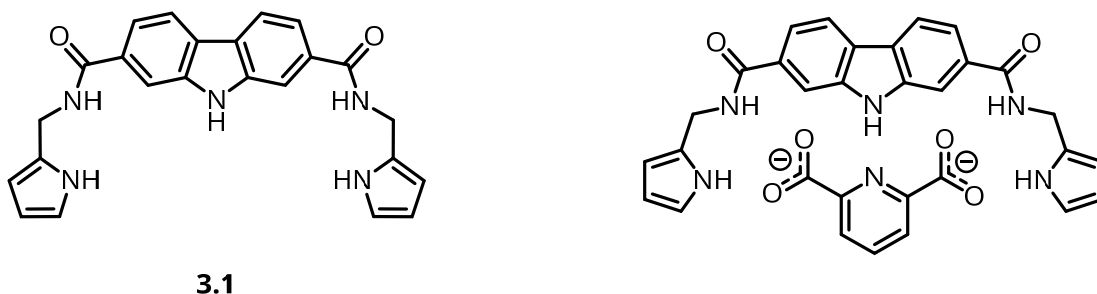


Figure 3.1: Dipicolinate fluorescent receptor by Curiel *et al.* and an example of its binding motif with the DPA anion.

Curiel *et al.* showed high selectivity towards the dipicolinate anion over similar structures such as isophthalates (see Figure 3.2). The exceptional binding strength of 34600 M^{-1} was achieved when tested in a competitive environment of water-acetone (2% v/v). When tested in polar, aprotic solvents such as DMSO there was a significant increase in binding strength to more than 10^6 M^{-1} .

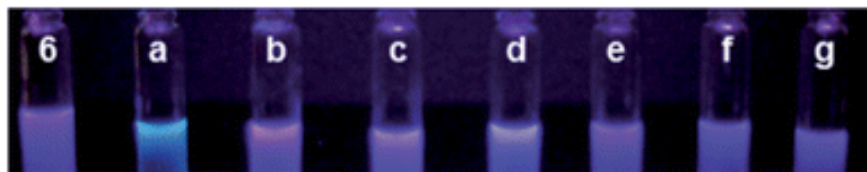
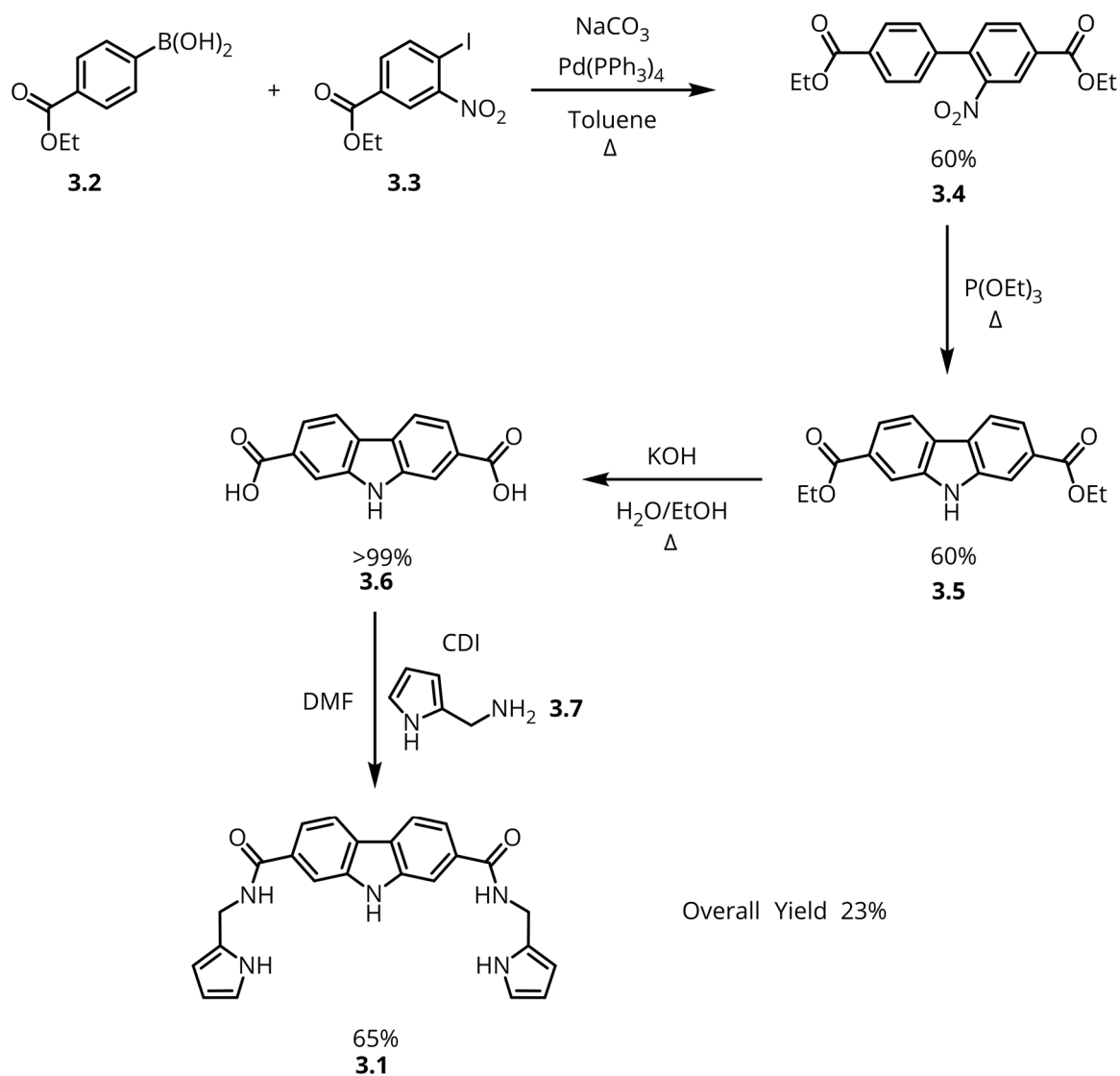


Figure 3.2: Fluorescent response of **3.1** to anions: (a) dipicolinate, (b) phthalate, (c) isophthalate, (d) terephthalate, (e) picolinate, (f) nicotinate and (g) isonicotinate.^{4*}

The synthesis outlined by Curiel *et al.* shown in Scheme 3.1 utilised a Suzuki-Miyaura coupling of a carboxyphenyl boronic acid **3.2** and iodo-nitro-phenyl ester **3.3** at the outset, using tetrakis-(triphenylphosphine)-palladium as the catalyst. The published yield for this reaction of 60% lies towards the lower end of the range for yields obtained from this type of reaction.⁵ The subsequent step in this synthesis was a Cadogan nitrene insertion to yield the carbazole diester **3.5**. Base catalysed hydrolysis of the corresponding ester yielded the diacid **3.6**. The (1H-pyrrol-2-yl)-methanamine **3.7** receptor unit was then introduced using 1,1-carbonyl diimidazole (CDI) as the coupling reagent to yield the final detector (**3.1**).

* Reproduced from Ref. ⁴ with permission from The Royal Society of Chemistry.



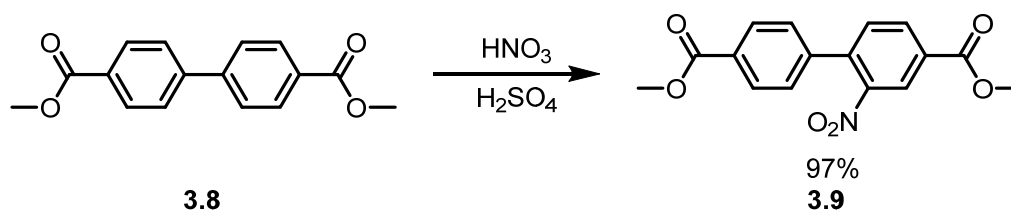
Scheme 3.1: Literature synthesis of the fluorescent receptor **1** by Curiel *et al.*⁴

This chapter describes the optimisation of methods to synthesize the fluorescent detector **3.1** to determine its suitability for use in an aqueous formulation. It also discusses attempted modifications made to the detector to alter its colorimetric and/or its fluorometric response as well as altering its physical characteristics such as water solubility and stability. The synthesis reported by Curiel *et al.* was repeated here to assess its suitability for use in this application.

3.2 Results and Discussion

3.2.1 Synthesis of the DPA sensor **3.1**

The synthesis reported by Curiel *et al.* began via the Suzuki-Miyaura cross coupling of carboxyphenyl boronic acid **3.2** and iodo-nitro-phenyl ester **3.3**, utilised expensive metal catalysts such as tetrakis(triphenylphosphine)-palladium. Starting from dimethyl [1,1'-biphenyl]-4,4'-dicarboxylate (**3.8**) using well-known nitrating conditions (nitric acid dissolved in concentrated sulfuric acid cooled to 5 °C) and a stoichiometric quantity of nitric acid, it was possible to selectively obtain the mono-nitrated product dimethyl 2-nitro-[1,1'-biphenyl]-4,4'-dicarboxylate (**3.9**) in a high yield (97%) as shown in Scheme 3.2. By restricting the stoichiometric quantity of nitric acid to one equivalent with respect to the starting material, in addition to maintaining the temperature of the reaction below 5 °C whilst slowly adding the nitric acid ensured that formation of the bis-nitrated by-product was kept to a minimum. The use of this method demonstrated that the use of substantially lower cost reagents can achieve higher yields than the comparative palladium and boronic acid chemistries employed by Curiel *et al.*



Scheme 3.2: Nitration of dimethyl [1,1'-biphenyl]-4,4'-dicarboxylate.

The ^1H NMR spectrum of **3.9** (see Figure 3.3) revealed the conversion to the desired mono-nitrated product. Since the nitrated biaryl framework is no longer symmetric, a downfield shift of the proton resonances of the methyl ester group H_b as well as protons attached to the functionalised ring was observed. The functionalised ring protons H_d , H_f and H_g were assigned by two-dimensional correlation NMR: HSQC, HMBC and ^1H - ^1H COSY.

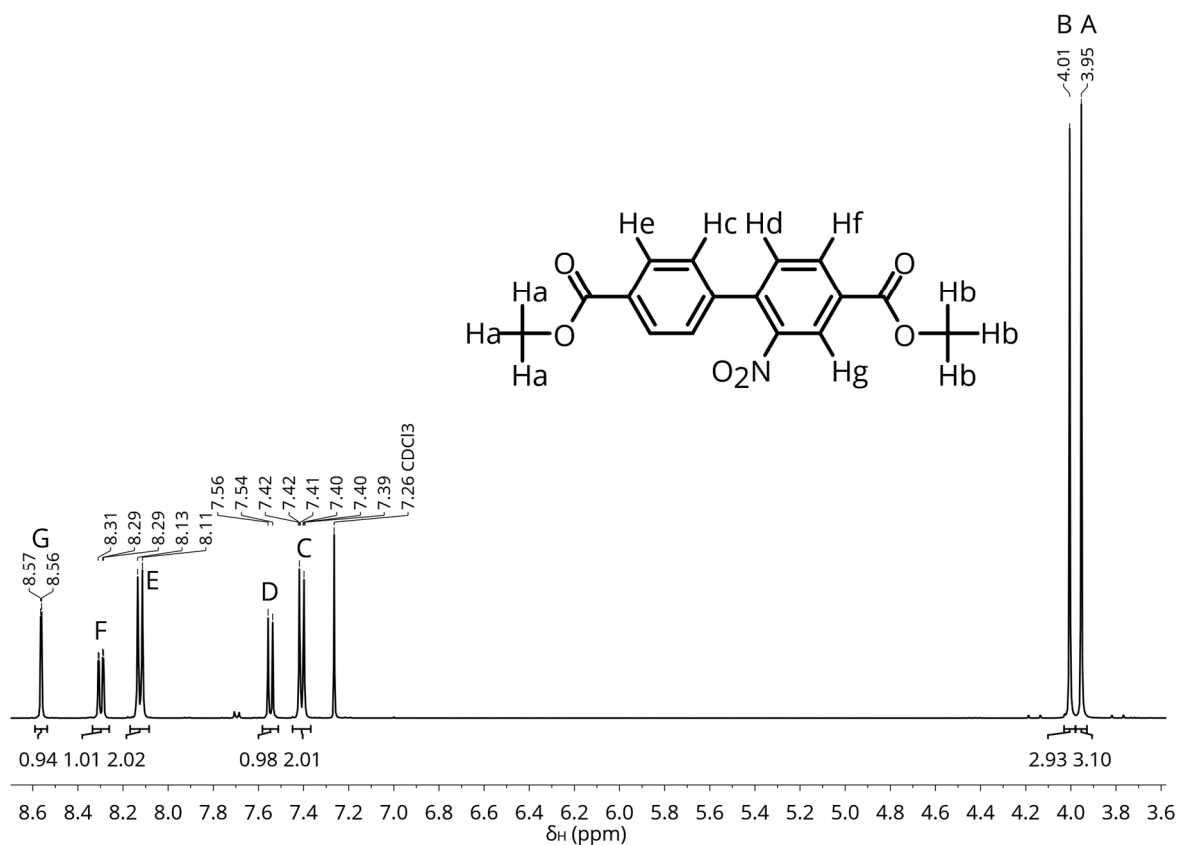
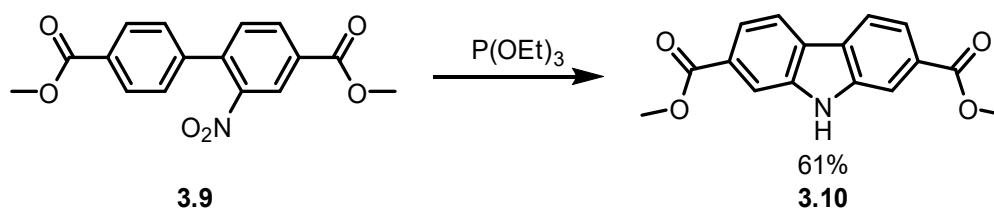


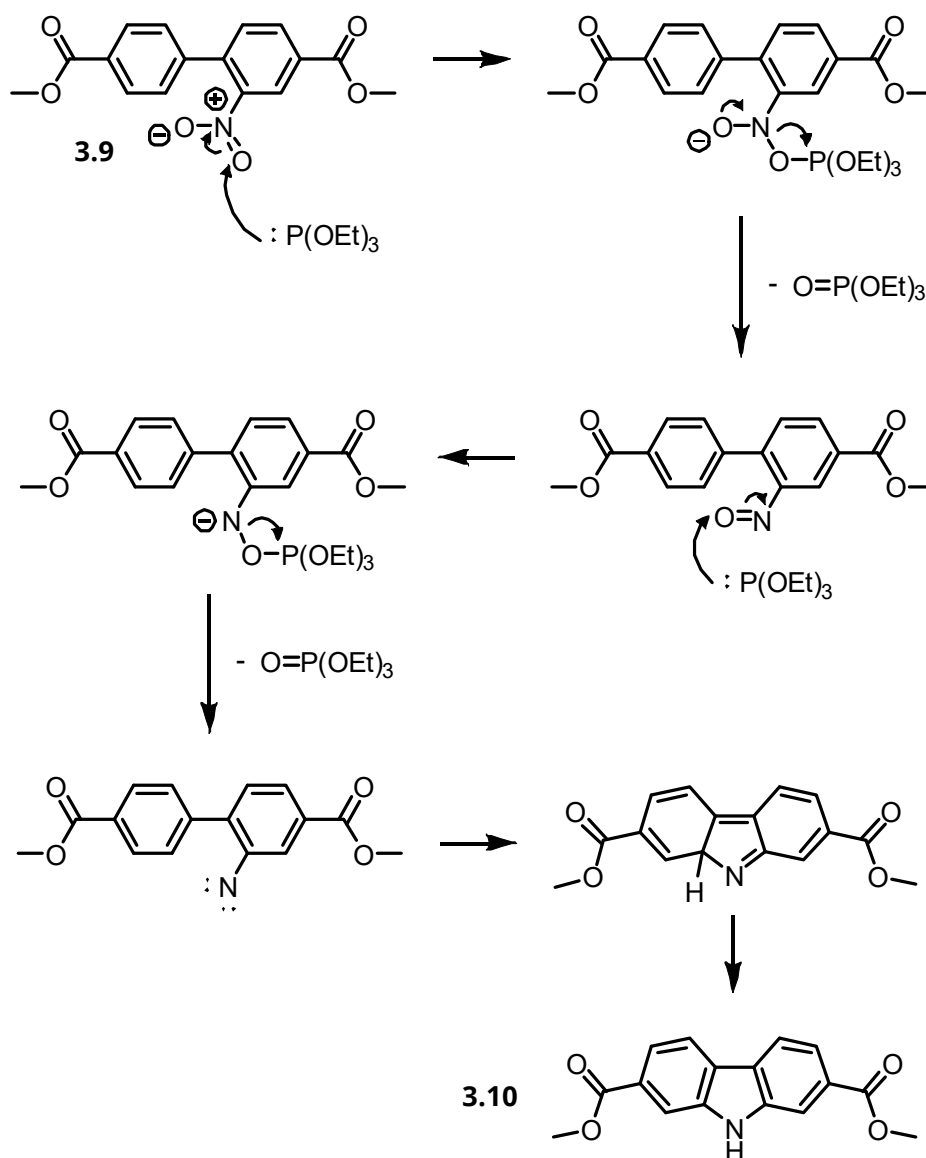
Figure 3.3: ¹H NMR spectrum of **3.9** in CDCl₃ at 293 K.

The conversion of nitrobiaryl **3.9** to the corresponding dimethyl 9*H*-carbazole-2,7-dicarboxylate (**3.10**) was carried out via a Cadogan nitrene insertion reaction using triethylphosphite.⁶



Scheme 3.3: Cadogan nitrene insertion of dimethyl 2-nitro-[1,1'-biphenyl]-4,4'-dicarboxylate.

The affinity of phosphorus for oxygen is so great⁷ that it can abstract oxygen from the aryl nitro and resulting intermediate nitroso group (see Scheme 3.4). The reactive nitrene that is formed then undergoes rapid cyclisation breaking the aromaticity of the neighbouring ring which in turn is quickly re-established by proton transfer to the nitrogen atom.



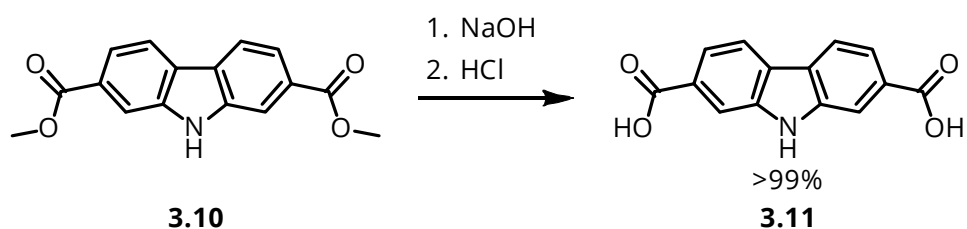
Scheme 3.4: Proposed mechanism for the Cadogan nitrene insertion of dimethyl 2-nitro-[1,1'-biphenyl]-4,4'-dicarboxylate.

The isolated carbazole diester **3.10** exhibited the predicted strong blue fluorescence expected of carbazole (see Scheme 3.4). Once the reaction was complete as, indicated by the thin layer chromatographic analysis (TLC), the excess triethylphosphite was distilled from the reaction before triturating the solid residue with methylene chloride.



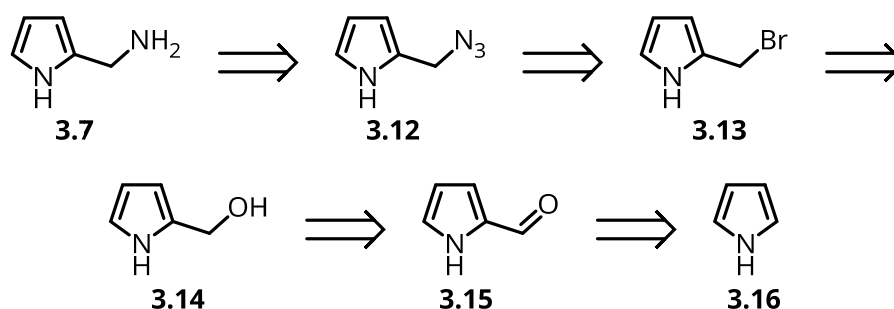
Figure 3.4: Saturated solution of **3.10** in ethyl acetate under natural light (left) and 254 nm lamp (right).

Hydrolysis of the resulting dimethyl [1,1'-biphenyl]-4-4'-dicarboxylate **3.11** under basic conditions yielded the diacid (**3.11**) in high yield (>99%) as shown in Scheme 3.5.



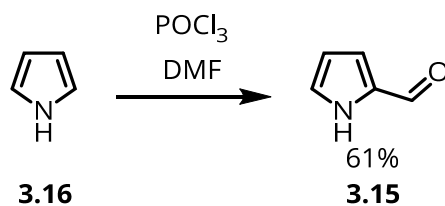
Scheme 3.5: Base hydrolysis of dimethyl [1,1'-biphenyl]-4-4'-dicarboxylate.

Sourcing the (1*H*-pyrrol-2-yl)-methanamine (**3.7**) used by Curiel *et al.* proved to be very difficult. Commercial prices as high as USD \$700 g⁻¹, led to the decision to synthesize it in house. The proposed method (see Scheme 3.6) was based on formation of an aldehyde precursor followed by reduction to the alcohol and conversion to the bromide before converting through to the free base amine.



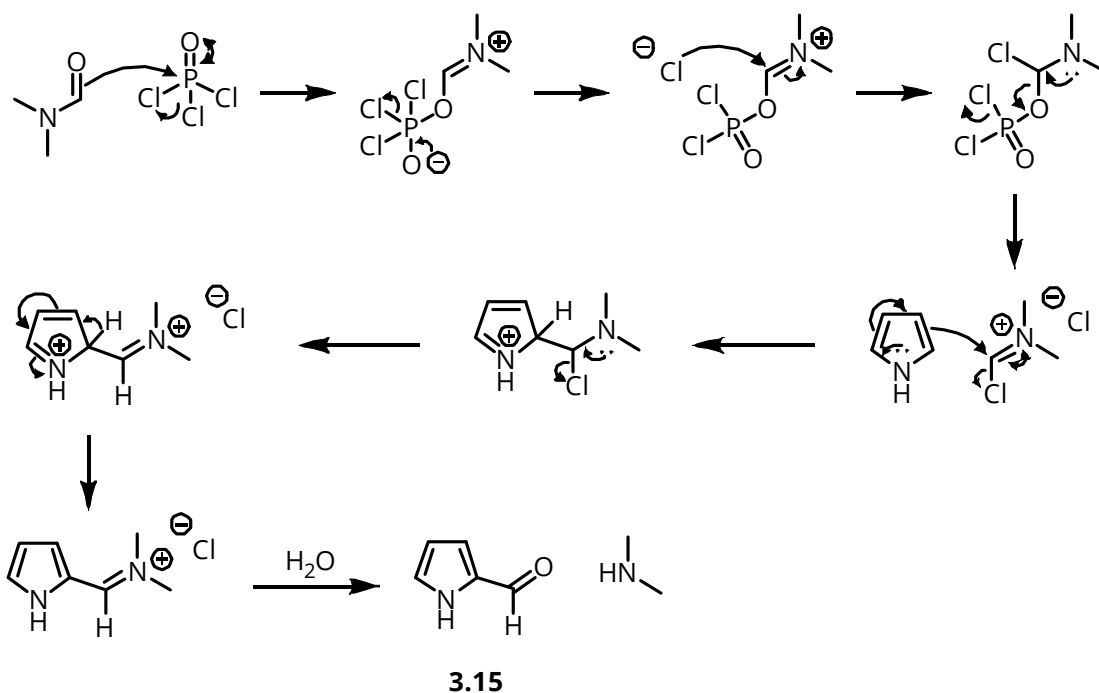
Scheme 3.6: Retrosynthetic analysis of (1*H*-pyrrol-2-yl)-methanamine.

For this procedure pyrrole was used as a starting material and converted to the respective 1*H*-pyrrole-2-carbaldehyde (**3.15**) by a Vilsmeier-Haack reaction (Scheme 3.7).



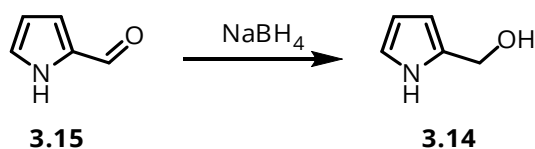
Scheme 3.7: Vilsmeier-Haack reaction of pyrrole.

The formation of the chloroiminium ion is central to this reaction. Slow addition of phosphorus oxychloride to dimethylformamide yields the chloroiminium chloride complex (Scheme 3.8). The complex is then attacked by the nucleophilic pyrrole to yield the (1*H*-pyrrol-2-yl)-carbiminium chloride which quickly hydrolyses on addition of water to yield the desired pyrrole-2-carbaldehyde.



Scheme 3.8: Mechanism for the Vilsmeier-Haack reaction of pyrrole.

Following formation of the aldehyde, it was reduced with the mild reducing agent sodium borohydride (Scheme 3.9). The conversion was successful. However, it became apparent that the (1*H*-pyrrol-2-yl)-methanol (**3.14**) is particularly unstable, turning from a clear amber oil to a dark brown amorphous solid. The ¹H NMR spectrum in Figure 3.5 shows the formation of large broad resonances around 5.7 and 3.5 ppm as well as a complete loss of the H_a proton resonance for the corresponding hydroxyl group.



Scheme 3.9: Reduction of pyrrole-2-carbaldehyde by sodium borohydride.

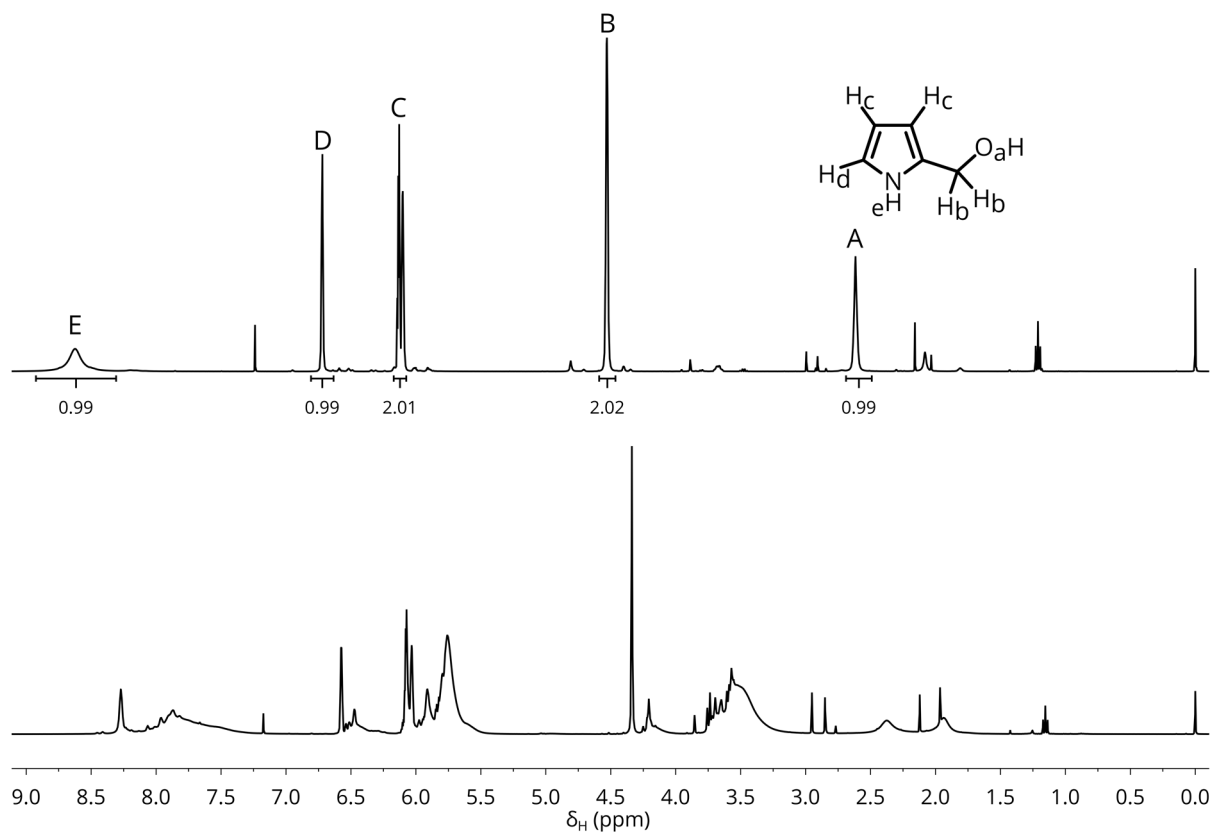
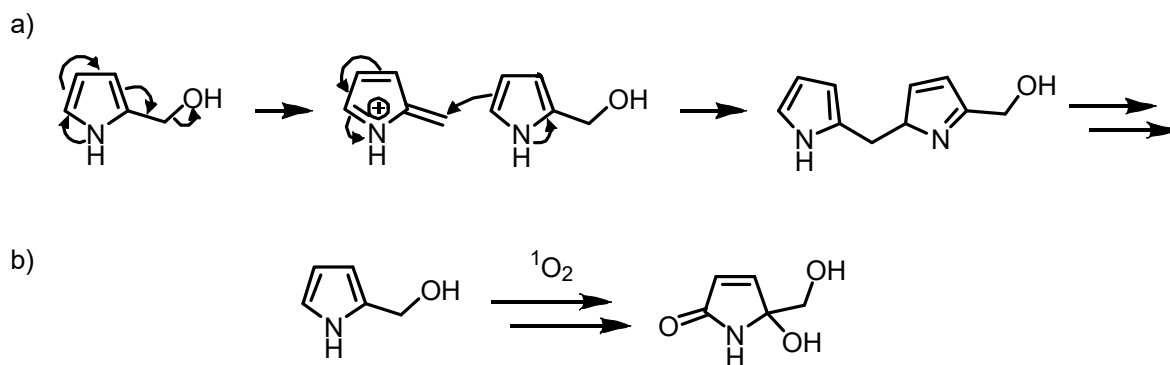


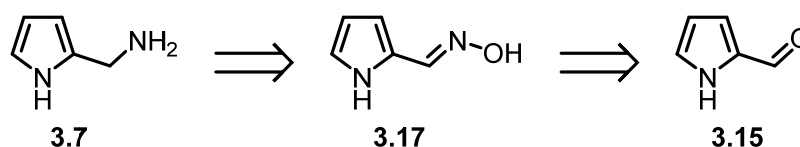
Figure 3.5: ^1H NMR spectra of **3.14** methanol (top) and its degraded structure (bottom) CDCl_3 at 293 K.

Pyrrole is known to be prone to uncontrolled oxidation, degradation and polymerisation leading to a rapid change of colour in air.⁸ Broad resonances are commonplace in the spectra of polymeric materials. The degradation of **3.14** is believed to be accelerated by the presence of the hydroxyl group which can act as a leaving group (see Figure 3.10). This issue is compounded by pyrroles known reactivity with singlet oxygen.⁹

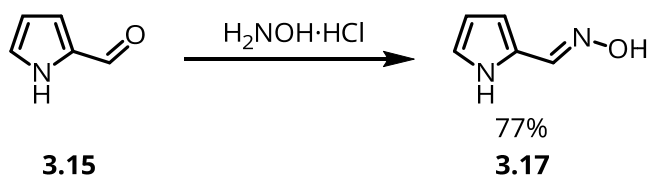


Scheme 3.10: Degradation mechanisms of (1H-pyrrol-2-yl)-methanol: a) polymerisation and b) oxidation.

Considering this reactivity (which would be exacerbated by conversion to a more labile leaving group such as a bromide suggested previously) the reaction plan was altered. As shown in Scheme 3.11 it was proposed that (1H-pyrrol-2-yl)-methanamine could be generated through reductive amination from the corresponding oxime (**3.17**) (Scheme 3.12).



Scheme 3.11: Retrosynthetic approach to (1H-pyrrol-2-yl)-methanamine.

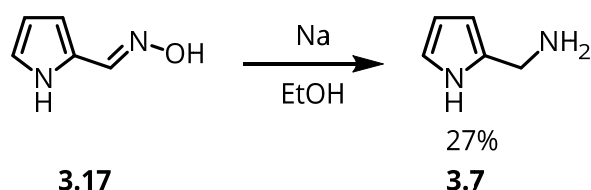


Scheme 3.12: Synthesis of 1H-pyrrole-2-carbaldoxime using hydroxylamine hydrochloride.

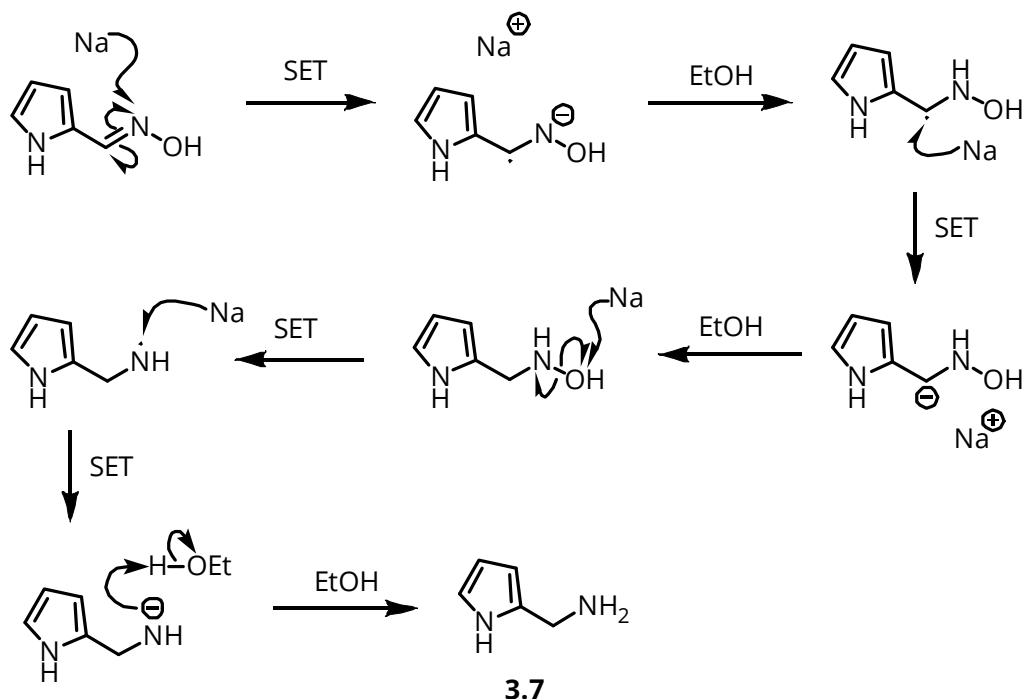
The oxime **3.17** was synthesized in a good yield of 77% and was identified by the appearance of a new broad resonance in the ^1H NMR spectrum at 11.16 ppm corresponding to the oxime hydroxyl proton. Subsequent reduction by hydrogen with palladium on carbon was attempted, but this reaction yielded a complex mixture from which the desired compound could not be isolated. It has been shown by Müller *et al.*¹⁰ that palladium on carbon predominantly results in the formation of secondary amine dimers. Also tested in this study was nickel on silica and alumina, Raney[®]-cobalt and rhodium on carbon, all of which had poor selectivity. The best candidate was nickel on silica which gave 71:29 preference to the primary amine.¹⁰ A variety of other reductive and

reductive amination methods were attempted on pyrrole oxime **3.17** and pyrrole carbaldehyde **3.15** respectively. Examples of these methods include sodium cyanoborohydride, ammonium formate on zinc and magnesium, but unfortunately these yielded comparable results or indeed no reaction at all.

After many unsuccessful attempts, a publication by Putochin in 1926 was found whereby they utilised the Bouveault–Blanc reduction of pyrrole oxime **3.17** to yield the (1*H*-pyrrol-2-yl)-methanamine (see Scheme 3.13).^{11†} In the mechanism outlined in Scheme 3.14 sodium provides a source of electrons for the single electron transfer (SET) steps involved. The compound passes through several radical compounds before reaching the desired pyrrole methylamine **3.7**.



Scheme 3.13: Bouveault–Blanc reduction of 1*H*-pyrrole-2-carbaldoxime.¹¹



Scheme 3.14: Mechanism for the Bouveault–Blanc reduction of 1*H*-pyrrole-2-carbaldoxime.

[†] The author is grateful to Mr Marcus Knappert for translation of this publication.

Promisingly, this reaction was successful in producing the desired amine. However, the isolated yields were poor (27%) affording an overall yield from pyrrole of 13%. Figure 3.6 shows a new resonance in the NMR spectrum at 3.9 ppm, with an integral of 2 corresponds to the newly formed methylene at the 2 position of pyrrole.

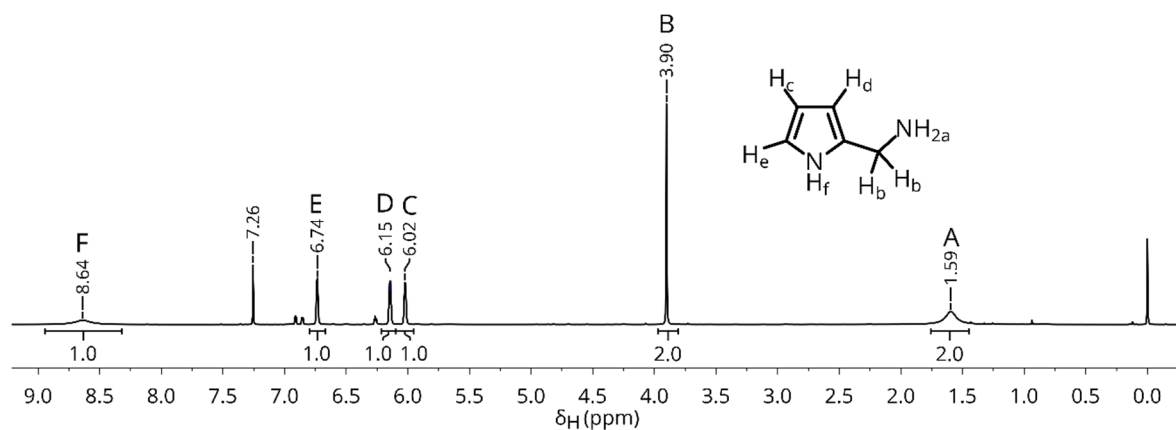
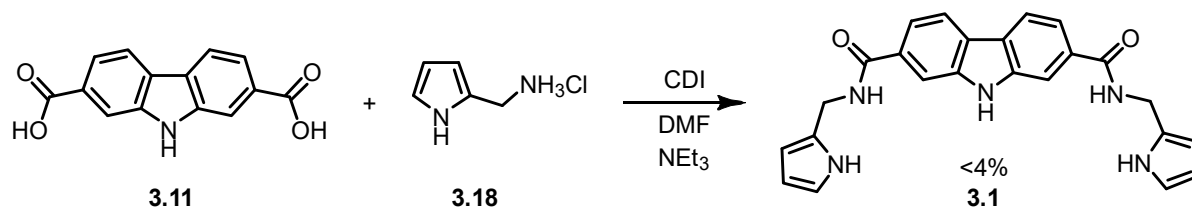


Figure 3.6: ^1H NMR spectrum of **3.7** in CDCl_3 at 293 K.

Fortunately, as a result of price fluctuations in the commercial market the cost of the hydrochloride salt of (1H-pyrrol-2-yl)-methylamine dropped to £88 g^{-1} during this study. Sourcing this compound allowed for the reaction outlined in Scheme 3.15.



Scheme 3.15: Synthesis of **1** using (1H-pyrrol-2-yl)-methylammonium hydrochloride.

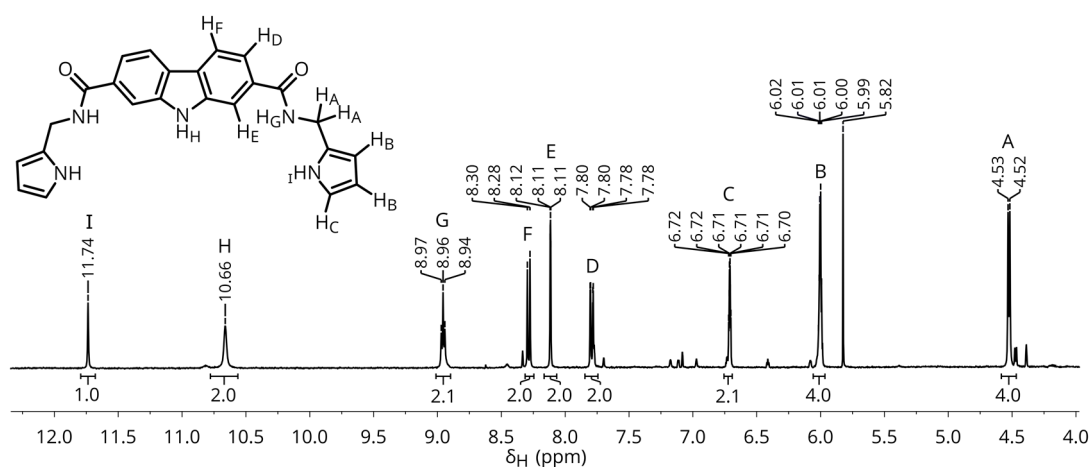
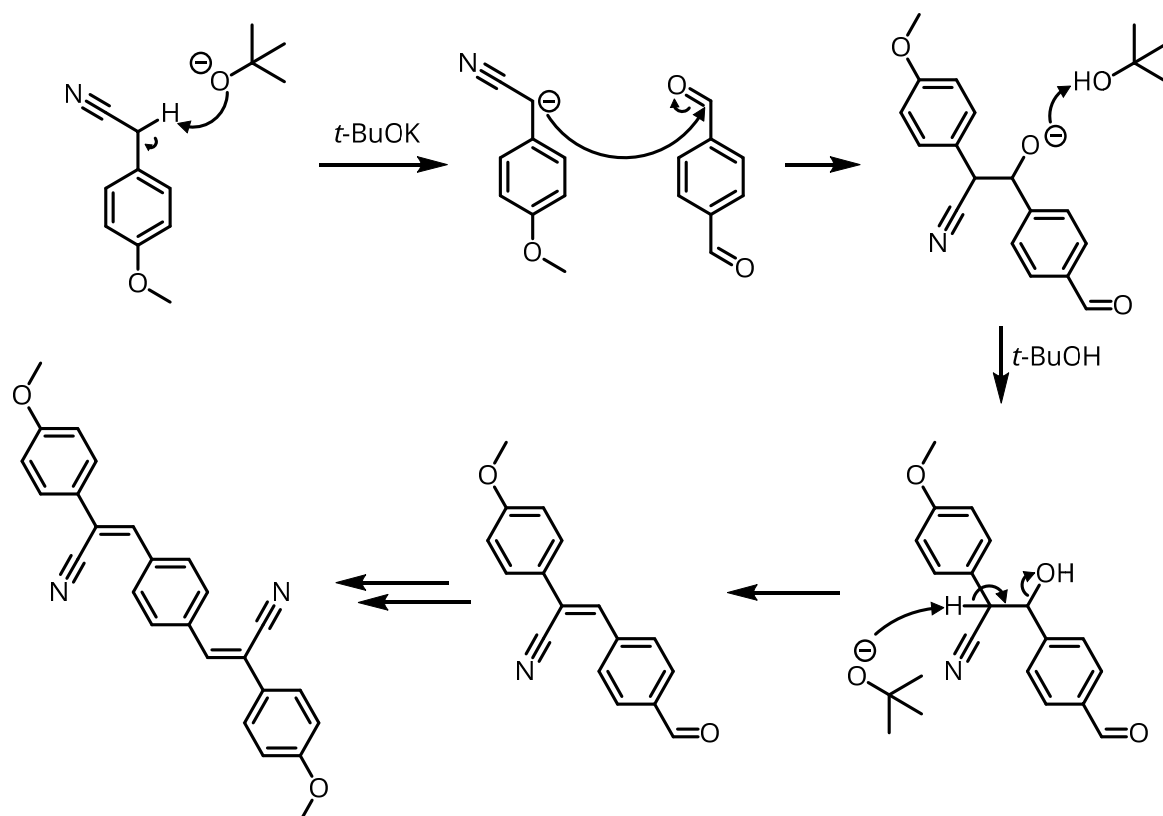
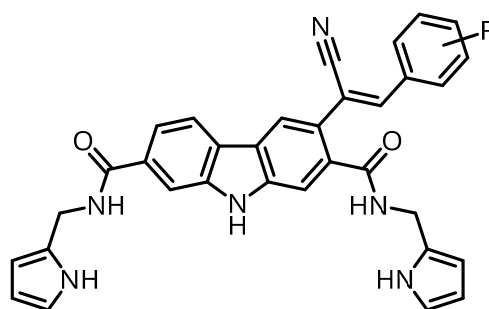


Figure 3.7: ^1H NMR spectrum of DPA sensor **3.1**.



Scheme 3.17: Proposed mechanism for the Knoevenagel condensation of 4-methoxyphenylacetonitrile and terephthalaldehyde.

It was proposed that the extended π -system resulting in addition of such structures to the aromatic framework of the carbazole component of the detector system **3.21** could induce significant changes to the emission or excitation wavelengths. This would require the presence of a formyl moiety on the carbazole ring to which these compounds could be attached. In addition to this, varying the substituents attached to the selected phenylacetonitrile compound can yield altered electronics, increased water solubility or even enable attachment of the detector to a polymeric substrate.



3.21

Figure 3.8: Phenylcyanovinylene modified carbazole sensor.

The software package GAMESS-US was used to optimise the structures and calculate the molecular orbitals.¹³ The electron density within HOMO and LUMO (Highest Occupied Molecular Orbital and Lowest Unoccupied Molecular Orbital) were shown to be evenly spread over the phenylcyanovinylene moiety on the target molecule as shown in Figure 3.9. This is substantially different to the original detector by Curiel *et al.* where the two highest electron density orbitals are located on the two pyrrole rings with the third highest electron density orbital on the ring. This reinforced the theory and provided justification for this approach to form the colorimetric detector.

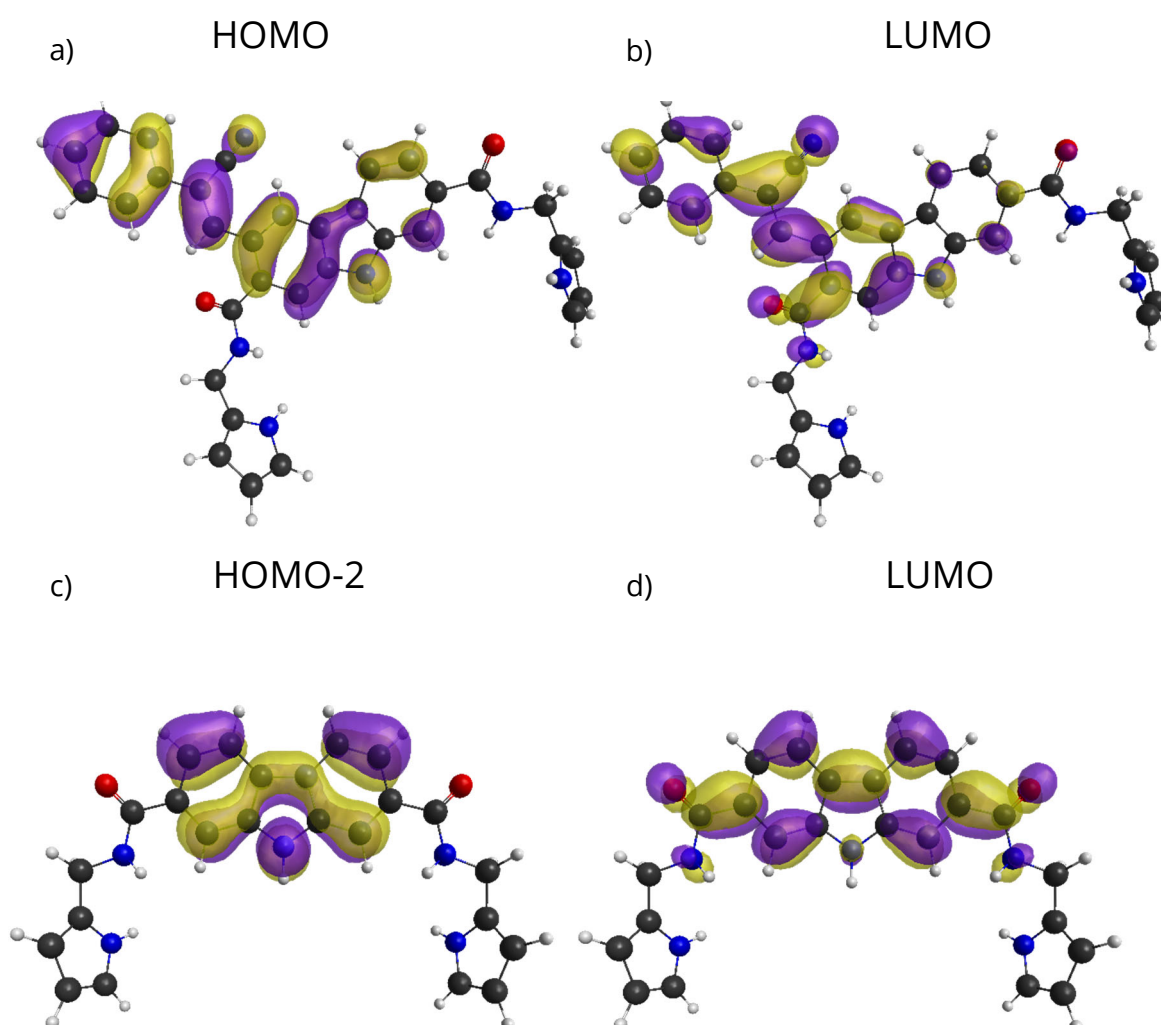
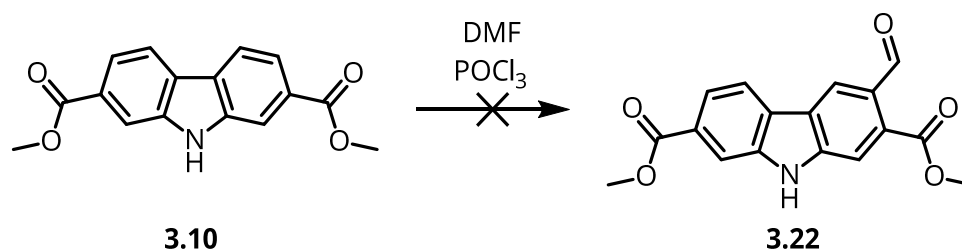


Figure 3.9: Contour plots of the a) HOMO and b) LUMO for the optimized structure of **3.21** and the c) HOMO-2 and d) LUMO for the optimized structure of **3.1**.

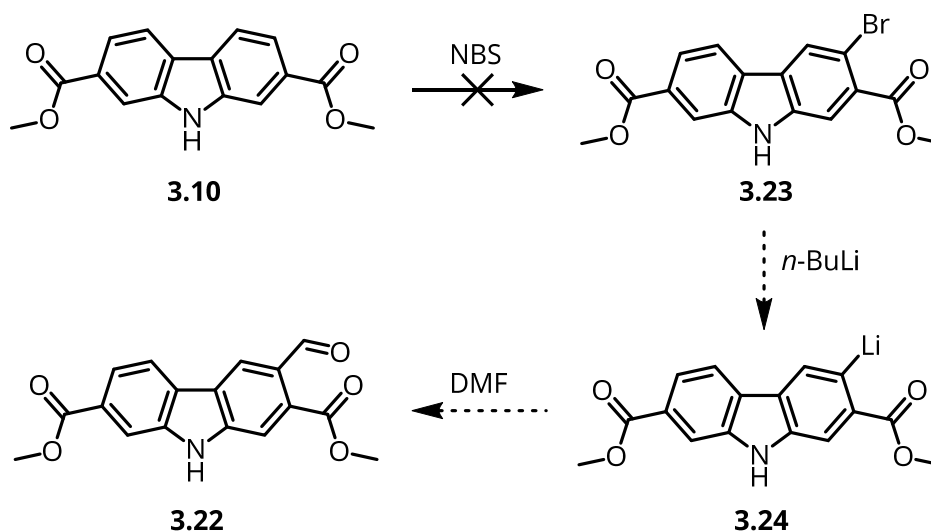
The first step towards this goal was to install the necessary formyl group in the 3-position of carbazole. Using similar chemistries to those that had been previously implemented on pyrrole, the Vilsmeier-Haack reaction was selected as a potential route to the

vinylphenylene substituted carbazole. However, use of these reagents proved unsuccessful, leaving only starting material.



Scheme 3.18: Vilsmeier-Haack reaction with 3.10.

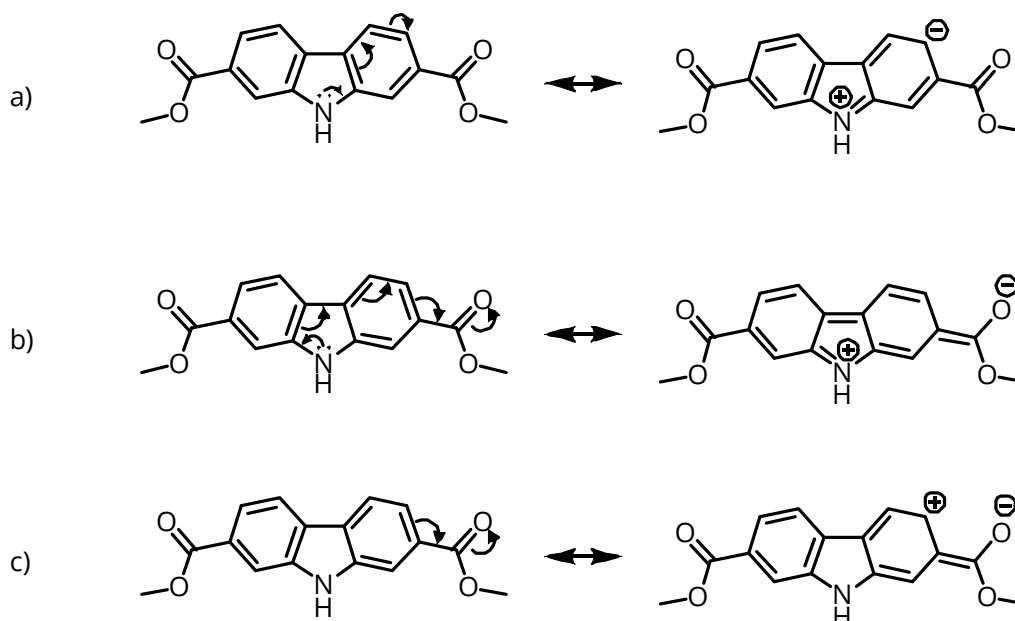
Following this unsuccessful approach to the 3-formyl derivative **3.22**, an alternative route was devised utilising metal-halogen exchange. The addition of a bromine substituent allows for exchange with a alkyllithium salt to yield the aryl lithium compound (see Scheme 3.19). N-bromosuccinimide (NBS) was selected as a brominating agent as it has been shown to effectively mono-brominate the 3-position of carbazole at high yields of up to 98%.¹⁴⁻¹⁶



Scheme 3.19: Attempted route to 3.22 via halogenation and metal-halogen exchange.

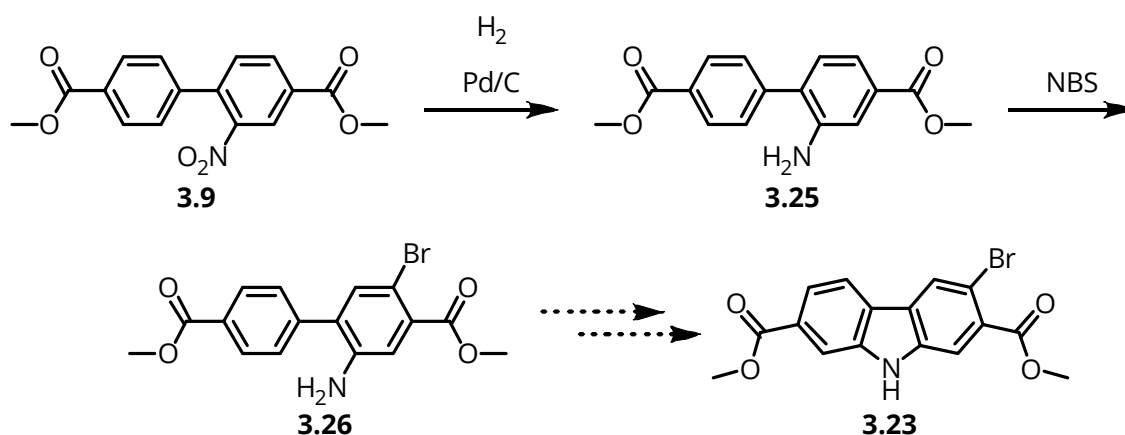
Despite this alteration in strategy, numerous unsuccessful attempts to install the bromide onto the carbazole led to the abandonment of this approach. It was originally hypothesized that the availability of the lone pair of the carbazole nitrogen to resonate into the ring and activate the para position as shown in Scheme 3.20a. The lack of reactivity observed towards electrophilic reagents used thus far suggests that presence of the ester groups is more detrimental than previously thought. The opportunity for

resonance from the nitrogen into the carbonyl (Scheme 3.20b) combined with the inherent deactivating nature of the ester group (Scheme 3.20c) overcomes this reactivity.



Scheme 3.20: Resonance structures of dimethyl 9H-carbazole-2,7-dicarboxylate.

To overcome the difficulties encountered with the bromination of carbazole there needed to be more electron density in the aromatic rings. An alternative route was devised whereby **3.9** would be reduced to its corresponding amine (**3.25**). This amine could enhance the reactivity of the ring such that bromination could occur. Following this the amine could be converted by oxidation back to the nitro by means of a peroxyacid to allow for the Cadogan nitrene insertion (see Scheme 3.21).



Scheme 3.21: Proposed approach to carbazole bromination by reduction and oxidation.

Nitrobiaryl **3.9** was reduced by catalytic hydrogenation using palladium on carbon (Pd/C) yielding dimethyl 2-amino-[1,1'-biphenyl]-4,4'-dicarboxylate (**3.25**) in an acceptable yield of 63%. The increased electron donation into the aromatic system was evident in the ^1H NMR spectrum as an upfield shift of the aromatic resonances. This reaction was found to be particularly sensitive to acid impurities. Oxidation of the catalyst occurred rapidly and the reaction would only leave starting material even after reacting for multiple days at elevated temperatures.

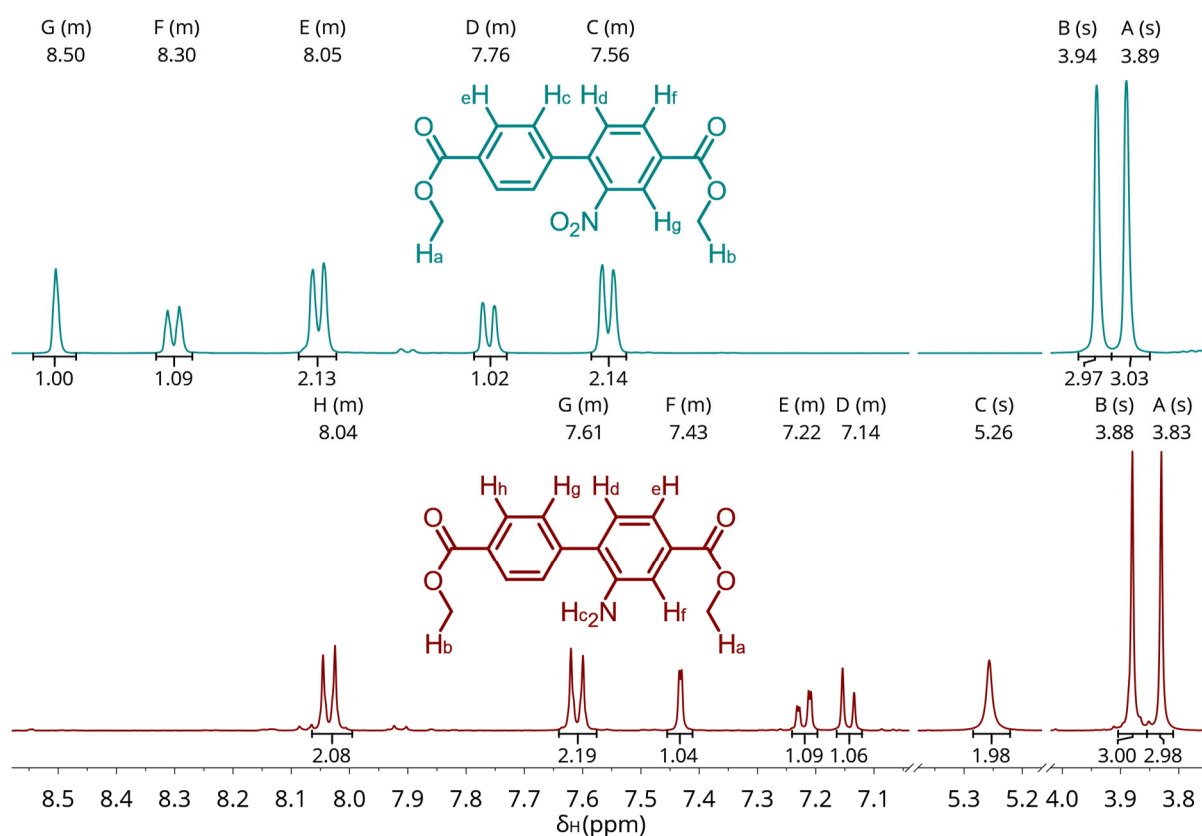


Figure 3.10: ^1H NMR of dimethyl 2-amino-[1,1'-biphenyl]-4,4'-dicarboxylate (bottom) and its precursor dimethyl 2-nitro-[1,1'-biphenyl]-4,4'-dicarboxylate (top) $\text{DMSO}-d_6$ at 293 K.

The bromination of **3.25** unfortunately yields an inseparable complex mixture of compounds suggesting the formation of multiple positional isomers most likely because of the increased reactivity of the ring system. There are three potential locations for installation of the bromine on the same ring as the amine (shown in Figure 3.11). The most favourable of these is position 5 with the least steric hindrance and para to the activating amine followed by ortho position 3. Position 6 is now least likely to be substituted because of its meta position relative to the amine. On the other ring there is now the opportunity to react in either the 2' or 3' position.

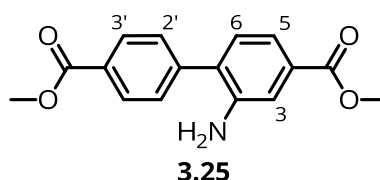


Figure 3.11: Potential bromination locations on **3.25**.

The 2' position is the more favourable position for attack as there is donation into the ring from the attached activating phenyl ring and amine as well as the deactivating but meta directing ester group. However, this enhancement may be reduced as a result of the dihedral angle between the rings preventing alignment of the p-orbitals. Should substitution occur at this 2' position then the Cadogan reaction should be able to proceed without hindrance as the nitrene that is formed has been shown to favourably insert between C-H bonds over carbon-halogen bonds.¹⁷

Should reaction have occurred at the 3' position the carbon-carbon free rotation could cause issues regarding the detection capability of the receptor for DPA. When the Cadogan nitrene insertion process takes place, the conformation of the biphenyl unit is vital since it can result in incorporation of the bromide into the binding pocket rendering it ineffective (see Figure 3.12). The conformer leading to **3.23a** is a higher energy conformation in contrast to conformer leading to **3.23b** because of the proximity of the more sterically hindering nitro and bromine substituents. However, the difference between the two energy levels of conformers leading to **3.23a** and **3.23b** is only 6 Kcal mol⁻¹ with the barrier to rotation from **3.23b** to **3.23a** being only 9 Kcal mol⁻¹ (see Figure 3.13). These low energies mean that at the high temperatures present in the Cadogan reaction there would be little population difference between the two conformers.

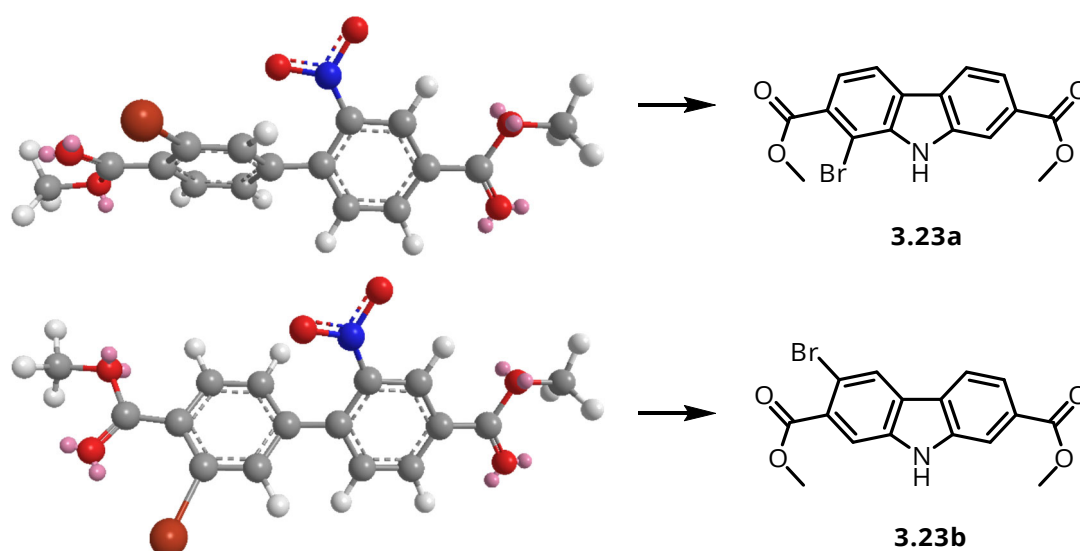


Figure 3.12: MM2 energy minimised conformer a (top) conformer b (bottom).

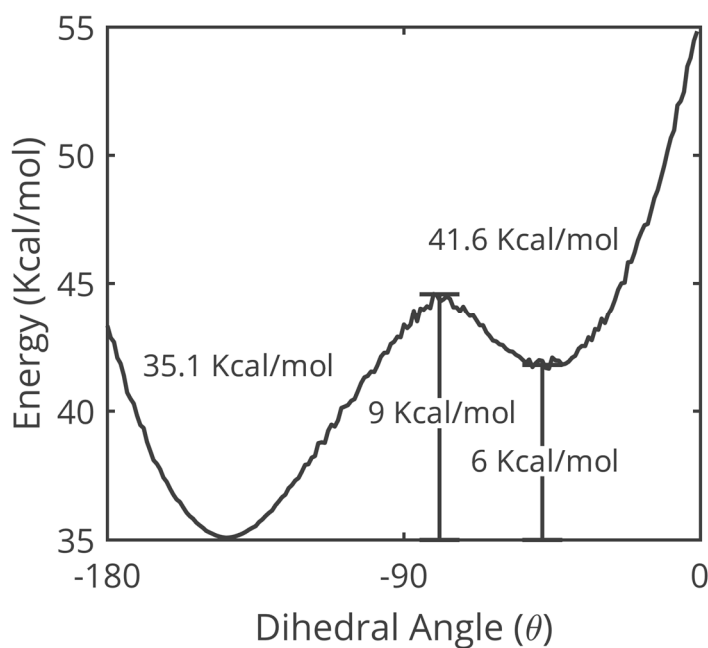


Figure 3.13: MM2 dihedral driver measured with energy minimisation using PerkinElmer Chem3D™.

3.2.3 Binding site modification

The limited progress with modification of the carbazole led to the search for alternative options in order to increase water solubility and suitability for the application. A potential target for alteration was the pyrrole chelating groups that provide hydrogen bonding to the DPA. An alternative to hydrogen bonding as the primary recognition motif is electrostatic attraction. Using the previous (1H-pyrrol-2-yl)-methylamine as the basis for a new design the compound the bisimidazolium compound **3.26** was deemed a potential

alternative (see Figure 3.14). The chain from the primary amine to the nitrogen of DPA is maintained but instead of the hydrogen bond donation the use of an imidazolium moiety provides potential for association via electrostatic forces of attraction. The added benefit of this structure is that it is anticipated that the charged moieties of the imidazolium moieties will aid water solubility of the DPA receptor compound. This modification allows for the use of similar chemistries to those used for the by substitution of the (1H-pyrrol-2-yl)-methylamine **3.7** with 3-(2-aminoethyl)-1-methyl-1H-imidazol-3-ium (**3.27**).

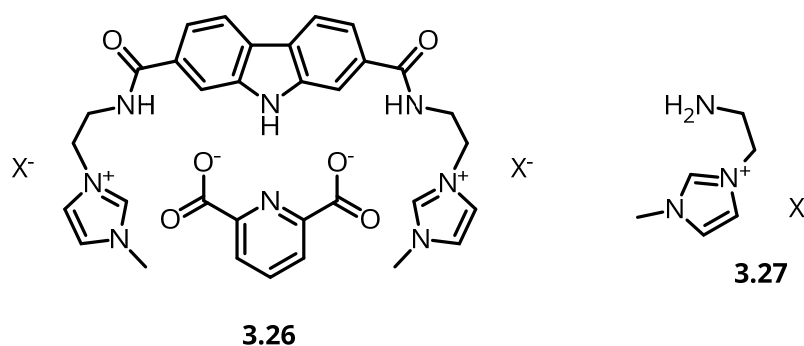
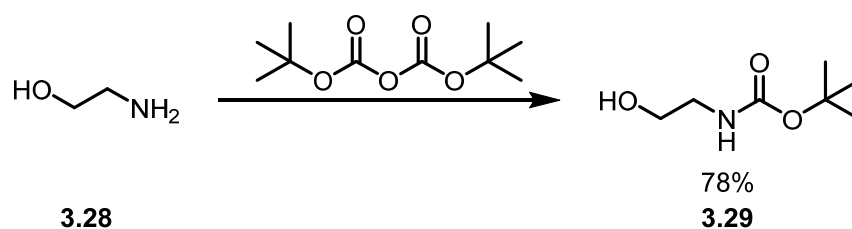


Figure 3.14: Proposed alternative detector showing binding pocket for DPA and the required imidazolium precursor.

In order to generate the desired imidazolium receptor units, the synthetic approach adopted involved at the outset the protection of ethanolamine **3.28** in the form of *N*-Boc-ethanolamine. Using Boc anhydride and sulfamic acid as a catalyst, the reaction was performed in the bulk and afforded the amine protected derivative **3.29** as a clear oil in good yield (78%).



Scheme 3.22: Boc protection of ethanolamine.

The ^1H NMR spectrum in Figure 3.15 shows the successful protection of the amine with the alcohol resonance at 5.28 ppm and the carbamate N-H resonance obscured by one of the methylene resonances at 3.61 ppm. However, it also shows there was residual Boc anhydride left in the product visible at 1.46 ppm.

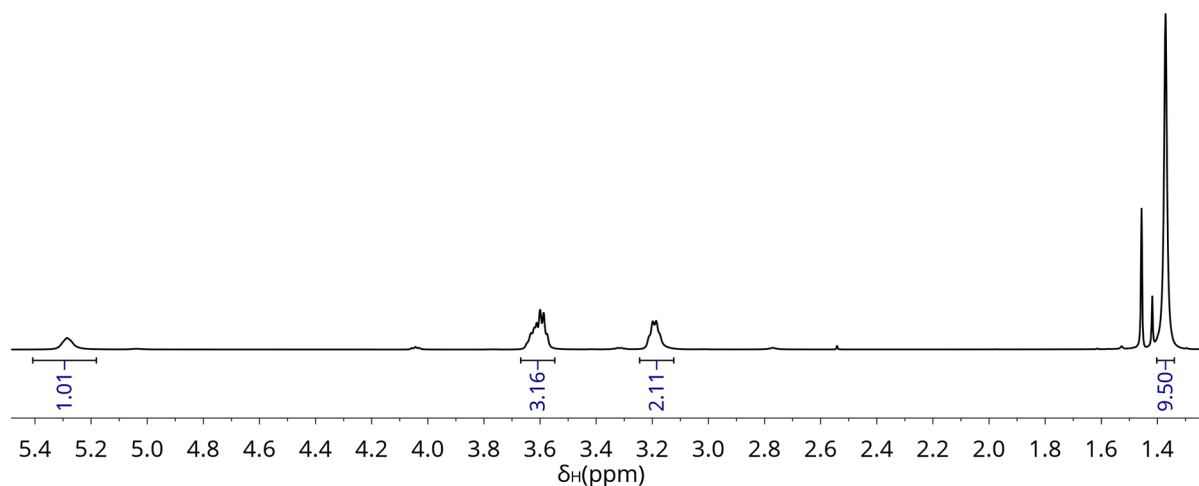
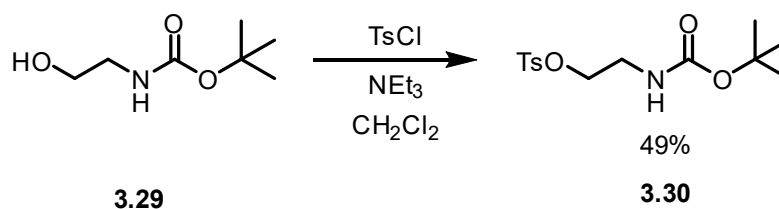


Figure 3.15: ^1H NMR spectrum of *N*-Boc-ethanolamine **3.29** in CDCl_3 at 293 K.

N-Boc-ethanolamine **3.29** was used without purification as it was found that the residual impurities could be removed in tandem with impurities formed from the following conversion of the alcohol to the tosyl ester **3.30**. This reaction was successful and following purification gave a moderate yield of 49%.



Scheme 3.23: Tosyl ester conversion of boc protected ethanolamine.

Comparison of the FTIR spectra of the alcohol **3.29** with the product of the reaction with tosyl chloride clearly reveals the absence of the broad hydroxyl stretch at 3339 cm^{-1} along with the appearance of the $\text{S}=\text{O}$ stretch at 1174 cm^{-1} as shown in Figure 3.16.

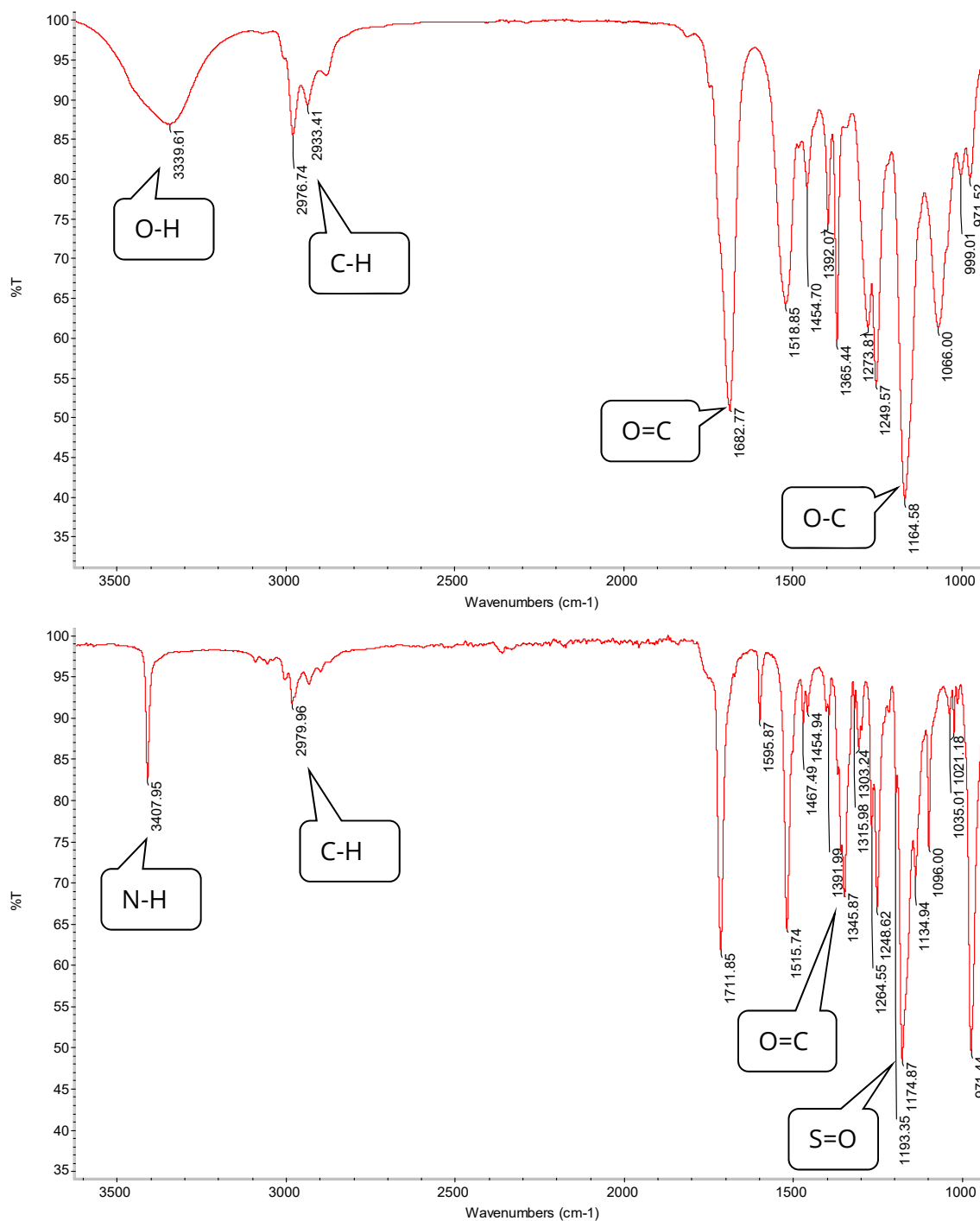
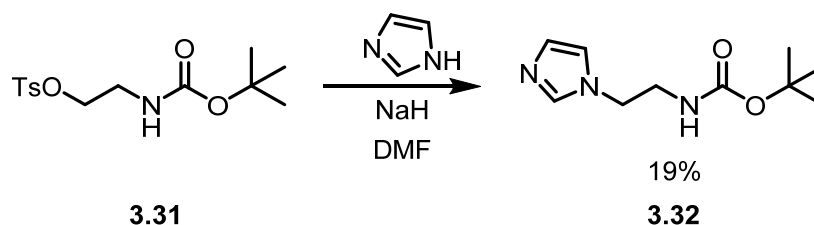


Figure 3.16: FTIR spectra of N-Boc-ethanolamine **3.29** (top) and O-Tosyl-N-Boc-ethanolamine **3.30** (bottom).

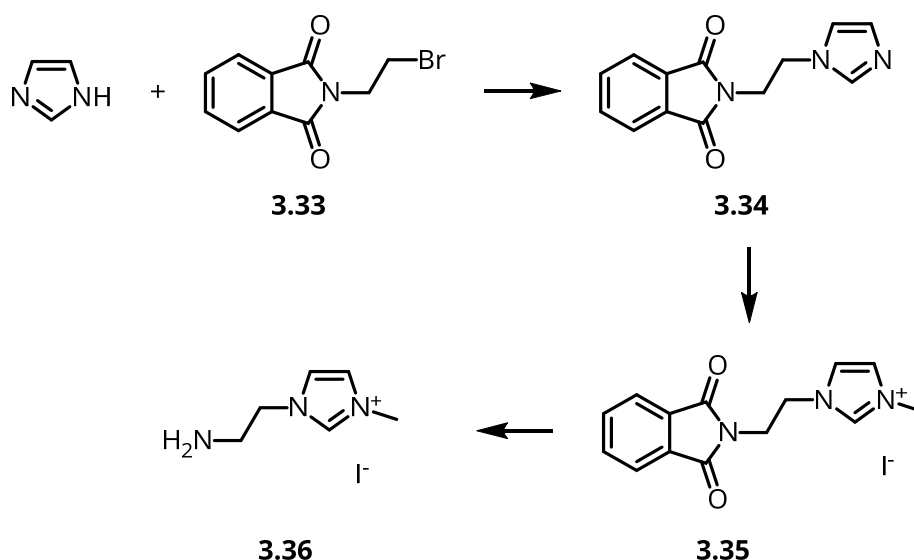
The confirmation of the reaction was further reinforced by means of mass spectrometry with compound **3.29** giving a sodiated mass ion at 184.0947 m/z matching the expected value of 184.0944 m/z. Similarly, the expected mass ion of 338.1033 m/z for the corresponding compound **3.30** was found at 338.1033 m/z.

The formation of the effective leaving group allows for facile substitution by means of an S_N2 reaction. Sodium hydride was used to deprotonate the imidazole in a solution of dimethyl formamide (DMF) followed by addition of **3.30** (Scheme 3.24).



Scheme 3.24: S_N2 displacement of a tosyl group by imidazole.

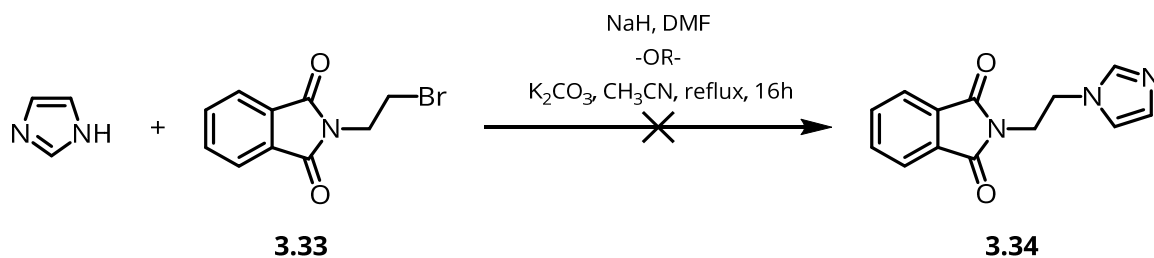
This reaction gave a light-yellow coloured oil in a poor yield (19%) taking the overall yield of this synthetic approach at this point to only 7.2%. With two reactions left to take place the approach was re-evaluated in search of a more efficient and scalable approach. A new route was identified, that would lead to the final product in three steps rather than the previous five. This new approach also gives a greatly improved overall atom economy of 45% compared to the previous approach which is only 20%.



Scheme 3.25: Proposed synthetic route to imidazolium precursor.

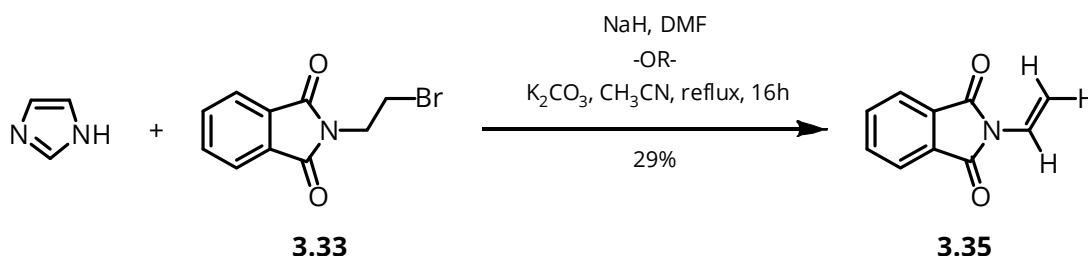
The use of the bromide as a labile leaving group allows for facile substitution by means of an S_N2 reaction. Sodium hydride was again used to deprotonate the imidazole in a solution of dimethyl formamide (DMF) followed by addition of *N*-(2-bromoethyl)-phthalimide. However, upon analysis by ^1H NMR spectroscopy expected resonances for

the imidazole ring were not observed. An alternative procedure was attempted using potassium carbonate in acetonitrile but produced similar results.



Scheme 3.26: Unsuccessful attempts at the S_N2 reaction to **3.33**.

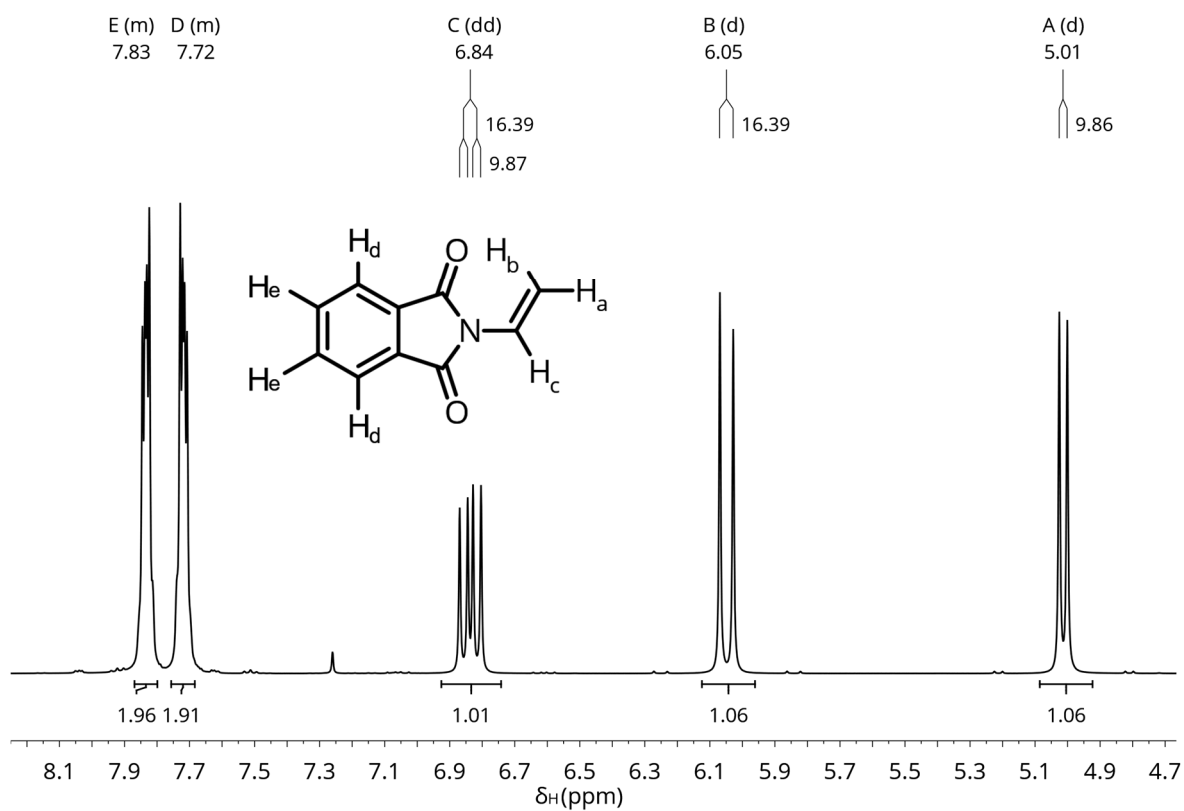
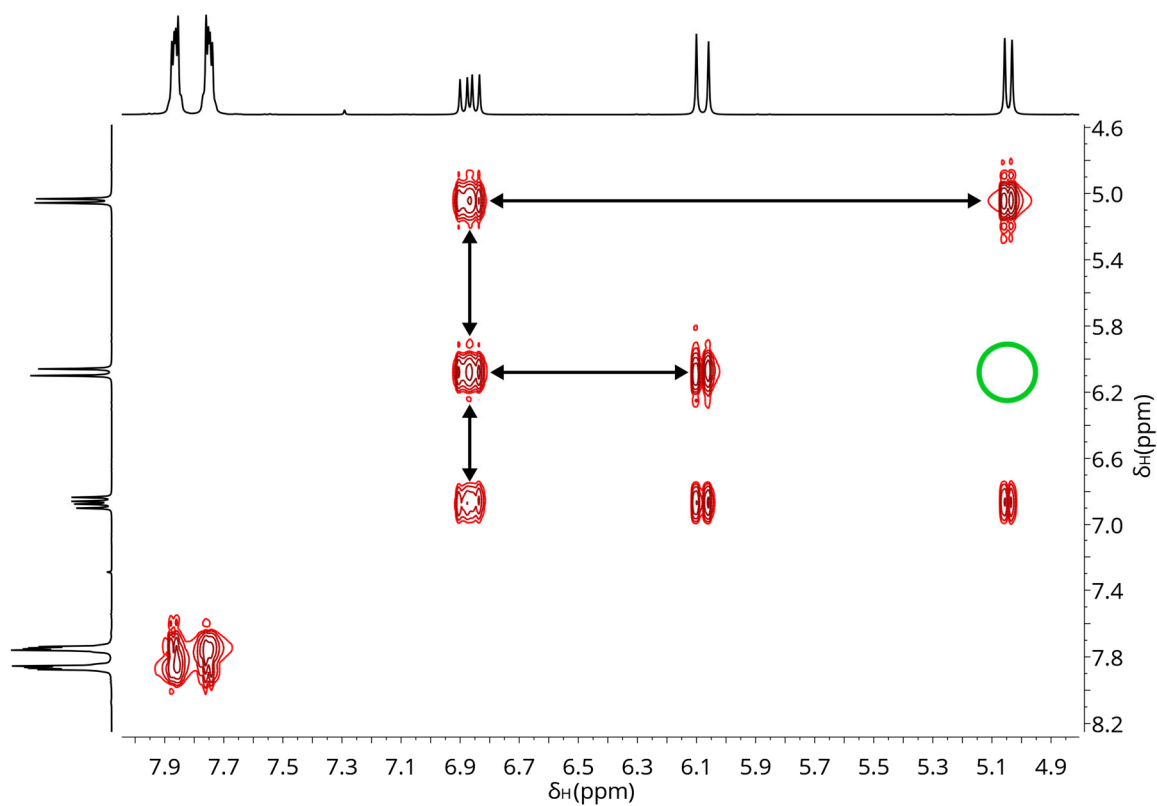
The ^1H NMR spectra (Figure 3.17) from these reactions suggested the formation of the elimination product **3.35** (Scheme 3.27). The expected multiplet with an integral of 4 protons arising from the aromatic phenyl ring was observed. However, the other proton resonances consist of a double doublet and two doublets with matching coupling values. Upon further inspection by means of 2D NMR techniques including ^1H - ^1H COSY, ^1H - ^{13}C HSQC and ^1H - ^{13}C HMBC it became apparent that the signals at 5.01 and 6.01 ppm corresponded to geminal protons. It is widely known that alkene proton coupling is greater for trans pairs of protons than cis pairs of protons. Using this the resonance with the larger coupling value can be attributed to the trans proton and *vice versa*.



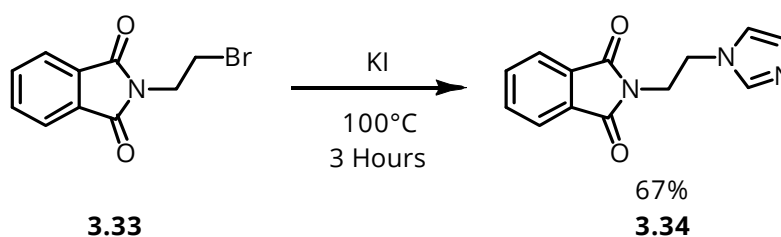
Scheme 3.27: Elimination product from **3.33**.

This is an example of an ABC type system where each signal comprises of two different coupling values leading to the formation of a double doublet (e.g. proton C exhibits coupling from J_{AX} and J_{BX} splitting twice to show a double doublet). However, in this particular case $J_{AB} \approx 0$, which causes very little splitting resulting in the appearance of one double doublet and two doublets. This is also the reason why the expected resonances in the 2D ^1H - ^1H COSY at 5.01, 6.01 ppm were not observed as shown in Figure 3.18.

$$J_{AB} \approx 0 \text{ Hz} \quad J_{AC} = 10.0 \text{ Hz} \quad J_{BC} = 16.0 \text{ Hz}$$

Figure 3.17: ^1H NMR spectrum of **3.35**.Figure 3.18: ^1H - ^1H COSY spectroscopy with green circle denoting missing signal at 5.01 ppm, 6.05 ppm.

An alternative procedure was found where potassium iodide and excess imidazole were combined in the melt at 100 °C to which was added **3.33**. Following extraction by Soxhlet in toluene, the resulting solution could be concentrated and recrystallized from ethyl acetate and petroleum ether. Recrystallization by this method, while successful in reducing the amount of residual imidazole, failed at removing it completely. It was found that trituration with water was a more effective method of purification that exploited the high solubility of imidazole and allowed for its easy isolation as can be seen in Figure 3.19.



Scheme 3.28: synthesis of 1H-1-methyl-3-(2-phthalimidylethyl)-imidazole

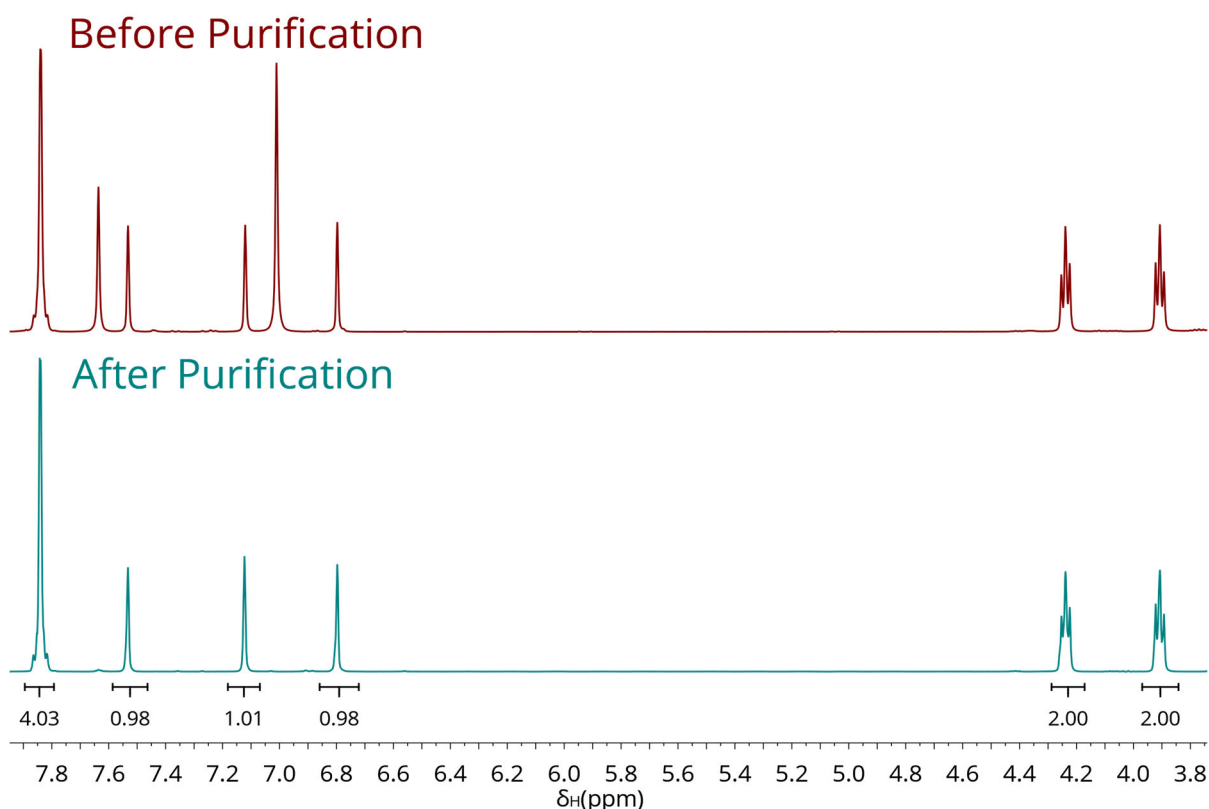
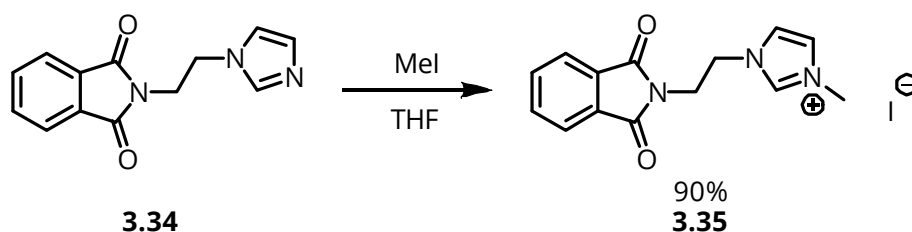


Figure 3.19: ^1H NMR spectrum of 1H-1-methyl-3-(2-phthalimidylethyl)-imidazole before and after trituration.

Following purification, the imidazole ring can be converted to the imidazolium iodide salt by addition of methyl iodide in THF as shown in Scheme 3.29. This reaction results in

precipitation of the iodide salt and affords high yields (*ca.* 90%). The ^1H NMR spectrum of **3.35** shows a downfield shift of the imidazole resonances, which is an indication of increased deshielding as a result of the positive charge now present.



Scheme 3.29: Methylation of **3.34**.

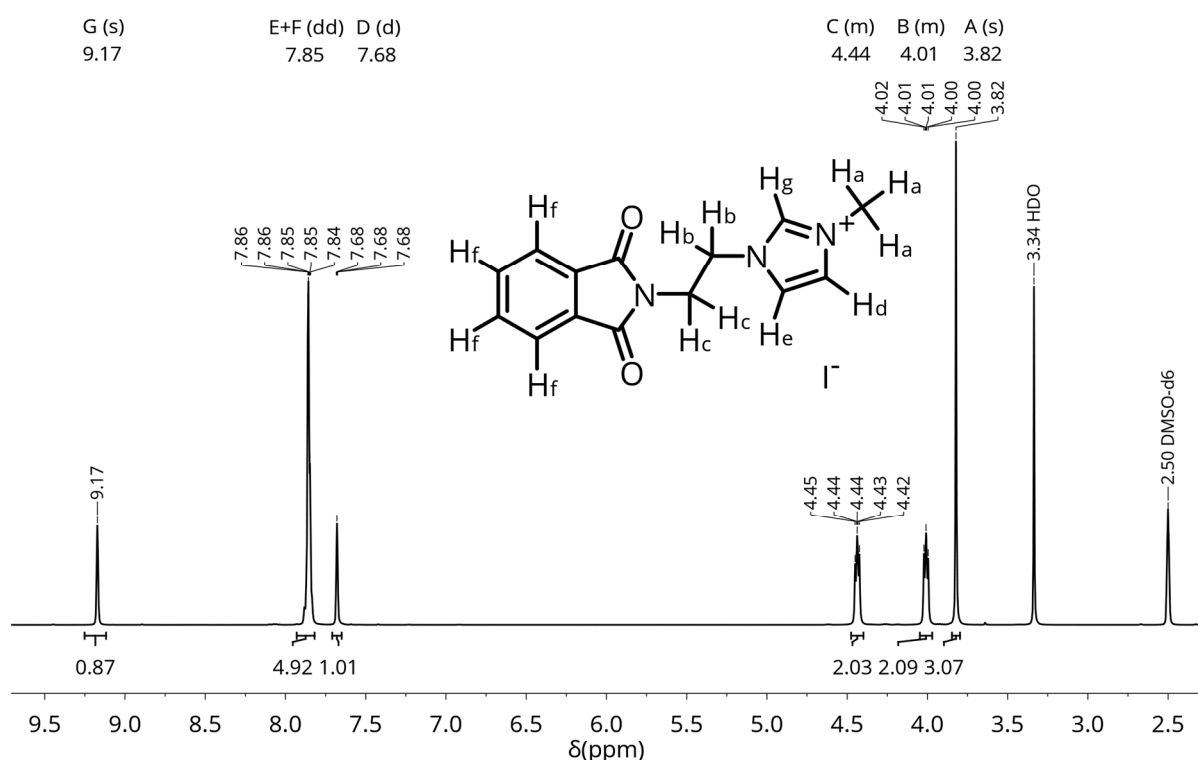
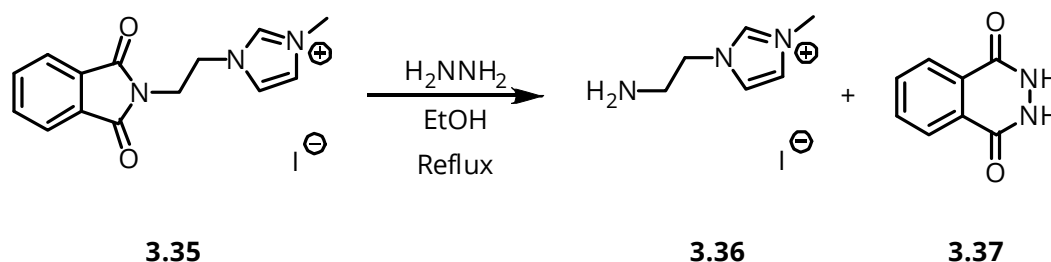


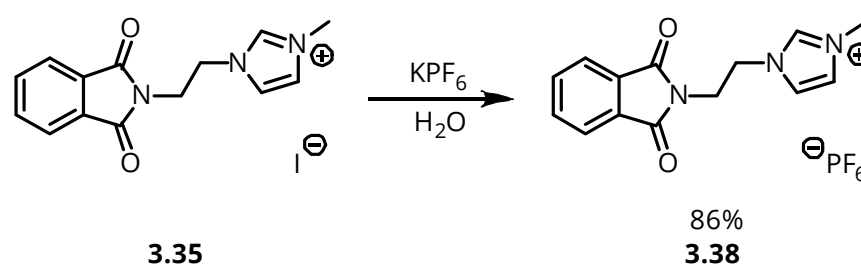
Figure 3.20: ^1H NMR of 1H-1-methyl-3-(2-phthalimidylethyl)-imidazole iodide **3.35**.

Once the methylation was completed, the phthalimide protecting group could be removed using hydrazine hydrate. (see Scheme 3.30) However, in this instance it was complicated by the relative solubility of the by-product. While the majority of the phthalhydrazide precipitated from solution as the ethanol was cooled to room temperature, substantial quantities remained. A variety of biphasic solvent extractions failed to purify the compound. Reverse phase column chromatography was attempted in the hope that the charged ionic species would elute faster than the phthalhydrazide but this was also unsuccessful.



Scheme 3.30: Hydrazinolysis of 1H-1-methyl-3-(2-phthalimidylethyl)-imidazolium iodide **3.35**.

In order to alter the solubility of the ionic compound **3.36** the precursor material could be exchanged with an alternative counterion. The counterion selected was hexafluorophosphate because of its well-known solubility characteristics in organic solvents. The iodide salt **3.35** dissolves readily in water and the resulting ion exchanged product formed an insoluble white precipitate that was isolated by filtration in good yield (86%).



Scheme 3.31: Counter-ion exchange of 1H-1-methyl-3-(2-phthalimidylethyl)-imidazolium hexafluorophosphate **3.38**.

Hydrazinolysis was carried out on **3.38** with the same method used in Scheme 3.30. Unfortunately, the arising product was also inseparable from the phthalhydrazine by-product.

3.3 Conclusion

The original detector **3.1** proposed by Curiel *et al.* has been synthesized and shown to be inappropriate for deployment in a surface spray type disclosure formulation as a result of its lack of water solubility and compound instability.

Following this discovery attempts were made to improve the colorimetric response of **3.1** by introducing structural changes to the carbazole moiety that would expand the π system. Computational studies showed that this could be effective as the HOMO and

LUMO were now clearly spread wider. This approach was restricted by the unexpected low reactivity of **3.10** which could not be resolved with the alternative routes attempted.

The issue of water solubility was tackled by attempting to introduce a charged imidazolium species **3.27**. Routes to this compound were optimized using the *N*-(2-bromoethyl)-phthalimide approach but were not concluded because of difficulties encountered with purification at the final stage.

Disappointingly, as a result of the numerous setbacks encountered during this work the proposed electrostatic detector **3.26** was not synthesized. The mixture of **3.36** and **3.37** could not be separated in order for the coupling synthesis to take place.

The priority for continuation of this work would be completion of the synthesis of modified of the sensor **3.26** with optimisation of purification procedures following the hydrazinolysis of phthalimide imidazolium iodide **3.35** leading to the synthesis of the amine imidazolium salt **3.27**.

Further to this, continuation of the modification of the ring structure of the carbazole component of the detector could still yield the intended colorimetric response as suggested by the computational calculations (see page 85). Alternative procedures to those already attempted here were considered, such as palladium coupling of phenyl groups directly to the carbazole moiety. However most of these rely on the formation of the aryl halide. As such, further investigation into successful halogenation methods for the dicarbonyl carbazole could assist results for multiple reaction pathways.

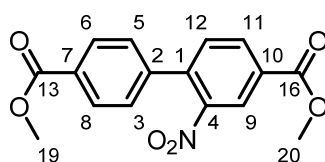
3.4 Experimental

3.4.1 Materials

All materials used were purchased from Sigma-Aldrich and Alfa Aesar with the exception of (1*H*-pyrrol-2-yl)-methylamine which was purchased from Fluorochem. Pyrrole was purified by distillation before use. Thin layer chromatography (TLC) carried out on Merck silica gel aluminium backed plates (20 × 6 mm) and visualised via UV fluorescence, ninhydrin or potassium permanganate staining solutions. Column Chromatography was carried out using Aldrich Silica gel (particle size 40-63 μm).

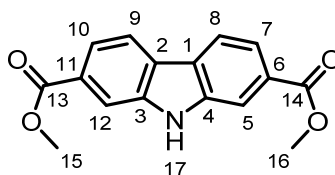
3.4.2 General Experimental

In addition to the methods cited in chapter 2; melting points were determined either using an Omega MPS10 for range values or a TA instruments TA-Q2000 DSC for point values. Mass spectrum data was collected by ESI analysis on a Thermo Scientific LTQ-Orbitrap XL mass spec using the Orbitrap detector operating at 100 K resolution, in positive ion mode. Mass tolerance of matching to proposed compound was limited to 5 ppm. Molecular orbital calculations were carried out with the GAMESS-US program.¹³ The electronic absorption spectra for the different compounds were calculated with the time-dependent density functional theory (TD-DFT) at the B3LYP/6-31G* level of theory on the relaxed geometries calculated at the same B3LYP/6-31G* level of theory.

3.4.3 Synthesis of dimethyl 2-nitro-[1,1'-biphenyl]-4,4'-dicarboxylate (**3.8**).

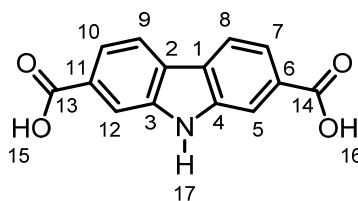
Dimethyl [1,1'-biphenyl]-4,4'-dicarboxylate (11.30 g, 41.81 mmol) was dissolved in conc. H₂SO₄ (150 mL) before being cooled to 0 °C. A solution of HNO₃ (2.90 mL, 70%, 45.42 mmol) in H₂SO₄ (6 mL) was added dropwise over 20 minutes keeping the solution between 0 and 5 °C. Once complete the solution was poured over ice, extracted with ethyl acetate (4 × 150 mL) and washed sequentially with saturated sodium hydrogen carbonate (150 mL) and brine (150 mL). The resulting solution was concentrated *in vacuo* to yield an off-white solid (12.77 g, 97%). mp(*i*PrOH) 98-99 °C, ν_{\max} (cm⁻¹) 3092 (C-H), 1718 (C=O), 1527 (NO₂), 1283 (NO₂), 1240 (C-O), 1114 (C-O), δ_{H} (400 MHz, d₆-DMSO) 8.50 (1 H, s, **9**), 8.30 (1 H, d, *J* 8.0, **11**), 8.05 (2 H, d, *J* 8.5, **8+6**), 7.75 (1 H, d, *J* 8.0, **12**), 7.55 (2 H, d, *J* 8.5, **5+3**), 3.93 (3 H, s, **20**), 3.88 (3 H, s, **19**) ppm, δ_{C} (100 MHz, d₆-DMSO) 165.7 (**16**), 164.2 (**13**), 148.4 (**4**), 140.9 (**10**), 138.5 (**7**), 133.1 (**11**), 132.7 (**12**), 130.5 (**1**), 129.8 (**2**), 129.5 (**8+6**), 128.2 (**5+3**), 124.9 (**9**), 52.9 (**20**), 52.3 (**19**) ppm, *m/z* expected 316.0743 found 316.0815 [M+H].

3.4.4 Synthesis of dimethyl 9*H*-carbazole-2,7-dicarboxylate (**3.10**).



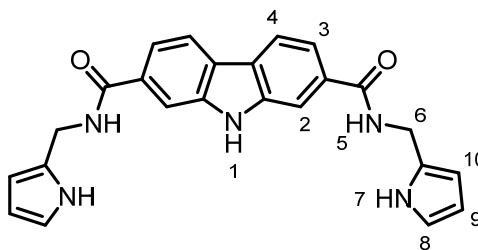
Dimethyl [1,1'-biphenyl]-4-4'-dicarboxylate (5.0 g, 15.9 mmol) and triethylphosphite (100 mL) were combined and maintained under reflux overnight. Excess triethylphosphite was distilled off under reduced pressure. The resulting orange residue was filtered and washed with dichloromethane to yield an off-white solid (2.69 g, 60%). mp_{DSC} 264 °C, ν_{\max} (cm⁻¹) 3289 (N-H), 2950 (C-H), 1692 (C=O) 1206.7381 (C-O), 1284.841(C-O), δ_{H} (400 MHz, d₆-DMSO) 11.83 (1 H, s, **17**), 8.34 (2 H, d, *J* 8.5, **9+8**), 8.18 (2 H, d, *J* 1.5, **12+5**), 7.82 (2 H, dd, *J* 8.5, 1.5, **10+7**), 3.91 (6 H, s, **16+15**) ppm, δ_{C} (100 MHz, d₆-DMSO) 166.7 (**13+14**), 140.3 (**6+11**), 127.7 (**1+2**), 125.2 (**4+3**), 121.2 (**9+8**), 119.6 (**10+7**), 112.8 (**12+5**), 52.2 (**16+15**) ppm. *m/z* expected 284.0845 found 284.0917 [M+H].

3.4.5 Synthesis of 9*H*-carbazole-2,7-dicarboxylic acid (**3.11**).



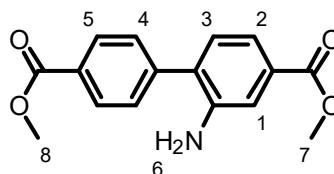
Dimethyl 9*H*-carbazole-2,7-dicarboxylate (2.0 g, 7.1 mmol) was suspended in sodium hydroxide solution (0.44 M, 125 mL) and brought to and maintained under reflux. Once the dimethyl 9*H*-carbazole-2,7-dicarboxylate had completely dissolved the reaction was cooled and slowly acidified with hydrochloric acid (0.12 M, 500 mL). The resulting solid was filtered and washed with distilled water to yield a beige coloured solid (1.8 g, >99%), mp. >350 °C, ν_{\max} (cm⁻¹) 3291 (N-H), 2951 (C-H), 1707 (C=O), 1207 (C-O), δ_{H} (400 MHz, d₆-DMSO) 12.94 (2 H, s, **15+16**), 11.78 (1 H, s, **17**), 8.29 (2 H, d, *J* 8.0, **9+8**), 8.14 (2 H, d, *J* 1.5, **12+5**), 7.80 (2 H, dd, *J* 8.0, 1.5, **10+7**) ppm, δ_{C} (100 MHz, d₆-DMSO) 166.8, 140.4, 127.8, 125.2, 121.3, 119.6, 112.84, 52.2 ppm.

3.4.6 Synthesis of *N*²,*N*⁷-bis((1*H*-pyrrol-2-yl)-methyl)-9*H*-carbazole-2,7-dicarboxamide (**3.1**).

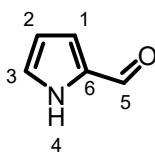


9*H*-carbazole-2,7-dicarboxylic acid (77 mg, 0.3 mmol) was dissolved in anhydrous DMF (20 mL) followed by addition of carbonyl diimidazole (200 mg, 1.23 mmol). The reaction was stirred under nitrogen for 2 hours after which (1*H*-pyrrol-2-yl)-methylammonium hydrochloride (200 mg, 1.5 mmol) was added and left to stir overnight. The solution was concentrated *in vacuo* and purified by column chromatography (EtOAc:Hexane) yielding a white solid (< 5 mg, < 4%), δ_{H} (400 MHz, d_6 -DMSO) 11.74 (1 H, s, **1**), 10.66 (2 H, s, **7**), 8.96 (2 H, t, *J* 5.5, **5**), 8.29 (2 H, d, *J* 8.0, **4**), 8.12 (2 H, s, **2**), 7.79 (2 H, d, *J* 8.0, **3**), 6.76 – 6.69 (2 H, m, **8**), 6.06 – 5.97 (4 H, m, **9+10**), 4.52 (4 H, d, *J* 5.5, **6**) ppm. *m/z* expected 412.1768 found 412.1768 [M+H].

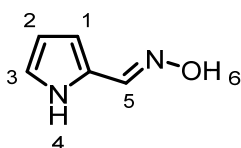
3.4.7 Synthesis of dimethyl 2-amino-[1,1'-biphenyl]-4,4'-dicarboxylate (**3.25**)



Dimethyl 2-nitro-[1,1'-biphenyl]-4,4'-dicarboxylate (1.00 g, 3.17 mmol) and 10% Pd/C (0.1154 g) were combined and purged with argon before addition of methanol (30 mL) and methylene chloride (6 mL). The solution was then purged with H₂ for 12 hours. The solution was purged with argon then filtered through diatomaceous earth. The residue was washed with methanol (30 mL) and dichloromethane (30 mL) to yield a clear yellow coloured liquid which was concentrated *in vacuo* to yield yellow crystals, dimethyl 2-amino-[1,1'-biphenyl]-4,4'-dicarboxylate (0.569 g, 63%); mp_{DSC} 166 °C, ν_{max} (cm⁻¹) 3458 (N-H), 3365 (N-H), 2952 (C-H), 1703 (C=O), 1273 (C-O); δ_{H} (400 MHz, d_6 -DMSO) 8.05 (2 H, d, *J* 8.5, **4/5**), 7.62 (2 H, d, *J* 8.5, **4/5**), 7.44 (1 H, d, *J* 1.5, **3**), 7.23 (1 H, dd, *J* 8.0, 1.5, **2**), 7.16 (1 H, d, *J* 8.0, **1**), 5.27 (2 H, s, **6**), 3.89 (3 H, s, **8**), 3.85 (3 H, d, *J* 8.5, **7**) ppm; δ_{C} (100 MHz, CDCl₃) 167.0, 166.8, 143.5, 143.4, 130.7, 130.5, 130.4, 130.3, 129.5, 128.9, 119.8, 116.7, 52.3 ppm; *m/z* expected 286.1001 found 286.1074 [M+H].

3.4.8 Synthesis of 1*H*-pyrrole-2-carbaldehyde (**3.15**).

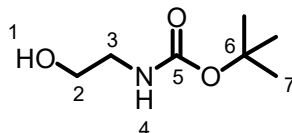
Phosphorus oxychloride (21 mL, 224 mmol) was added to anhydrous diethyl ether (70 mL) under argon and cooled to 0 °C. Anhydrous dimethyl formamide (21 mL, 271 mmol) was added dropwise maintaining the temperature of 0 °C and stirred for 30 minutes. A white precipitate formed to which was added anhydrous pyrrole (15.5 mL, 223 mmol) and the solution was slowly warmed to room temperature and left to stir overnight. The reaction was then cooled to 0 °C and quenched with saturated sodium carbonate to pH 7. The solution was extracted with ethyl acetate (4 × 100 mL) washed with brine (100 mL) and then dried over anhydrous magnesium sulfate. The solution was filtered, concentrated *in vacuo* and recrystallised from hexane to yield white crystals (12.9 g, 61%), mp 45-47 °C, ν_{\max} (cm⁻¹) 3139 (N-H), 2977 (C-H), 1614 (C=O), δ_{H} (400 MHz, d₆-DMSO) δ 12.10 (1H, s, **4**), 9.48 (1H, s, **5**), 7.22 (1H, s, **3**), 7.00 (1H, dd, J 3.5, 1.0 Hz, **1**), 6.28 (1H, dd, J 3.5, 2.5 Hz, **2**) ppm. δ_{C} (100 MHz, DMSO) 179.1 (**5**), 132.9 (**6**), 127.0 (**3**), 121.9 (**1**), 110.5 (**2**). *m/z* expected 96.0371 found 96.0440 [M+H].

3.4.9 Synthesis of 1*H*-pyrrole-2-carbaldehyde oxime (**3.17**).

1*H*-Pyrrole-2-carbaldehyde (0.8907g, 9.37 mmol) was finely powdered and added to a conical flask followed by a solution of potassium carbonate (0.8769, 6.34 mmol) in water (75 mL). To this suspension was added hydroxylamine hydrochloride (1.0631 g, 15.30 mmol) and stirred for 30 minutes then transferred to the fridge and left overnight. The resulting white precipitate was filtered, dissolved in ethyl acetate (100 mL) and dried over anhydrous magnesium sulfate. Following filtration, the solution was then concentrated *in vacuo* to yield a white solid (0.7945 g, 77%), mp_{DSC} 169 °C, ν_{\max} (cm⁻¹) 3408.57 (O-H), 3113 (N-H), 2981 (O-H), 1643 (C=N), 737 (O-N), δ_{H} (400 MHz, d₆-DMSO) 11.16 (1 H, s, **6**), 11.12

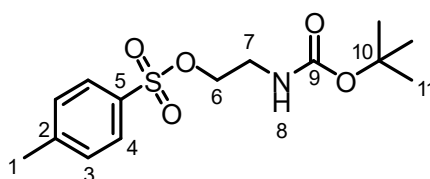
(1 H, s, **4**), 7.25 (1 H, s, **5**), 6.88 (1 H, m, **1/2/3**), 6.55 (1 H, m, **1/2/3**), 6.10 (1 H, m, **1/2/3**) ppm.
m/z expected 111.0480 found 111.0552 [M+H].

3.4.10 Synthesis of *N*-Boc-ethanolamine (**3.29**)



Di-*tert*-butyl dicarbonate (15.7280 g, 72.04 mmol) and sulfamic acid (0.3256 g, 3.27 mmol) were combined followed by 2-aminoethan-1-ol (3.9 mL, 65.15 mmol) dropwise. The reaction was stirred under argon at room temperature for 1 hour, monitored by TLC analysis and visualised with potassium permanganate. Upon completion the product was extracted with ethyl acetate (20 mL). The organic extraction was washed sequentially with water (3 × 20 mL), brine (2 × 20 mL) and sat. NaCO₃ (2 × 30 mL) then dried over MgSO₄, filtered and concentrated *in vacuo* to yield a clear colourless viscous oil, *N*-Boc-ethanolamine (**5**) (6.8194 g, 78%); *R*_f = 0.02 (1:4 ethyl acetate : hexane) *v*_{max} (cm⁻¹) 3339 (O-H), 2976 (C-H), 1682 (C=O), 1164 (C-O); δ_{H} (400 MHz, CDCl₃) 5.29 (1 H, s, **1**), 3.68 – 3.61 (1 H, m, **4**), 3.61 – 3.53 (2 H, m, **3**), 3.20 (2 H, m, **4**), 1.37 (9 H, s, **7**) ppm; δ_{C} (100 MHz, CDCl₃) 156.9 (**5**), 79.5 (**3**), 62.1 (**2**), 43.0 (**6**), 28.34 (**7**) ppm; *m/z* expected 184.1052 found 184.0944 [M+Na].

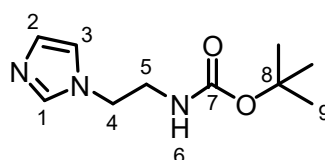
3.4.11 Synthesis of 2-((Boc-amino)-ethyl 4-methylbenzenesulfonate (**3.30**)



N-Boc-ethanolamine (**5**) (2.9293 g, 18.17 mmol) was mixed with dichloromethane (8 mL), placed under an inert atmosphere (argon) and cooled to 0 °C. Trimethylamine (5.2 mL, 37.31 mmol) was added dropwise followed by *p*-toluenesulfonyl chloride (5.3925 g, 28.29 mmol). The solution changed from a clear to a cloudy opaque white mixture. This was left stirring for 12 hours at room temperature after which time it turned a deep, opaque orange/brown. Upon completion the product was extracted with dichloromethane (20 mL). The organic extraction was washed sequentially with iced water (2 × 20 mL) and brine

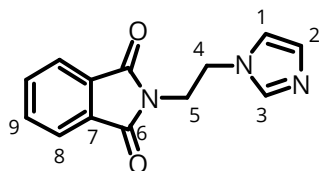
(1 × 20 mL) then dried over MgSO₄, filtered and concentrated *in vacuo* to yield a brown/orange viscous liquid product. The crude material was purified via column chromatography (1:4 ethyl acetate:hexane) to yield a pale yellow crystalline solid (2.8225 g, 49%); R_f = 0.10 (DCM), mp_{DSC} 81 °C, ν_{max} (cm⁻¹) 3407 (N-H), 2979 (C-H), 1711 (C=O), 1345 (S=O), 1174 (S=O), δ_H (400 MHz, CDCl₃) 7.80 (2 H, d, **4**), 7.37 (2 H, d, **3**), 4.91 (1 H, s, **8**), 4.07 (2 H, t, J 10.0, 6.0, **6**), 3.38 (2 H, q, J 5.0, **7**), 2.45 (3 H, s, **1**), 1.41 (9 H, s, **11**); δ_C (100 MHz, CDCl₃) 155.7 (**9**), 145.1 (**2**), 132.7 (**5**), 130.0 (**3**), 128.0 (**4**), 79.7, (**10**) 69.5 (**6**), 39.8 (**7**), 28.4 (**11**), 21.8 (**1**) ppm, *m/z* expected 338.1140 found 338.1033 [M+Na].

3.4.12 Synthesis of *Tert*-butyl (2-(1H-imidazol-1-yl)-ethyl)-carbamate (**3.32**)



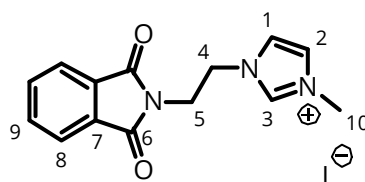
A mixture of NaH (0.1594 g, 6.63 mmol, 60% in mineral oil) and DMF (8 ml) was placed under an inert atmosphere (argon). A solution of imidazole (0.2451 g, 3.60 mmol) in DMF (2 ml) was added with stirring and left for 45 minutes before a solution of 2-((*tert*-butoxycarbonyl)-amino)-ethyl 4-methylbenzenesulfonate (1.1715 g, 3.71 mmol) in DMF (6 ml) was added and the mixture was left stirring at room temperature for 12 hours. A change from an opaque pale pink to an opaque pale amber solution was observed, before finally becoming a clear pale amber liquid. The solvent was then removed under reduced pressure and the crude product was extracted with ethyl acetate (25 mL). The organic extraction was washed sequentially with water (2 × 25 mL) and brine (1 × 25 mL) before being dried over MgSO₄, filtered and concentrated *in vacuo* to yield a pale yellow, viscous liquid; *tert*-butyl ((1H-imidazol-1-yl)-methyl)-carbamate (**7**) (0.1481 g, 19%); R_f = 0.1 (DCM); ν_{max} (cm⁻¹) 3250 (N-H), 2927 (C-H), 1698 (C=O), 1168 (C-O); δ_H (400 MHz, CDCl₃) 7.42 (1 H, s, **1**), 7.03 (1 H, s, **3**), 6.92 (1 H, s, **2**), 5.47 (1 H, s, **6**), 4.07 (2 H, t, **4**), 3.42 (2 H, q, **5**), 1.44 (9 H, s, **9**); δ_C (100 MHz, CDCl₃) 155.8 (**7**), 137.2 (**1**), 129.5 (**2**), 118.6 (**3**), 79.7 (**8**), 46.4 (**4**), 41.2 (**5**), 28.1 (**9**); *m/z* expected 212.1321 found 212.1394 [M+H].

3.4.13 Synthesis of 2-(2-(1H-imidazol-1-yl)-ethyl)-isoindoline-1,3-dione. (**3.34**)



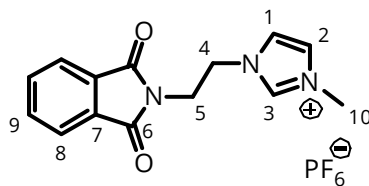
KI (326 mg, 1.9 mmol) was added to a RBF containing molten imidazole (13.4 g, 197 mmol) under an inert atmosphere. After stirring for 10 minutes at 90 °C, *N*-(2-bromoethyl)-phthalimide (10 g, 39 mmol) was slowly added and the reaction was left stirring at 100 °C for a further three hours. The reaction was cooled and extracted by Soxhlet in toluene for 20 hours. The extract was condensed *in vacuo* yielding a white solid which was triturated with water to yield white crystals (6.34 g, 67%). mp_{DSC} 161 °C, ν_{\max} (cm⁻¹) 3455 (C-H), 1694 (C=O), δ_{H} (400 MHz, d₆-DMSO) 7.87 – 7.81 (4 H, m, **9+8**), 7.53 (1 H, s, **3**), 7.12 (1 H, s, **2**), 6.80 (1 H, s, **1**), 4.24 (2 H, t, *J* 6.0, **5**), 3.91 (2 H, t, *J* 6.0, **4**), *m/z* expected 242.0851 found 242.0924 [M+H].

3.4.14 Synthesis of 1-(2-(1,3-dioxoisoindolin-2-yl)-ethyl)-3-methyl-1-imidazolium iodide. (**3.35**)



2-(2-(1H-Imidazol-1-yl)-ethyl)-isoindoline-1,3-dione (1.0 g, 4.15 mmol) was dissolved in anhydrous THF to which iodomethane (0.5 mL, 8.03 mmol) was added and stirred for three hours. The precipitate was filtered and washed with THF to yield a light-yellow powder (1.43 g, 90%). mp_{DSC} 233 °C, ν_{\max} (cm⁻¹) 3128 (C-H), 1708 (C=O), δ_{H} (400 MHz, d₆-DMSO) 9.15 (1 H, s, **3**), 7.92 – 7.81 (5 H, m, **1+9+8**), 7.66 (1 H, d, *J* 2.0, **2**), 4.43 (2 H, t, *J* 5.0, **5**), 4.01 (2 H, t, *J* 5.0, **4**), 3.81 (3 H, s, **10**), δ_{C} (100 MHz, d₆-DMSO) 167.6, 137.1, 134.5, 131.5, 123.6, 123.2, 122.8, 47.8, 38.0, 35.8 ppm, *m/z* expected 256.1086 found 256.1080 [M-I].

3.4.15 Synthesis of 1-(2-(1,3-dioxoisoindolin-2-yl)-ethyl)-3-methyl-1-imidazolium hexafluorophosphate. (**3.38**)



1-(2-(1,3-Dioxoisindolin-2-yl)-ethyl)-3-methyl-1-imidazolium iodide (2.0 g, 5.2 mmol) was dissolved in water to which potassium hexafluorophosphate was added (0.96 mg, 5.2 mmol). A white precipitate immediately began to form and was left to stir overnight to ensure complete exchange. The precipitate was filtered and washed with water (2×20 mL) to yield a white powder (1.85 g, 86%). mp_{DSC} 188 °C, ν_{\max} (cm⁻¹) 3160 (C-H), 1709 (C=O), δ_{H} (400 MHz, d₆-DMSO) 9.15 (1 H, s, **3**), 7.91 – 7.81 (5 H, m, **1+9+8**), 7.66 (1 H, s, **2**), 4.43 (2 H, t, *J* 5.5, **5**), 4.01 (2 H, t, *J* 5.5, **4**), 3.81 (3 H, s, **10**), *m/z* expected 256.1086 found 256.1080 [M-PF₆].

3.5 References

- 1 H. Liu, N. H. Bergman, B. Thomason, S. Shallom, A. Hazen, J. Crossno, D. A. Rasko, J. Ravel, T. D. Read, S. N. Peterson, J. Yates and P. C. Hanna, *J. Bacteriol.*, 2004, **186**, 164–78.
- 2 P. Setlow, *Curr. Opin. Microbiol.*, 2003, **6**, 550–556.
- 3 V. Gonzalez, D. A. L. Vignati, C. Leyval and L. Giamberini, *Environ. Int.*, 2014, **71**, 148–157.
- 4 D. Curiel, G. Sánchez, M. Más-Montoya, A. Tárraga and P. Molina, *Analyst*, 2012, **137**, 5499–5501.
- 5 A. F. Littke, C. Dai and G. C. Fu, *J. Am. Chem. Soc.*, 2000, **122**, 4020–4028.
- 6 J. I. G. Cadogan and M. J. Todd, *Chem. Commun.*, 1967, 178–179.
- 7 T. Cottrell, *The Strengths of Chemical Bonds*, Butterworths Scientific Publications, London, 1954.
- 8 H. A. Ludwig, *Ullmann's Encycl. Ind. Chem.*, 2000.
- 9 H. James, R. Kieran, B. Alex and S. Jason, *Chem. – An Asian J.*, 2015, **11**, 155–167.
- 10 E. Gebauer-Henke, W. Leitner, A. Prokofieva, H. Vogt and T. E. Muller, *Catal. Sci.*

- Technol.*, 2012, **2**, 2539–2548.
- 11 N. Putochin, *Berichte der Dtsch. Chem. Gesellschaft (A B Ser.)*, 1926, **59**, 1987–1998.
 - 12 C. Löwe and C. Weder, *Synthesis (Stuttg.)*, 2002, **2002**, 1185–1190.
 - 13 X. Fradera and M. Solà, *J. Comput. Chem.*, 2002, **23**, 1347–1356.
 - 14 X. Chen, J. Mihalic, P. Fan, L. Liang, M. Lindstrom, S. Wong, Q. Ye, Y. Fu, J. Jaen, J.-L. Chen, K. Dai and L. Li, *Bioorg. Med. Chem. Lett.*, 2012, **22**, 363–366.
 - 15 M. Majchrzak, M. Grzelak and B. Marciniak, *Org. Biomol. Chem.*, 2016, **14**, 9406–9415.
 - 16 K. Sun, X. Xie, Y. Liu, W. Jiang, X. Ban, B. Huang and Y. Sun, *J. Mater. Chem. C*, 2016, **4**, 8973–8979.
 - 17 B. J. Stokes, B. Jovanović, H. Dong, K. J. Richert, R. D. Riell and T. G. Driver, *J. Org. Chem.*, 2009, **74**, 3225–3228.

Chapter 4

In Vitro studies of bacterial germination and disclosure

4.1. Introduction

The occurrence of the disease Anthrax in humans typically results from exposure to a large quantity of *B. anthracis* endospores.^{1,2} Once situated in a favourable environment with suitable moisture and nutrient levels, the endospores undergo germination returning the bacteria to its vegetative state. This process is irreversible, and the vegetative cell cannot return to the endospore state without following the sporulation process (see Figure 1.8). This sporulation process comprises of the axial filament formation whereby unsymmetrical cleavage within the cell begins. Following this the forespore is formed and then engulfed by the remaining intracellular material. At this point the main body of the endospore has been created and is now prepared for release by forming the endospore cortex and coat. Once this is complete the remainder of the cell undergoes lysis and the endospore is released.

Based on this principle of irreversibility and the context of the objectives of this project, if germination can be induced then the success of any subsequent decontamination efforts will be increased greatly. The aims of this section of work are to provide insight into the interactions between materials synthesized and the target *B. anthracis* bacteria. Ideally the materials need to enable rapid and complete germination of the endospores while preventing the onset of resporulation.

The materials produced in this study would be tested directly against *B. anthracis* endospores. However, access and use of *B. anthracis* is restricted to certain institutions as a direct result of its capacity for use as a BWA. In order to circumvent this, a biological simulant can be used in its place. This is common practise when highly infectious pathogens need to be studied.

Bacteria and Viruses are separated into four categories, also known as Biological Safety Levels (BSL), dependent on the hazard they pose to human life as shown in Figure 4.1. Category 1 comprises species that pose no little to no risk to human health as they are

unlikely to cause disease such as *B. subtilis* and species within the *Lactobacillus* genus. Category 2 pathogens have the potential to cause human disease, but treatment is widely available. Such examples of this are *B. cereus*, a common cause of food poisoning and the measles virus. Category 3 pathogens have the capacity to cause severe human disease. *B. anthracis* falls in this category along with the causative agents of a variety of well-known diseases including West Nile virus, SARS virus, Tuberculosis, Yellow fever and Malaria. While treatment is available for these diseases the extent of their symptoms raises these pathogens above those of category 2. Category 4 pathogens can cause severe human disease and have no known treatments available. This category is almost entirely comprised of viruses such as Ebola virus. There are only a handful of laboratories in the UK with the facilities to handle Category 4 pathogens as their use is heavily restricted.³ Category 3 laboratories, though more widespread, require their workers to have a large amount of expertise and training.

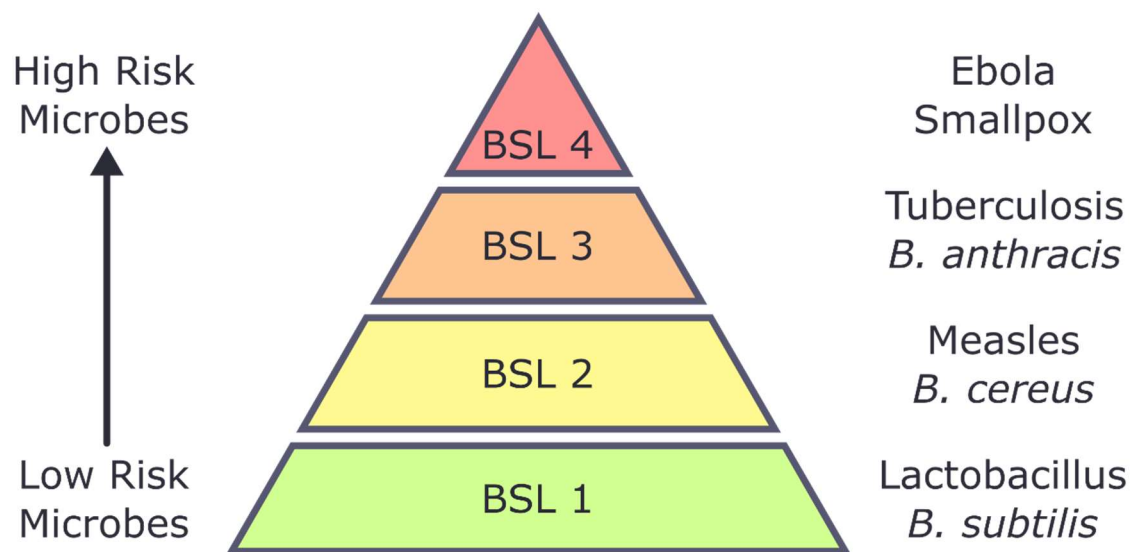


Figure 4.1: Depiction of biological safety levels and species that belong to these categories.

B. thuringiensis represents an ideal candidate for use as a simulant. The specific strain developed by Bishop and Robinson at Dstl belongs to the *subspecies* *kurstaki*.⁴ Typically, this subspecies is used as a biological pesticide. It acts in this method by producing proteins known as Cry proteins which are activated by the basic environment of the insects' digestive tract. As these proteins are not present in *B. anthracis* a specific strain HD-1 cry was used. This strain does not produce these Cry proteins and therefore more accurately reflects the response expected from *B. anthracis*.

The relationship between strains is typically visualized by a phylogenetic tree as shown in Figure 4.2. The distance between terminals indicates the similarities between the genetic variants. In this case *B. thuringiensis* is shown to be one of the closest relatives to *B. anthracis* compared to other *Bacillus* species such as *B. subtilis* and *B. cereus*.⁵

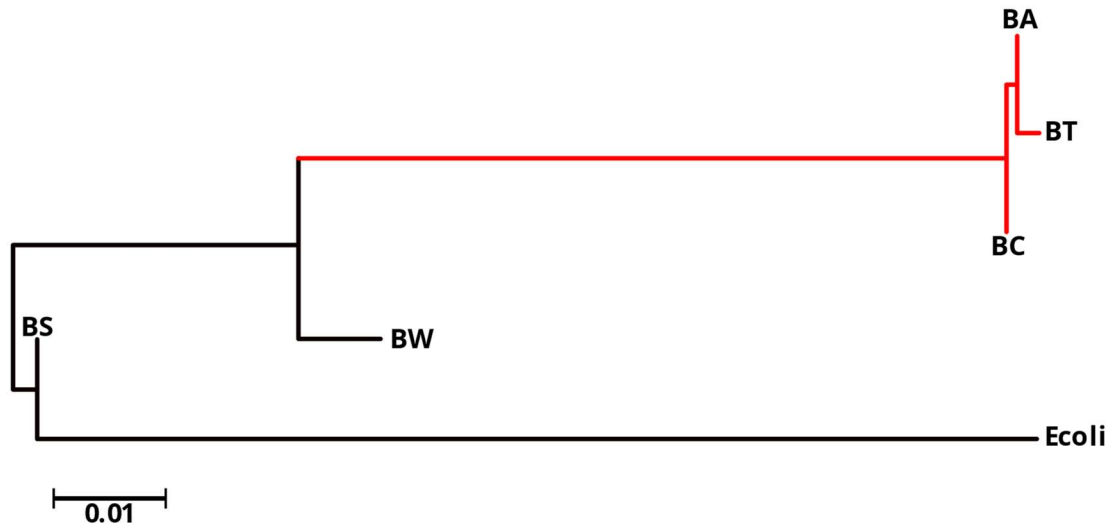


Figure 4.2: Phylogenetic tree of *B. anthracis*. the scale bar represents a 1% sequence difference (BA:*B. anthracis*; BT:*B. thuringiensis*; BC:*B. cereus*; BW:*B. weihenstephanensis*; BS:*B. subtilis* and *B. clausii*, *B. halodurans*, *B. licheniformis*)⁵

It has been found that this strain of *B. thuringiensis* is a particularly effective simulant for *B. anthracis* as it exhibits similar germination patterns and cell recovery from soil media.⁶ The added benefit of using this species of bacteria is that it is classified as a BSL category one bacteria.⁷ This greatly reduces the risk to human health during its use and permits a wider range of experimental freedom.

4.2. Results and Discussion

Stock suspensions of *B. thuringiensis* were prepared by inoculating a solution of trypticase soy nutrient broth (TSB). TSB comprises amino acid sources from the peptide mixes Tryptone and Soytone, carbon sources in the form of dextrose and essential salts such as sodium chloride and dipotassium phosphate.⁸ These were incubated for 2 days at 37 °C before being harvested by centrifugation. By leaving the bacteria for this extended incubation period most of the nutrients are consumed. As the *B. thuringiensis* senses the loss of these nutrients the process of sporulation is triggered. The resulting endospores

* Reproduced from reference ⁵ under the Creative Commons Attribution 4.0 International License.

can be visualised by staining with malachite green as shown in Figure 4.3. To assist in this visualisation safranin is used as a counter stain allowing for the identification of the any vegetative cells.

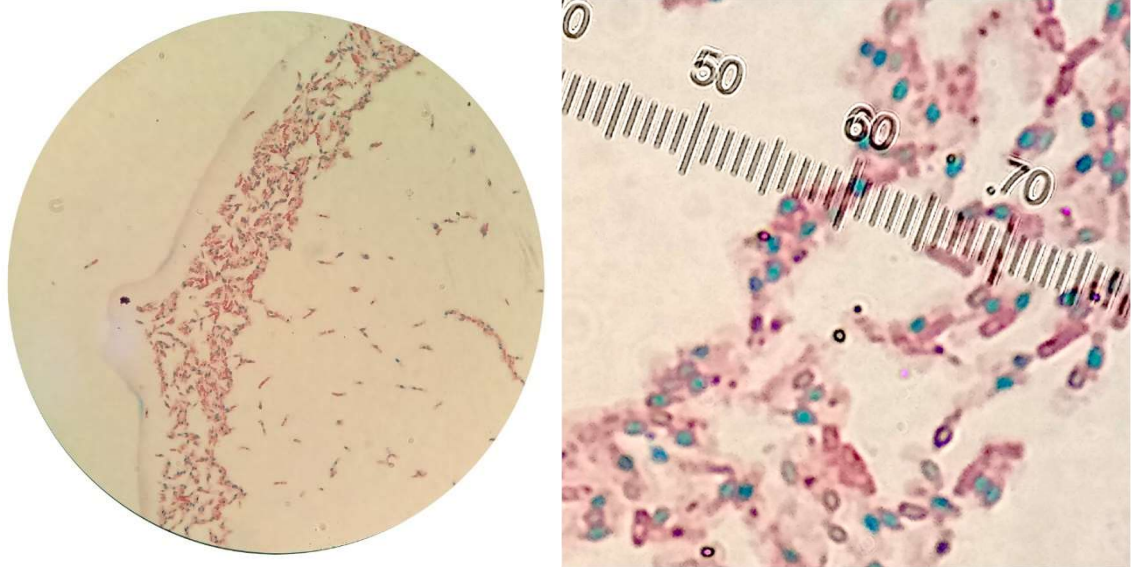


Figure 4.3: Images of *B. thuringiensis* endospores stained with malachite green and safranin O. (Scale in μm)

The evident red colouration in Figure 4.3 was thought to be a result of cellular debris left behind from the sporulation process. To verify this a small aliquot of the spores were exposed to germinants and stained with malachite green and safranin O (see Figure 4.4).

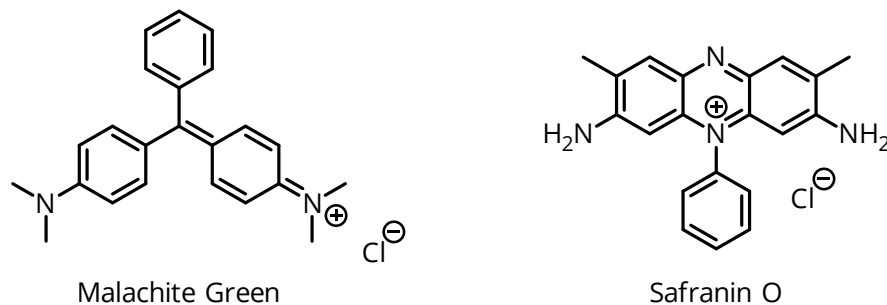


Figure 4.4: Structures of stains used for the visualisation of bacteria and endospores.

There is a clear difference between the light red cellular debris and the much darker red vegetative cells. These dark red vegetative cells can also be seen to have replicated to form linear filaments (Figure 4.5). This linear filament morphology is due to the binary fission method of asexual reproduction.

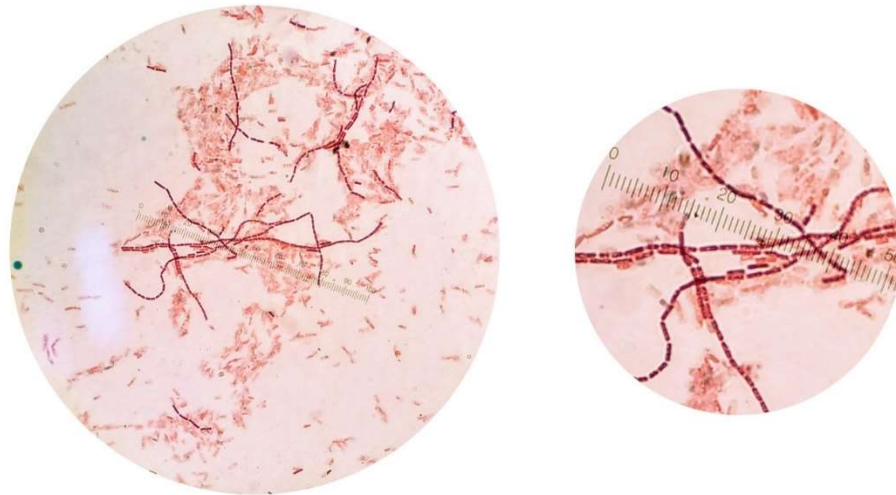


Figure 4.5: Images of *B. thuringiensis* vegetative cells stained with malachite green and safranin. (Scale in μm)

Germination testing by plate counting is not affected by the presence of this cellular debris. However, should alternative quantification methods be used in the future this debris could cause issues. Tavares and Souza *et al.* developed a procedure where lysozyme was utilized to breakdown remnants of the vegetative cells.⁹ Applying this procedure to the *B. thuringiensis* endospores shown in Figure 4.3 affords a cleaner stain as shown in Figure 4.6. The lysozyme enzyme effectively cleaves the glycosidic bonds present between sugars that form the peptidoglycan cell wall in gram-positive bacteria. The use of lysozyme on vegetative cells is common practice to kill the cell and liberate its contents. As the coat that protects the endospore is formed from different components it is resistant to the effects of this enzyme while its former mother cell is highly susceptible.

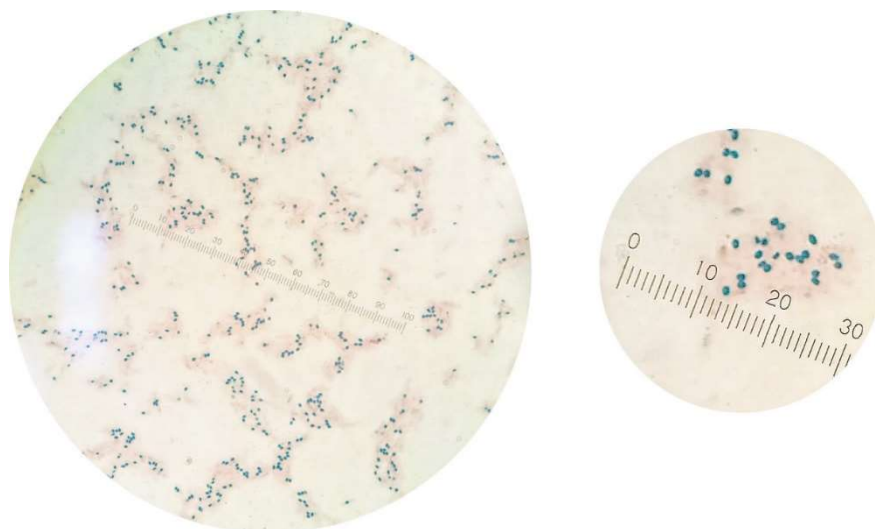


Figure 4.6: Images of *B. thuringiensis* endospores post lysozyme treatment. stained with malachite green and safranin. (Scale in μm)

The use of transmission electron microscopy (TEM) to examine the cells revealed the large quantity of fine debris particles even more evidently (see Figure 4.7). In the right micrograph shown below the remnants of a mother cell is clearly visible.

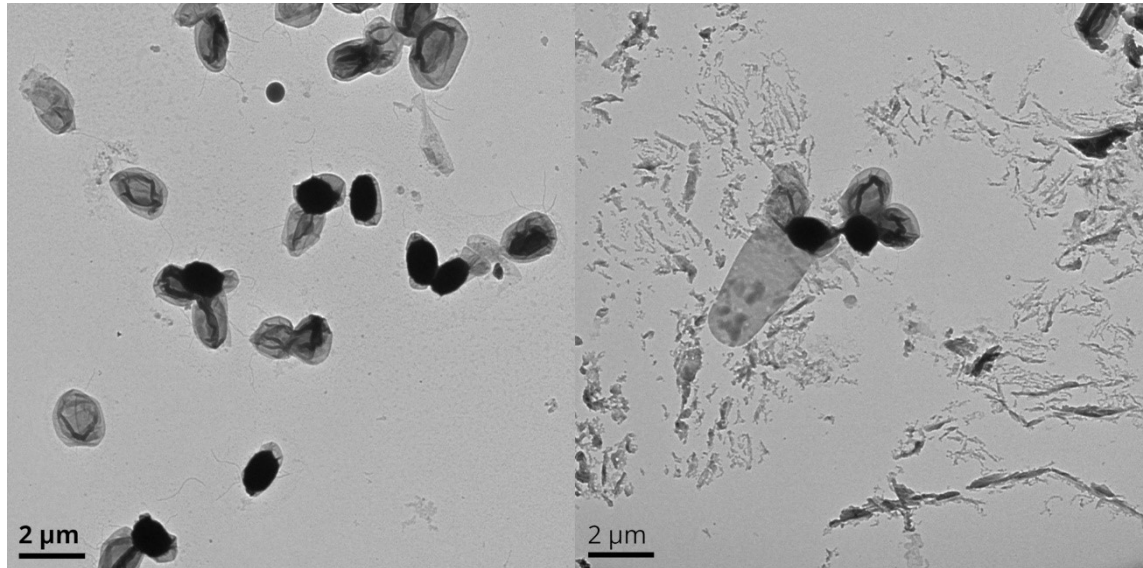


Figure 4.7: Micrographs of cellular debris and endospores obtained via TEM analysis.

Following treatment by the lysozyme purification method the microscopy images are noticeably free from debris with only the exosporium layers of the endospore remaining (see Figure 4.8).

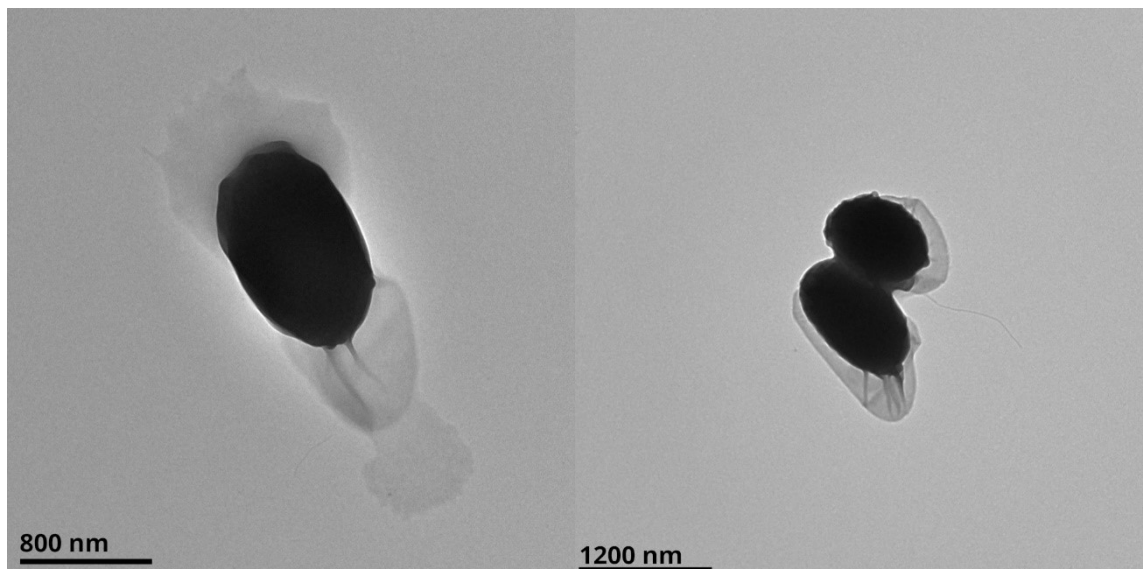


Figure 4.8: Endospores and their exosporium layers.

To begin the testing, the methodology for the germination experiment needs to be determined. In this case the number of cells that germinate need to be calculated. To

accomplish this the non-reversible nature of the germination process can be exploited. Once the cell has germinated it cannot return quickly to its endospore form without first passing through the lengthy sporulation process. Therefore, if germination is induced followed by thermal shock to kill ensuing vegetative cells the remaining cells are an indication of the remaining endospores. Stock concentration of *B. thuringiensis* endospores are firstly thermal shocked to ensure that vegetative cells are not present before the test.

In work published by Bishop⁶ it was found that the amino acid L-alanine and the nucleoside inosine provided high germination rates in *B. anthracis* and *B. thuringiensis* at concentrations of 100 mmol L⁻¹ and 10 mmol L⁻¹, respectively.⁶ This combination of germinant was selected as it provides the required rapid germination and the treated bacteria showed no evidence of growth and replication which is vital for the accuracy of the plate counting experiment.

The germination sample is comprised of a water polymer solution (800 µL), stock endospore suspension (100 µL) and stock solution of germinants prepared at 10-fold the final concentration required (100 µL). This method of preparation allows for the rapid addition of the germinants.

The germination sample is then prepared and incubated for one hour at 37 °C followed by repeating the thermal shock at 65 °C for a further one hour (see Figure 4.9).

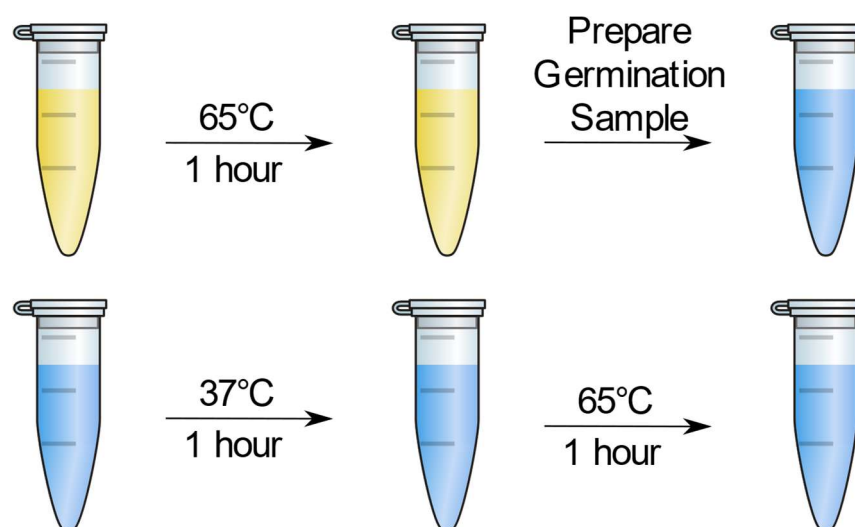


Figure 4.9: Schematic representation of the sample preparation procedure used.

4.2.1. Plate Counting

The plate counting method is widely used in the field of microbiology to quantify the number of colony forming units (CFU) per millilitre of suspension. Three 100 μL aliquots were taken from the germination samples and diluted sequentially. These dilutions were then used to inoculate trypticase soy agar (TSA) plates in triplicate and incubated overnight at 37 °C (see Figure 4.10). The resulting colonies can then be counted for each dilution level where they are clearly distinguishable.

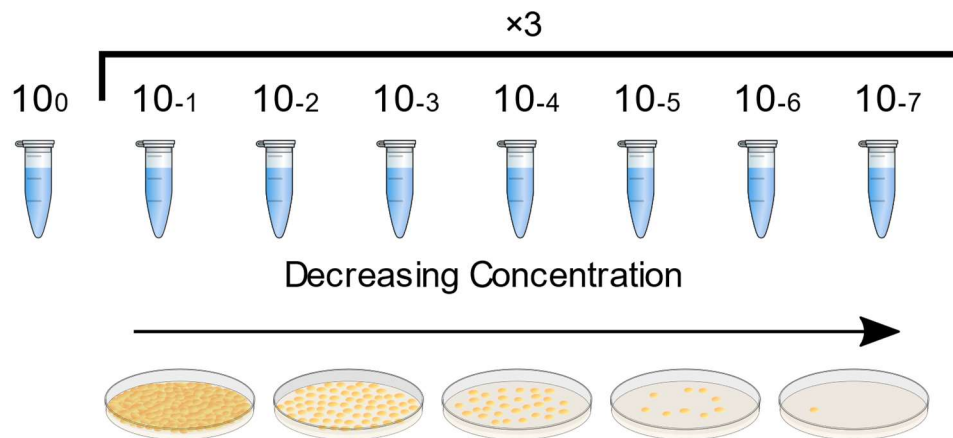


Figure 4.10: Schematic representation of the plate counting procedure used in this study.

The germination samples were prepared with a water-polymer-germinant solution. The final concentration of the germinants was identical across all samples. Alongside each germination sample was a control sample, this had no germinants added but was subjected to the same temperature cycles. This control sample provides a comparison such that the germination samples effectiveness can be determined.

The 4-nitro hydrogelator **2.6** was tested for its efficacy at a concentration of 0.5 mg mL^{-1} using the δ -gluconolactone gelation method discussed in Chapter 2. Alongside this gelator was also tested the cyano derivative **2.6CN**. The degree of germination for these materials was exceedingly poor with the nitro gelator performing the best with a germination of 36% when compared to the control. The cyano derivative **2.6CN** performed significantly poorer with an exhibited degree of germination of 8% compared to the control.¹⁰

The cause of this decrease in germination could be caused by a variety of factors, such as incompatibility with δ -gluconolactone method of gelation because of the resulting low pH.

Other potential causes include potential bactericidal properties of the urea derivatives **2.6** and **2.6CN**.

Following the negative germination result with the hydrogels tested, the SMA polyglycerol polymer was tested for its capability to assist with germination. The concentration of the polymer solution used at the outset of these tests was 20% w/w. This concentration provides contingency for adjustment should higher or lower concentrations be required. The data shown in Table 4.1 comprises individual sample measurements where each sample is sequentially plated in triplicate and averaged to give the degree of germination. The data suggests that the polymer solution enhances the germination rate of the endospores.

Germinants Only (%)	Polymer Solution (%)
69.9	88.3
50.7	85.0
60.2	83.7
44.0	84.3
72.3	85.3
62.8	83.7
75.3	91.0
67.4	89.1
59.2	89.2

Table 4.1: Average values from plate counts from 20% w/w SMA polymer solution.

This is further confirmed by the statistical model one-way analysis of variance (ANOVA) which compares the means of distributions for significant difference. This data exhibits $p < 0.01$ (3.9×10^{-6}), supporting the hypothesis that these data are significantly different.

The box plot shown in Figure 4.11 displays this data in a more visual manner where it can be seen that the mean values of the analysed data are clearly separated and there is no overlap of the minimum and maximum ranges and interquartile range.

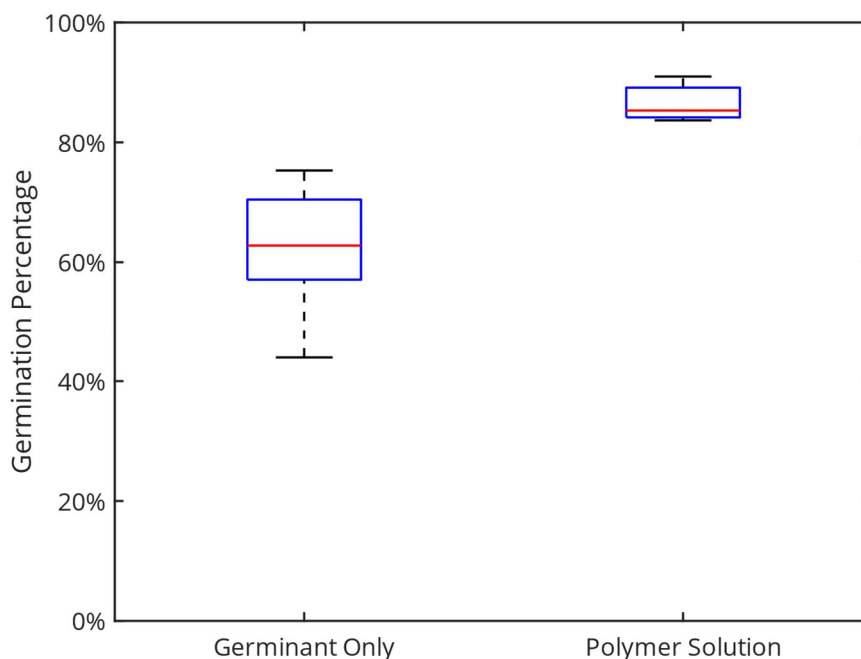


Figure 4.11: Box plot of degree of germination data from plate counts from 20% w/w SMA polymer solution showing the mean (red line), interquartile range (blue box) and range (black lines). (n=9)

In comparison to other materials previously tested at Dstl¹⁰ the polyglycerol formulated at 20% v/v offers greatly improved degree of germination over a period of one hour. The benefit of polyglycerol over the materials that performed similarly (see Table 4.2) is its high degree of functionality and exceptional affinity for water. The xanthan gum in glycerol solution requires large quantities of glycerol to achieve the required viscosity and water retention. The use of hyaluronic acid appears promising as it provides excellent germination properties. However, the cost of the biopolymer can reach as high as £11000 g⁻¹ which makes it prohibitively expensive for the desired application.¹¹ Finally, Poloxamer 407, an A-B-A copolymer made of polyethylene glycol and polypropylene glycol (EG₁₀₀PG₆₅EG₁₀₀)¹², offers a similar degree of germination to that of the polyglycerol at similar concentrations and a low cost. However, the benefit of the branched nature of the polyglycerol is that it is capable of further functionalization with little effect on its solubility and water retention capacity.

Material	Germination (%)
<i>p</i> -cyano hydrogelator (0.5 mg mL ⁻¹)	8
<i>p</i> -nitro hydrogelator (0.5 mg mL ⁻¹)	36
Gum arabic (0.4 % w/v in 40% v/v glycerol)	50
Xanthan gum (1 % w/v in 40% v/v glycerol)	98
Hyaluronic acid mol. wt. 750-1,000 kDa (in 0.15 M NaCl)	98
Agarose (1 % w/v)	30
Polyglycerol (20 % v/v)	95
Poloxamer 407 (20 % w/v)	98
Glycerol (40 % v/v)	50

Table 4.2: Degree of Germination for materials in water and L-alanine and inosine germinants.^{10†}

4.2.2. Alternative Methods for measuring Germination

While plate counting provides very accurate quantitative results there are a few drawbacks to gauging germination by this process. This method is known to be very time and labour intensive as agar plates need to be sterilized and prepared and each germination sample requires 7-fold serial dilution and generates 21 agar plates which are reduced to a single data point. Considering this, other methods of quantifying germination were investigated.

4.2.2.1. Dynamic Light Scattering

Dynamic light scattering (DLS) is routinely used to measure the size of particles within a solution by means of scattered light from an incident beam. The scattered speckle pattern varies over time based on the Brownian motion of the particles in solution. Larger particles diffuse slower through the solution than smaller particles. At first glance this method would appear to be perfectly suited to this task since as the endospores germinate they grow in size by a significant factor. However, while this method could reliably measure the size of the endospore, the vegetative cells are much more difficult to characterise. As DLS relies on the size of the surface that scatters the light back the approximately spherical endospore provides an even surface at every orientation. The vegetative cells of *B. thuringiensis* and other members of the *Bacillus* genus are rod shaped as such the traditional methods of DLS analysis would detect an average of different sizes

[†] The author is grateful for the testing of the hydrogelators and supply of data on previously tested materials by Dstl.¹⁰

of particles depending on the orientation of the cell relative to the incident beam.¹³ The example shown in the schematic of Figure 4.12 exemplifies this effect through the rotation of an endospore and vegetative cell.

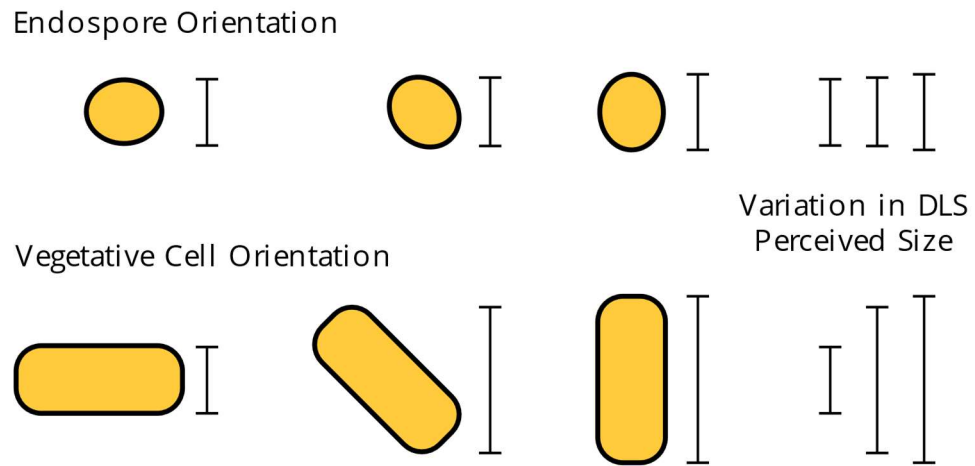


Figure 4.12: Comparison of endospore and vegetative cell perceived size by DLS.

Additional calculations for the Brownian motion of rotation are required in order to accurately determine the size of these rods which significantly increases the complexity of this method.^{14,15} Further compounding these limitations is the requirement that an accurate refractive index is given for the material being analysed. However, as the endospore germinates the opacity and refractive index changes dramatically thereby altering the measurements taken.

4.2.2.2. Optical Density

Optical density measurements are common place in microbiology research as a method of measuring the density of cells in a solution. In a similar fashion to DLS, the bacteria in the solution scatter the incident light beam resulting in a lower transmission. It is this transmission that can be used to measure cell replication, since optical density is known to be linear with respect to cell density.¹⁶

Optical density measurements are typically taken at 600 nm (OD_{600}), but this can be altered between 400 and 800 nm depending on the species being analysed. This minimises damage that can occur when using shorter wavelength radiation such as UV while still providing accurate readings.

This method has previously been used for quantification of *B. thuringiensis* cells and endospores and therefore could provide insight into the germination over time.^{17,18} Using a UV-Vis spectrophotometer an absorption spectrum was taken of a diluted sample of endospores every minute for two hours (see Figure 4.13). During this time the suspension was kept at 37 °C to match the conditions used previously. There was a noticeable decrease in absorption over time while the line shape of the spectrum remained the same.

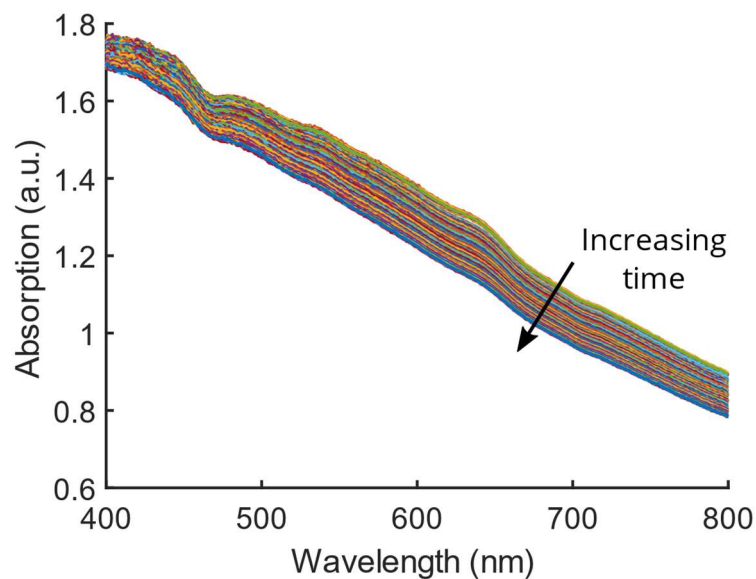


Figure 4.13: UV-Vis spectrum of *B. thuringiensis* endospores over time at 37 °C.

This can be visualised more easily by taking the normalised absorption values at 600 nm over time (see Figure 4.14). There is a slight decrease in this absorption most likely as a result of sedimentation of the endospores. Though this effect was not visible by eye the greater sensitivity of the spectrophotometer allows for this determination. Using this data as a baseline the germination measurements can be adjusted to take this into account.

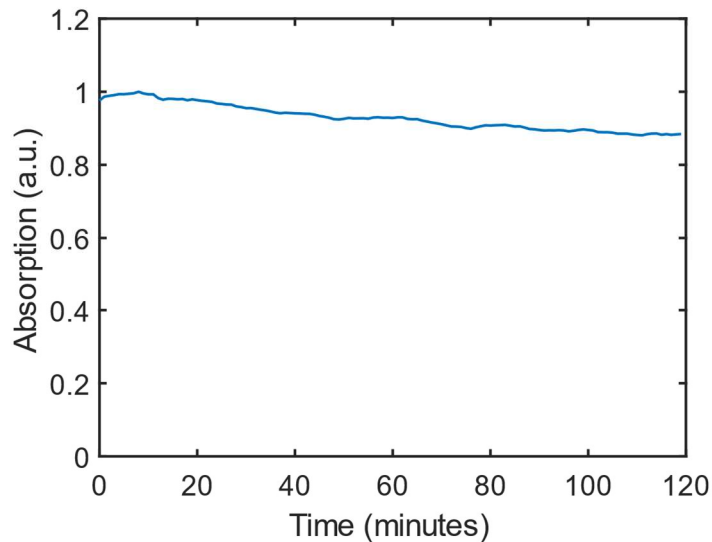


Figure 4.14: Absorption at 600 nm vs. time for *B. thuringiensis* endospores at 37 °C.

The graph in Figure 4.15 shows an initial sharp drop in relative optical density for both samples. This correlates to the first stage of germination as the cells begin to rehydrate and expel the salts within.¹⁹ This shows similar germination rates for both the germinant only as well as the germinant polyglycerol solution within the first five minutes. After this point the germination in polymer solution can be seen to continue at a greater rate than that of the germinant only solution. At a period of 20 minutes after germination began the polyglycerol enhanced solution exhibited a 33% greater loss in optical density. After one hour this manifests as a ten percentage point lead for the polyglycerol solution which the germinants alone only reach after a further one hour of incubation time.

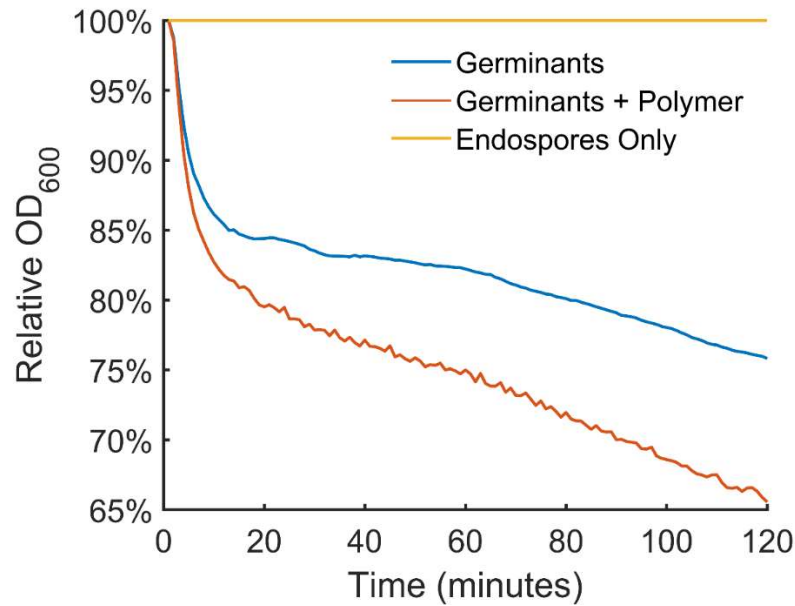


Figure 4.15: Optical density of germinating solutions relative to the endospores alone.

While this method does not provide the quantifiable accuracy found with the plate counting method it gives insight into the minute by minute process of germination and how this is affected by the material. As well as greater temporal insight this method offers rapid results with usable data being return with two to three hours compared to the plate counting technique which can take up to two days including preparation of materials.

4.3. Conclusion

B. thuringiensis HD-1 cry endospores were cultivated and purified by means of a lysozyme based method.⁹

The nitro and cyano urea hydrogels **2.6** and **2.6CN** were tested against *B. thuringiensis* as a potential effective material for encouraging germination and quantified by plate counting. They were found to be ineffective for this purpose with the degrees of germination of 36% and 8% respectively, significantly lower than previously tested alternatives.

SMA polyglycerol was also tested by means of plate counting and shown to be highly effective at encouraging germination of the endospores. In order to gain greater insight into the process of germination the method of measuring optical density was investigated. Using the endospores alone as a baseline the polyglycerol enhanced

solution showed a 33% greater loss of optical density compared to that of the endospores and germinants alone after 20 minutes. This improved over time with the polyglycerol solution reaching 75% relative OD₆₀₀ within 60 minutes compared to the 120 minutes for the endospores and germinants alone.

This study provides an excellent foundation for further investigation into the germination rates of *B. thuringiensis* in polyglycerol solutions by means of OD₆₀₀ measurements. These data have been shown to provide greater insight into the temporal process of germination at the expense of quantitative accuracy. Since the exact CFU values do not carry inherent meaning for this analysis this method offers a high throughput alternative.

4.4. Methods

The growth media used in these studies was trypticase soy broth TSB (containing pancreatic digest of casein 17.0 g, enzymatic digest of soya bean 3.0 g, sodium chloride 5.0 g, dipotassium hydrogen phosphate 2.5 g, glucose 2.5 g and dH₂O 1 L). The plates used were tryptic soy agar and used the broth listed above with the addition of agar 15.0 g. Germination experiments were carried out with a final germinant concentration of L-alanine 100 mmol L⁻¹ and inosine 10 mmol L⁻¹. *B. thuringiensis* endospore stock solution of 2.5×10⁸ CFU mL⁻¹ was used to inoculate the germination samples. OD₆₀₀ measurements were recorded using a Varian Cary 300 UV-Vis spectrophotometer at 37 °C and analysed with MATLAB®. TEM micrographs were obtained on a JEOL JEM 2100 plus TEM.

4.5. References

- 1 W. F. Klietmann and K. L. Ruoff, *Clin. Microbiol. Rev.*, 2001, **14**, 364–381.
- 2 D. Thavaselvam and R. Vijayaraghavan, *J. Pharm. Bioallied Sci.*, 2010, **2**, 179–188.
- 3 House of Commons, *Biosecurity in UK research laboratories Sixth Report of Session 2007–08*, 2008.
- 4 A. H. Bishop and C. V Robinson, *J. Appl. Microbiol.*, 2014, **117**, 654–662.
- 5 A. Wang and G. J. Ash, *Sci. Rep.*, 2015, **5**, 13644.
- 6 A. H. Bishop, *J. Appl. Microbiol.*, 2014, **117**, 1274–82.

- 7 WHO (World Health Organization), *International programme on chemical safety (IPCS): microbial pest control agent Bacillus thuringiensis*, 1999, vol. 217.
- 8 BD Tryptic Soy Broth (TSB) Product Details,
<https://www.bd.com/europe/regulatory/Assets/IFU/HB/CE/BA/BA-257107.pdf>.
- 9 M. B. Tavares, R. D. Souza, W. B. Luiz, R. C. M. Cavalcante, C. Casaroli, E. G. Martins, R. C. C. Ferreira and L. C. S. Ferreira, *Curr. Microbiol.*, 2013, **66**, 279–85.
- 10 C. Robinson, *Pers. Commun.*, 2017.
- 11 Hyaluronic acid sodium salt from Streptococcus equivalent molecular weight 750,000-1,000,000 | Sigma-Aldrich, <https://www.sigmaaldrich.com/catalog/product/sigma/53163>, (accessed 31 August 2018).
- 12 A. Bodratti and P. Alexandridis, *J. Funct. Biomater.*, 2018, **9**, 11–34.
- 13 S. E. Harding and P. Johnson, *Biochem. J.*, 1984, **220**, 117–123.
- 14 S. R. Aragón and R. Pecora, *J. Chem. Phys.*, 1976, **64**, 2395–2404.
- 15 J. Rodríguez-Fernández, J. Pérez-Juste, L. M. Liz-Marzán and P. R. Lang, *J. Phys. Chem. C*, 2007, **111**, 5020–5025.
- 16 E. G. Biesta-Peters, M. W. Reij, H. Joosten, L. G. M. Gorris and M. H. Zwietering, *Appl. Environ. Microbiol.*, 2010, **76**, 1399–1405.
- 17 R. M. Schmidt, M. M. Carter, M. L. Chu, C. J. Latario, S. K. Stadler and D. L. Stauff, *FEMS Microbiol. Lett.*, 2016, **363**, fnw076.
- 18 N. El-Khoury, R. Majed, S. Perchat, M. Kallassy, D. Lereclus and M. Gohar, *Front. Microbiol.*, 2016, **7**, 1222.
- 19 B. J. F. Keijser, A. Ter Beek, H. Rauwerda, F. Schuren, R. Montijn, H. van der Spek and S. Brul, *J. Bacteriol.*, 2007, **189**, 3624–34.

Chapter 5

Conclusions and Future Perspectives

The primary aim of this project was to produce a formulation capable of rapid disclosure of surfaces contaminated with *B. anthracis* endospores. In order to accomplish this the project was divided into 3 distinct sections of work: i) development of a formulation capable of retaining moisture without restricting germination, ii) synthesis of a disclosure agent capable of indicating the presence of *B. anthracis* and iii) testing products synthesized on a biological simulant to evaluate their use in the field.

5.1. Materials for BWA Disclosure - Gels and Polyols

Humidity is a major factor in encouraging germination of the endospores. To accomplish this while also maintaining the desired final chemical, physical and optical properties of the formulation a variety of methods were investigated. For endospore germination the formulation needs to be highly hygroscopic and water soluble.¹⁻³ The use of the final formulation in the field means care must be taken into account with regards to the environmental persistence to ensure that it does not contaminate land or water supplies.

The sub class of Low Molecular Weight Gelators (LWMGs) known as supergelators were thought to be suited to this application because of their ability to form rigid gels at concentrations of less than 1 wt%. The type of LMWG initially selected for these studies were nitro and cyano gelators **2.6** and **2.6CN** proposed by Hayes *et al.* These supergelators were synthesized and found to be very promising with regards to their ability to retain moisture over an extended period. Gels of **2.6** prepared with concentrations 5 mg mL⁻¹ in uncapped vials showed exceptionally low evaporation rates of less than 3% over 142 hours. When testing more realistic environmental conditions by means of glass slides the water retention was significantly affected by the greater surface area. While the duration of interest is only between one and two hours, the ability of these materials to retain moisture in ideal conditions is far in excess of these times was promising.

Following this work polyglycerols were investigated as a potential route to a formulation with high water retention, low colorimetric and fluorometric interference and high

viscosity. These hyperbranched materials are highly water soluble, possess extensive hydroxyl functionality for future functionalisation and are comprised of ether linkages rendering them particularly stable and unreactive.

Polyglycerols were synthesized using the slow monomer addition (SMA) procedures outlined by Frey *et al.*⁴ with the slight modification of the bases cation counterion to sodium from potassium. The lower cost and greater availability of the sodium methoxide prompted its selection. It was found during these syntheses that use of this cation prompted greater formation of cyclic structures within the polyglycerol material. The SMA procedure, while effective, is not a high throughput method and is heavily restricted by the capacity of the syringe pump equipment. In order to probe the necessity of the SMA procedure an alternative method was derived where the glycidol monomer was added in the bulk and slowly heated to 95 °C over two days. This slow heating was required in order to prevent thermal runaway and explosive polymerisation.

The bulk polymerisation method resulted in formation of predominantly cyclic structures. This was thought to be caused by the templating effect of the sodium cations whereas potassium cations used previously by Frey *et al.* are more likely to be chelated by the diglyme solvent. This effect was exacerbated by the low temperatures and long reaction times of the bulk procedure.^{5,6}

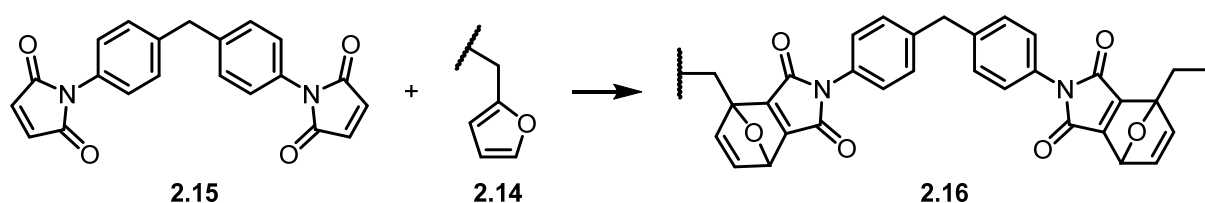
The polyglycerols generated via the SMA procedure exhibited ideal physical properties to the originally discussed requirements. The relatively low reactivity of the hydroxyl functionality and resilience of the ether linkage makes these materials particularly stable as is evident from the TGA analysis which showed these materials can endure the temperatures found within an autoclave meaning they could easily be prepared as an aseptic solution. This particular benefit would allow for mass production of final formulations and enable long-term storage without degradation. Since these formulations will contain sugars and amino acids to initiate germination the ability to sterilise them will prevent unintended biological growth. Unwanted proliferation of BWAs resulting from these solutions could pose significant risk to the end user.

In the light of the data obtained from studies on hydrogelators and hyperbranched polyglycerols, the priority for the continuation of the development of these materials

would be to investigate the potential alternative morphologies arising from the use of different cations, such as potassium, rubidium or caesium, during polymerisation. Variation of the alkali metal has been shown to produce differing templating effects as well as the use of more highly charged cations such as Ca^{2+} .^{5,6} The morphological variants produced from these studies should perform similarly to those already tested as they only differ by their degree of branching which is not expected to impact the germination of the bacteria.

The SMA polyglycerols provide an excellent hyperbranched backbone to which can be attached bioactive components such as sensors and cleavable decontamination groups. Orthogonal reactivity provided by addition of alternative functional groups enables facile further modification of the polymer while maintaining the high hydroxyl functionality. Installation of the pendant furfuryl alcohol groups allows for this via the well-known Diels-Alder thermoreversible reaction. The benefit of this method is that these reactions are typically conducted in very mild conditions and at low temperatures which allows for sensitive or less stable functional compounds to be attached to the polymer backbone without fear of degradation or damage to these materials.

Alongside these active compounds it would also be possible to introduce thermoreversible cross-linking compounds such as bismaleimide **2.15** (see Scheme 5.1). The introduction of this cross-linking moiety could greatly increase the viscosity and potential water retention capabilities by increasing the effective molecular weight of the polyglycerol.



Scheme 5.1: Bismaleimide facilitated cross-linking of polymer chains via Diels-Alder reaction.

It was noted that the furfuryl functionalised polyglycerols exhibited interesting lower critical solution temperature (LCST) characteristics in water (see Figure 5.1). This characteristic has only been observed previously with linear aliphatic modifications to the polyglycerol backbone as described recently by Liu and Chen *et al.* in late 2017.⁷

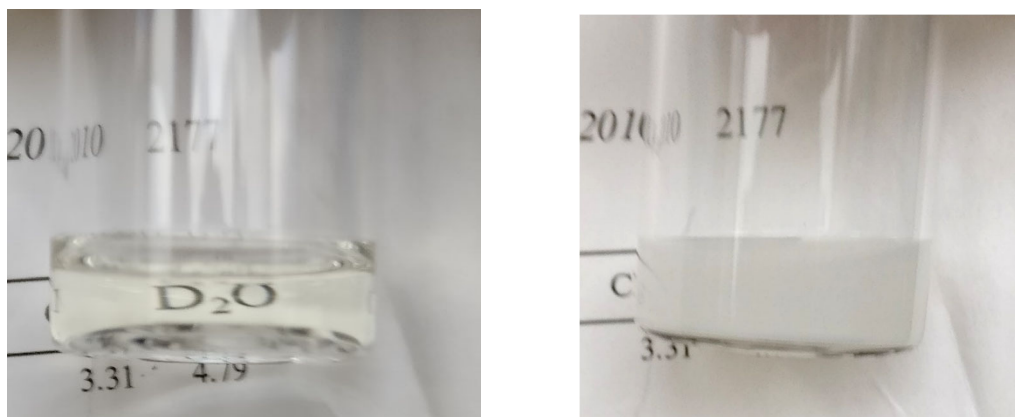


Figure 5.1: Left) 20 °C solution of FGE copolymer in water Right) 45 °C solution of polyglycerol in water.

The modified polyglycerols reported by Liu and Chen *et al.* were formed by functionalisation of polyglycerol post-polymerisation by carbonyl diimidazole (CDI) coupling on a milligram scale (≤ 300 mg polyglycerol). These results represent a proof of concept approach whereby very small quantities of material can be produced with the observable LCST effect. Conversely, the results described herein show an approach that can produce a similar observable LCST effect at much larger scale (*ca.* 50 g) by means of a process that is more suitable for industrial scaling. Combined with this is the ability of the furfuryl groups to act as functionalizable handles to provide further modification without reduction of the number of hydroxyl groups. Since the materials described by Liu and Chen *et al.* are only functionalised with aliphatic chains providing no further reactivity. In addition to the synthesis outlined by Liu and Chen *et al.* their chosen method of analysis was using fluorescence spectroscopy with the dye Nile red as the fluorescent probe to determine the solutions' cloud point. The method selected for use in this study was DLS analysis. The advantage of this measurement technique is the insight it provides into particle size distribution within the solution.

The method of synthesis for these materials can be easily adjusted and by varying the point of addition hyperbranched block copolymers could be achievable which will dramatically affect the physical properties of the material. Should the FGE monomer be introduced to the reaction separately to the glycidol monomer the resulting polymer will likely develop significant amphiphilic properties due to the more defined separation of hydrophilic and hydrophobic segments.

The increased amphiphilic or bolaamphiphilic nature of the resulting material could lead to increased formation of micellar structures and other self-assembling networks.⁸⁻¹¹

5.2. Disclosure Agent

During the process of germination, *B. anthracis* endospores release the biomarker calcium dipicolinate (CaDPA) which is used to improve the thermal stability of the endospore.^{2,3} This biomarker has been targeted by researchers as a highly specific indicator for the presence of endospores.

The majority of these sensors are based on the inherent chelation of the terbium trivalent cation by the dipicolinate anion.¹²⁻¹⁵ The first organic disclosure agent capable of identifying DPA was originally synthesized by Curiel *et al.* In order to identify the suitability of this disclosure agent for the desired application outlined previously. For this purpose, the original disclosure agent **3.1** was synthesized. Subsequent tests determined it was inappropriate for the required application, primarily because of its lack of water solubility and instability, as the desired formulation is both aqueous-based and likely to be stored for extended periods of time of up to one year.

To mitigate these issues attempts were made to improve the colorimetric response of **3.1** by introducing structural changes to the carbazole moiety that would expand the π -system. This feature could also be utilised to attach to the disclosure agent to the polyglycerol backbone or solubilising groups to enable solvation in aqueous formulations. Computational studies showed that this could be effective as the HOMO and LUMO were now clearly spread over a larger conjugated area. This approach was restricted by the unexpected low reactivity of the carbazole diester **3.10** which could not be resolved with the alternative routes attempted.

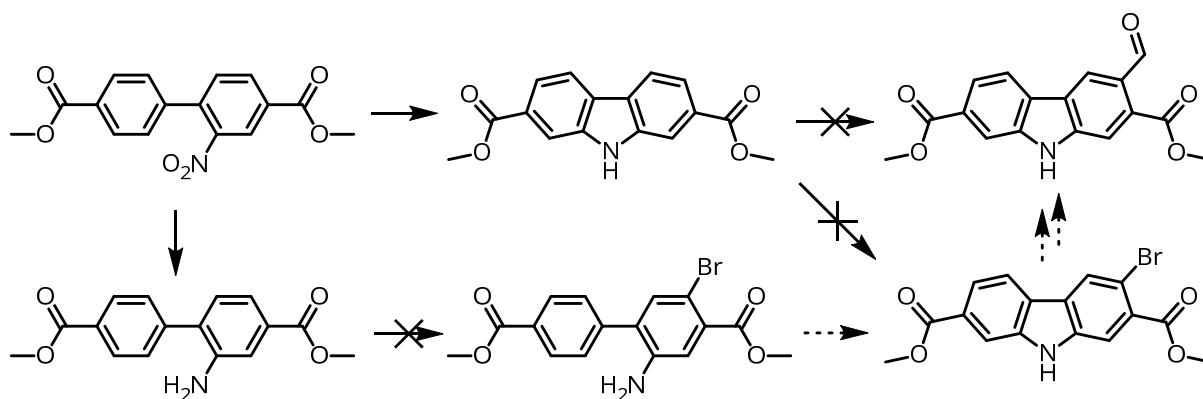


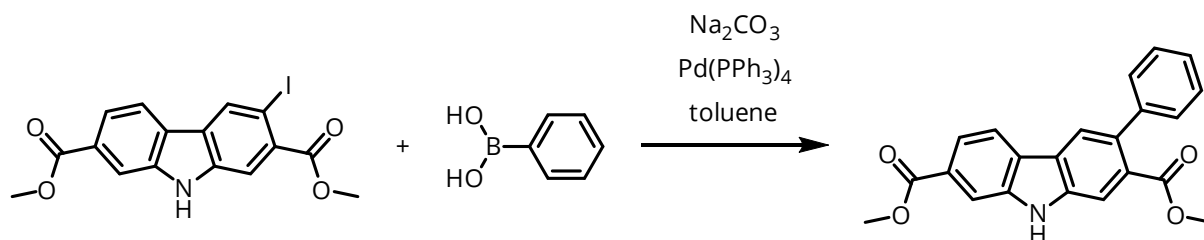
Figure 5.2: Alternative routes attempted to obtain formyl carbazole diester.

The issue of water solubility was tackled by attempting to introduce a charged imidazolium species **3.27**. Optimizations were performed in an attempt to reach the final ligand, such as the utilisation of *N*-(2-bromoethyl)-phthalimide. However, this was not concluded as a result of difficulties encountered with purification at the final stage. Disappointingly, because of this and other setbacks encountered during this study the proposed electrostatic detector **3.26** was not synthesized.

The priority for continuation of this work would be completion of the synthesis of modified of the sensor **3.26** with optimisation of purification procedures following the hydrazinolysis of phthalimide imidazolium iodide **3.35** leading to the synthesis of the amine imidazolium salt **3.27**.

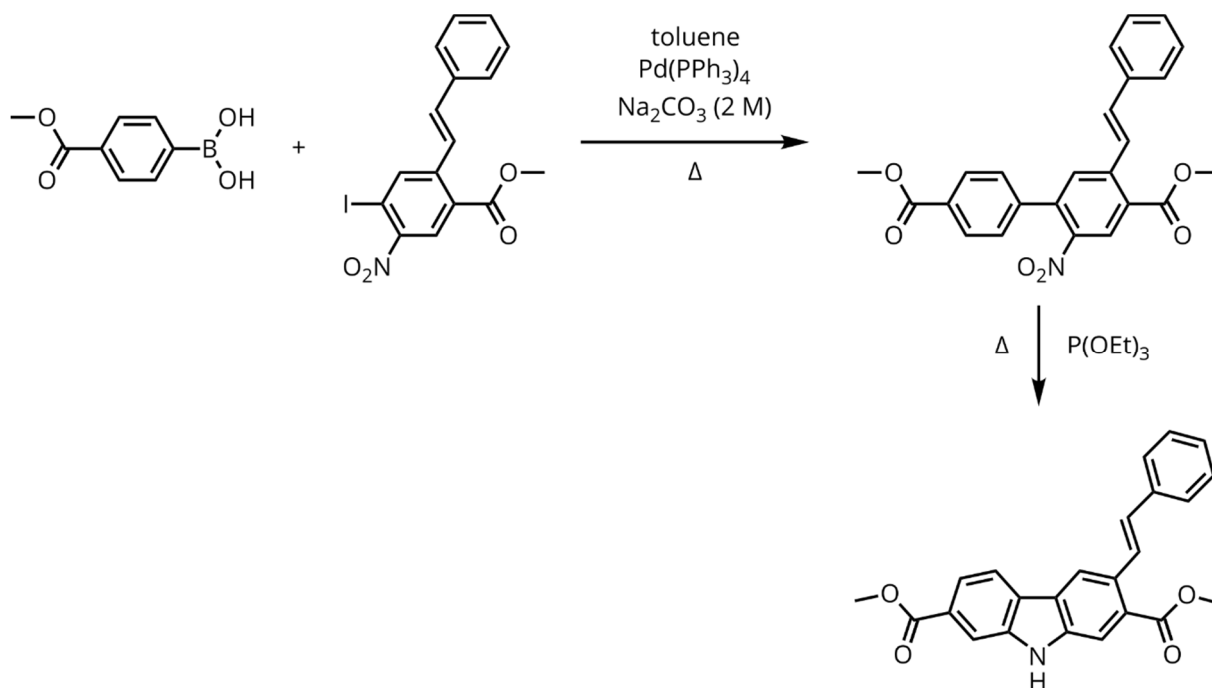
Further to this, the intended colorimetric response could still be achieved through the modification of the ring structure of the carbazole component of the detector. This was suggested by the computational calculations carried out on the theoretical structures.

An alternative procedure involving the direct coupling of phenyl groups to the carbazole moiety could also yield such a colourimetric detector as shown in Scheme 5.2. However, the majority of these reactions rely on the formation of the aryl halide which is obtained would also assist in opening up many other reaction pathways.



Scheme 5.2: Direct coupling of phenyl substituents to the carbazole ring via an iodo functionalized carbazole diester.

Alternatively, by utilising the synthetic pathway outlined by Curiel *et al.* the addition of the stilbene moiety prior to the palladium catalysed coupling of the phenyl ring precursor could yield the desired carbazole stilbene (see Scheme 5.3). The stilbene precursor **5.1** could be synthesized via the Heck coupling by employing a procedure developed by Morishita *et al.*¹⁶ The implementation of this functionality prior to the Cadogan nitrene insertion could avoid the drawbacks of the low reactivity of the resulting carbazole.



Scheme 5.3: Synthesis of stilbene carbazole disclosure agent precursor via palladium catalysed Suzuki reaction followed by Cadogan nitrene insertion.

5.3. Microbiological Studies

In order to evaluate the effectiveness of formulations at providing suitable environments for germination a series of microbiological studies were carried out. However, since the use of *B. anthracis* is restricted for obvious reasons an alternative simulant was used.

B. thuringiensis subsp. *kurstaki* HD-1 cry⁻ was selected for this purpose as it has been shown to be a particularly accurate replacement to its more hazardous relative.¹⁷

The cultivation of *B. thuringiensis* HD-1 cry⁻ endospores and subsequent further purification by means of a lysozyme based method¹⁸ was very successful at yielding the required simulant endospores.

Nitro and cyano urea hydrogels **2.6** and **2.6CN** were tested against *B. thuringiensis* as a potential effective material for encouraging germination and quantified by plate counting. They were found to be ineffective for this purpose with the degrees of germination of 36% and 8% respectively, significantly lower than previously tested alternatives.¹⁹

Polyglycerol produced via the SMA method was tested by means of plate counting to establish its efficacy towards encouraging germination endospores. To gain greater insight into the process of germination over time the method of measuring optical density was investigated. Using the endospores alone as a baseline, the polyglycerol enhanced solution was shown to give a 33% greater loss of optical density compared to that of the endospores and germinants alone after 20 minutes. This improved over time with the polyglycerol solution reaching 75% relative optical density at 600 nm (OD₆₀₀) within 60 minutes compared to the 120 minutes for the endospores and germinants alone.

The priority for continuation of this work would be the further development of the OD₆₀₀ technique for quantifying germination rates. This method has been shown to provide greater insight into the temporal development of the bacteria in response to a particular germination environment. Since the CFU values obtained via the plate counting method are relative to a control sample run at the same time the only benefit they provide is the ability to distinguish between viable and non-viable endospores. The high throughput offered by the OD₆₀₀ measurement method could enable more rapid data collection and faster formulation development compared to the two days and large quantity of agar plates it would typically take to run samples via the plate counting method.

5.4. References

- 1 B. Setlow, E. Melly and P. Setlow, *J. Bacteriol.*, 2001, **183**, 4894–9.
- 2 P. Setlow, *J. Appl. Microbiol.*, 2006, **101**, 514–525.
- 3 P. Setlow, *Curr. Opin. Microbiol.*, 2003, **6**, 550–556.
- 4 A. Sunder, R. Hanselmann, H. Frey and R. Mülhaupt, *Macromolecules*, 1999, **32**, 4240–4246.
- 5 L. Mandolini and B. Masci, *J. Am. Chem. Soc.*, 1977, **99**, 7709–7710.
- 6 G. Ercolani, L. Mandolini and B. Masci, *J. Am. Chem. Soc.*, 1981, **103**, 2780–2782.
- 7 Y. Zhang, R.-C. Wang, H.-J. Liu and Y. Chen, *Soft Matter*, 2017, **13**, 8136–8143.
- 8 N. Nuraje, H. Bai and K. Su, *Prog. Polym. Sci.*, 2013, **38**, 302–343.
- 9 F. Qiu, C. Tang and Y. Chen, *J. Pept. Sci.*, 2017, **24**, e3062.
- 10 P. Mosae Selvakumar, E. Suresh and P. S. Subramanian, *J. Mol. Struct.*, 2009, **919**, 72–78.
- 11 R. Nagarajan, in *Amphiphiles: Molecular Assembly and Applications*, American Chemical Society, 2011, vol. 1070, p. 1.
- 12 H. Chen, Y. Xie, A. M. Kirillov, L. Liu, M. Yu, W. Liu and Y. Tang, *Chem. Commun.*, 2015, **51**, 5036–5039.
- 13 D. L. Rosen, *Rev. Anal. Chem.*, 1999, 18, 1.
- 14 Q. Li, K. Sun, K. Chang, J. Yu, D. T. Chiu, C. Wu and W. Qin, *Anal. Chem.*, 2013, **85**, 9087–9091.
- 15 A. Makoui and D. K. Killinger, *Appl. Opt.*, 2009, **48**, B111–B118.
- 16 T. Izumi and N. Morishita, *J. Heterocycl. Chem.*, 2018, **31**, 145–152.
- 17 A. H. Bishop and C. V Robinson, *J. Appl. Microbiol.*, 2014, **117**, 654–662.
- 18 M. B. Tavares, R. D. Souza, W. B. Luiz, R. C. M. Cavalcante, C. Casaroli, E. G. Martins, R. C. C. Ferreira and L. C. S. Ferreira, *Curr. Microbiol.*, 2013, **66**, 279–85.
- 19 C. Robinson, *Pers. Commun.*, 2017.